

**Interaction of free surface waves
with elastic and air-cushion
platforms**

Interaction of free surface waves with elastic and air-cushion platforms

Proefschrift

ter verkrijging van de graad van doctor
aan de Technische Universiteit Delft,
op gezag van de Rector Magnificus prof. dr. ir. J.T. Fokkema,
voorzitter van het College voor Promoties,
in het openbaar te verdedigen

op dinsdag 7 januari 2002 om 13.30 uur
door

Renaud Alexandre Martin GUERET,

ingénieur de l'Ecole Supérieure des Ingénieurs de Marseille, France.

geboren te Clermont-Ferrand, Frankrijk.

Dit proefschrift is goedgekeurd door de promotor:

Prof. dr. ir. A.J. Hermans

Samenstelling promotiecommissie:

Rector Magnificus,
Prof. dr. ir. A.J. Hermans,
Prof. dr. B. Molin
Prof. dr. ir. T.J.C. van Terwisga
Prof. dr. ir. A.W. Heemink
Prof. Dr. ir. J.A. Pinkster
Dr. ir. R.H.M. Huijsmans
Dr. S. Malenica

voorzitter
Technische Universiteit Delft, promotor
Ecole Supérieure d'Ingenieurs de Marseille
Technische Universiteit Delft
Technische Universiteit Delft
Technische Universiteit Delft
Marin, Wageningen
Bureau Veritas, Parijs

Published and distributed by: DUP Science

DUP Science is an imprint of
Delft University Press
P.O. Box 98
2600 MG Delft
The Netherlands
Telephone: +31 15 27 85 678
Telefax: + 31 15 27 85 706 E-mail: Info@Library.TUdelft.NL

ISBN 90-407-2357-5

Copyright © 2002 by Renaud Guéret

All rights reserved. No part of the material protected by this copyright may be reproduced or utilized in any form or by any means, electronic or mechanical, including photocopying, recording or by any information storage and retrieval system, without written permission from the publisher: Delft University Press.

Printed in The Netherlands

Contents

List of symbols	v
General introduction	1
1 The behavior of large flexible platforms in waves	7
1.1 Introduction	7
1.2 Mathematical formulation	8
1.2.1 Formulation of integral equation	11
1.2.2 Drift force	13
1.3 One-dimensional platform	14
1.4 Two-dimensional platform	15
1.5 Behavior of a ship with elastic distortions in periodic waves	22
1.5.1 Mathematical model	22
1.5.2 Numerical method	24
1.5.3 Numerical results for a parallelepiped barge	25
2 Moving aircraft on a flexible platform	29
2.1 Introduction	29
2.2 Mathematical model	30
2.2.1 mathematical formulation	31
2.2.2 steady pattern in the moving frame with constant speed	33
2.3 Pattern for an arbitrary path of the source	42
3 Platform with air cushion	47
3.1 Introduction	47
3.2 Physical problem	49
3.3 Mathematical description	50
3.3.1 Boundary conditions	50
3.3.2 Boundary value problem	52
3.4 Wave forces on the body and hydrodynamic coefficients	56
3.4.1 Restoring coefficients	56

3.4.2	Added masses and damping	58
3.4.3	Equations of motion	59
3.5	Two dimensional test problem	61
3.5.1	Present model	61
3.5.2	Newman's acoustic model	64
3.5.3	Numerical results and comparison	67
3.6	Radiation problem for a cylindrical platform	69
3.7	Three-dimensional test problem, results for a barge	75
3.7.1	Numerical aspects	76
3.7.2	Pinkster's model and results	76
3.7.3	Comparison with Pinkster and Newman's results	77
3.7.4	Comparison with Malenica's results	81
4	Deformation of an elastic cylinder in waves	89
4.1	Introduction	89
4.2	Derivation of the main equations	90
4.3	Expansion of the solutions in eigenfunctions	92
4.4	Boundary conditions	94
4.5	Numerical method	94
4.6	Numerical results and test of convergence	95
A	Integral equations	101
A.1	General case for integral equations	101
B	Integral evaluation	103
B.1	Some integral calculus	103
	Conclusions and recommendations	107
	Bibliography	109
	Samenvatting (Summary in Dutch)	113
	Remerciements (In Dutch)	117
	Curriculum vitae (In Dutch)	119

List of symbols

The list of symbols gives an explanation of symbols which are used in different places in this thesis. The list is not exhaustive and we only present the ones occurring the most frequently or which meaning is not evident. Symbols only used once are explained close to the equation where they are used in and all symbols having a different meaning depending on the chapter where they are used in are also included in this list.

chapter 1 & 2

β	angle of incident wave	P	pressure applied on the platform
ϵ	small parameter	D	platform flexural rigidity
η	surface elevation	\mathcal{D}	platform reduced flexural rigidity
\mathcal{P}	platform area	m	platform mass per unit area
\mathcal{F}	free surface surrounding the platform	μ	platform reduced mass per unit area
h	platform's draft	\bar{F}_x	Drift force
\mathcal{D}^-	fluid region beneath the platform	\mathcal{G}	Green's function
\mathcal{D}^+	fluid region towards infinity	L	platform's length
$\partial\mathcal{D}$	interface between \mathcal{D}^- and \mathcal{D}^+	B	platform's width
W	time dependent platform elevation	λ_p	wavelength in the platform
w	complex platform elevation	ν	Poisson's ratio
ρ_s	platform density	H	water depth
ρ	water density	$C(k)$	wave celerity in the platform
		C_{min}	minimum of the wave celerity

C_{plate}	wave celerity for a plate without water	w_0	deflection under the wheel at rest
C_g	water wave celerity in shallow water	$b(x)$	width of the ship at abscissa x
U	plane speed	\mathcal{K}	restoring moment for a ship slice
w_p	deflection under the wheel		

chapter 3

Σ	platform boundary	P_{tam}	atmospheric pressure
Σ_1	wetted part of the platform	v_c	instantaneous volume of the air chamber
Σ_2	air-water interface of the air chamber	P_{cs}	pressure in the air chamber when the platform is at rest
C	platform center of volume	p_c	instantaneous pressure in the air chamber
S	surface area of Σ_2	αS	gas compression ratio
S_h	S_h projection of Σ_2 on the plane $z = 0$	γ	thermodynamic ratio
h_a	distance of Σ_2 from the sea level	ν	incoming wave number
S_p	intersection of the platform with the plane $z = 0$	ϕ^D	diffraction potential
s	surface area of S_p	ϕ_j^R	radiation potential
V_0	water displacement	\mathcal{M}	restoring moment
V_{cs}	volume of the air chamber when the platform is at rest	c	sound celerity
		σ	source strength

chapter 4

u	normal shell deflection
v	tangential shell deflection
w	vertical shell deflection
h	water depth
d	shell thickness

General introduction

This thesis has the peculiarity of presenting not one single main subject but four different studies. This introduction explains what is the aim of such a work and the reasons which motivate it. The four studied subjects are presented as well as the method we chose for their resolution.

Background

Hydrodynamics and the study of water waves propagation are not new subjects. They have furnished, since the nineteenth century, numerous study opportunities to both pure and applied mathematicians. Due to the simplicity of the equations formulations (contrary to electrodynamics, the equations are scalar), the treaties in mathematical physics still constantly refer to hydrodynamic phenomena for the presentation of the boundary value problem theory. In a sense, hydrodynamics is an "old science" and the main governing equations have for a long time been subject to extensive studies and are now well known.

It is the oil-industry which mainly, for it's ocean engineering needs, maintained, and still nowadays maintains, a constant interest in this field. In order to predict the behavior of floating platforms or tankers, for oil exploitation, a large effort has been put by mathematicians and engineers in the derivation of appropriate models. The complexity of the mathematical models followed the need of the description of new phenomena. Taking in account forward speed for the sailing tankers required new additional terms in the free surface equation and the computing of the drift forces led to more accurate free surface condition treatment and the development of the so-called "second order potential".

Up till now, whatever was the subject, efforts of modeling were then mainly focused on the free surface condition treatment. The floating bodies had the common characteristic of being solid and rigid, leading to mathematical sim-

plications for the boundaries equations treatment on their hull.

There is nowadays a growing interest for constructions in off-shore engineering which do not satisfy these last criterion. Either the body can not be considered as rigid, but is flexible -that's the case for floating platforms of very large dimensions and small draft which are candidates for floating airports concepts- or the body can not be considered as whole as solid - that's the case for platforms which possesses an air cushion ensuring their floatability-.

The objective of this thesis is the study of the behavior in waves of four of such constructions.

The first two chapters are devoted to the study of the deflections of a floating flexible platform subject to the forcing of incoming waves or the one of a moving plane on it's surface. The third chapter, is independent of the first two ones and we study the motion of a floating platform with air cushion in waves. The fourth and final chapter is devoted to the study of influence of periodic waves on the deflections of a flexible shell, mounted at the sea bottom.

Mathematically, we make use of the well known linearized potential theory to describe the physical phenomena involved. The originality of these analyzes originates in the new arising types of boundary conditions applied on the hull of the bodies. Indeed, the boundary condition on the flexible platform involves a fourth order partial differential equation for the normal derivative of the potential and the one applied on the water-air cushion interface is described by an integro-differential operator. In the fourth chapter, we derive the hydrodynamic problem for the fluid and the mechanical one for the shell. The kinematic relation between the fluid particle motion on the hull and the shell deflection couples the two problems.

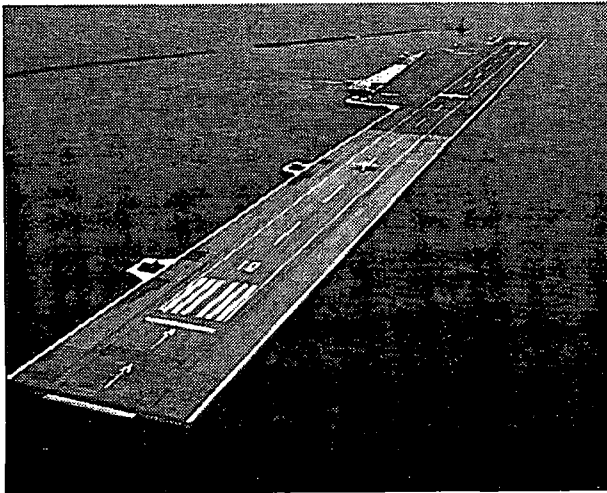


Figure I.1: 1000 m Mega-Float floating airport model in Tokyo

Problems description

Floating flexible platform

There exists today several projects, in the United States (San Diego), and in Japan (Osaka and Tokyo, see figure (1.1) ¹) of floating platform construction for the purpose of airports. Their dimensions are about several kilometers by several hundred meters while their thickness is several meters. These structures have a mat-like dynamic behavior which can be described by a plate equation. Due to their small draft, it is reasonable to model them geometrically as a thin layer of zero thickness laying at $z = 0$. Therefore, it is possible to consider the platform as a free surface, as it is done for water waves equation derivation. The classical Neumann boundary condition is modified in order to take in account the mass per unit area and rigidity of the plate, leading to a fourth order partial differential equation.

The solution for the plate deflection is derived with a Green function method and is found to fulfill an integro-differential equation. Contrary to classical floating bodies with a draft, both influencing and influenced points lay at $z = 0$. A special attention is therefor paid to the establishment of this last equation. The numerical problem is solved via a finite difference scheme in two and three dimensions and numerical results presented. We also show that the drift force, as expected small, can be obtained without difficulty as a simple post-calculus once the deflection is obtained.

In a last section, it is shown how the method used for a mat-like structure can, with small changes, be extended to the deflection determination of a thin and elongated ship, with a three dimensional geometry.

Moving pressure point

Using the same platform model as in the first chapter but considering for simplification the plate infinite, we follow our analyze by computing the deflection caused by a moving plane on the platform in absence of incoming wave. The problem has great resemblance with the one of a moving pressure point translating on an ice sheet and reference is made to the previous works done in this case. Our equation describing the deflection is derived in a slightly different way with the help of Laplace and Fourier transform. In the particular case of a plane moving with constant speed, our solution is drastically simplified and contrary to what has been done up to now, is accurate in the wheel vicinity as well as far away. Existence of critical speeds, earlier mentioned by other authors, is showed and analytic solution presented in some cases. An analogy with the Cherenkov electromagnetic radiation is also presented. The numerical determination of the platform deflection in the case of a plane with a translation motion with time varying speed, written in the form of a double integral,

¹photo found on internet on the site www.srcj.or.jp

in time and in the wave number, presents some difficulties and is time consuming. A contour deformation in the complex plane is used to speed up and make more accurate the involved numerical integration.

Platform with air cushion

In the third chapter, we analyze the behavior of a floating platform with air cushion in waves. A well known mechanical problem met in off-shore engineering is that very large bodies experience large moments and stresses in the structure. An air cushion device can remedy these problems because the pressure of the gas trapped in the chamber is almost uniform in space and tends to average the constraints acting on the hull.

The air chamber behaves like a spring. The incoming waves generate water elevation in the cushion and the gas compression, increasing the pressure, will force the body to move.

We model the gas compression in the air chamber with an adiabatic gas law. The interaction between the water flow and the gas at the interface in the air chamber leads to a new kind of free boundary condition. It is in a sense an extension of the classical Neumann condition on the linearized water free surface at $z = 0$ but is described by an integro-differential equation. Once the boundary equation have been established, as well on the air cushion interface, on the wetted part of the hull and on the ocean surface, we use a Green function method to derive the integral equations of which the potentials of diffraction and radiation are solution. As for classical rigid platforms, added masses and damping coefficients are computed. In order to evaluate the motions experienced by the platform in waves, we compute the restoring forces and moments acting on the body. The air cushion presence change drastically the restoring coefficients and special attention is paid to the derivation of these expressions. The air cushion is shown to confer a particularly bad stability to the platform. Analytical results are derived for bodies with very simple geometries in order to understand the underlying phenomena involved. Comparison is also carried out with acoustic models derived by other authors.

Finally, we test our numerical model on a real barge tested in model test basin by *Pinkster*. Our computed results agree well for the experiments.

Deformation of an elastic cylinder in waves

In the fourth and last chapter, we investigate the deflection of a thin shell cylinder, mounted at the sea bottom, by periodic waves. Contrary to the first three chapters, it will not be possible to establish an unique boundary equation on the hull. The mechanical shell equation and the hydrodynamic equations are given and the kinematic relation on the shell hull couples them. The harmonic water waves diffracted by the cylinder are described by means of the eigenmode expansion. Although these functions are not eigenfunctions for the

mechanical shell equation, we expand the highest derivatives involved in mechanical equations using the same set of orthogonal functions. Once we have shown with a simple example that our method converges when we increase the number of modes, we apply it for a real shell and present numerical results.

The behavior of large flexible platforms in waves

In this chapter, we present a method to study the behavior of large floating flexible bodies excited by waves. Our analysis is restricted to structures which dynamic behavior can be described by a rod (or a beam in 3D) model. We are mainly interested in the applications for large flexible artificial islands for the purpose of floating airports and ships of large dimensions.

1.1 Introduction

Very large floating structures (VLFS) are being considered as an airport in many projects around the world. These platforms are several kilometers long and a couple of hundreds meters large. In comparison their thickness, usually less than 10 m, is negligible.

Due to their important sizes, the structures, subjected to an external load, wave forcing or the load exerted by the plane, can no longer be considered as rigid. The goal of this study is then to determine the deflections of the platform and their associated stresses in the structure. Usually, structural and hydrodynamic analyzes are performed separately. The load is evaluated in a first stage, assuming that the body is rigid and the deflection is then computed. For those very long and thin structures, where the platform and fluid interact on each other, the elevation is mainly due to the elastic deformation and can be of large importance. It is expected to be much higher than the one that would be generated on a similar rigid body.

In this study, we do not consider the fluid elevation under the platform and the elastic deflection separately and their coupling gives rise to a new boundary condition at the plate-water interface.

We model the platform dynamically as a two-dimensional thin plate governed by the Euler beam theory. The free edge boundary condition will furnish the boundary equation for the plate. The choice of those boundary conditions has as consequence that continuity of the elevation between the plate and the water is not assured. The liquid is assumed ideal, incompressible, its motion is irrotational and we will make use of the classical linearized potential theory for the description of the fluid motion.

In the first section, we present an approach to describe the behavior of a platform of general shape influenced by long crested harmonic waves. Many authors presented some methods of resolution. Originally, *Stoker* [28] solved the two-dimensional problem (for a one-dimensional platform) using linear shallow water theory and obtained closed forms solutions for the beam elevation and stresses. Recently, other authors provided solutions for two-dimensional platforms. Some of them are based on the "generalized mode" decomposition where the motion of the structure is described in rigid and flexible modes, with associated potentials (*Lee and Newman*) [11]. Others use for the velocity-potential, an eigenfunction-expansion in vertical modes which satisfy the governing Laplace equation and the free surface condition (*Kim and Cengiz Ertekin*) [29].

Our method is based on a boundary element method. We use a free surface Green function and develop a integro-differential equation for the determination of the deflection. A detailed treatment of the resolution in the case of a two-dimensional platform and a rectangular three-dimensional platform is given and numerical results presented.

In the second part, we show how the integro-differential equation developed for a platform analysis, can be easily modified in order to study hydroelastic behavior of a ship in waves. The problem of deformations of a ship in calm water is, for a long time, a well known problem for ship builders. *Bishop and Price* [16] initiated, in the last seventies, the study of flexible ships submitted to waves. They use, nevertheless, simplified hydrodynamic models for this purpose. Our model presents the advantage of a full coupling between the waves forcing and the elastic distortion. Numerical results are given for the idealized case of a parallelepiped barge in waves.

1.2 Mathematical formulation

In this section we give the mathematical equations which describe the physical problem. We consider a platform of general shape, in open sea, submitted to regular incoming waves. The draft h is small compared to the horizontal dimensions so that we can consider it as a thin layer laying at $z = 0$, where z is assumed to point vertically upward.

The area occupied by the platform (at $z=0$) is denoted \mathcal{P} and the free surface surrounding the platform \mathcal{F} . The fluid domain is split up in two regions. The

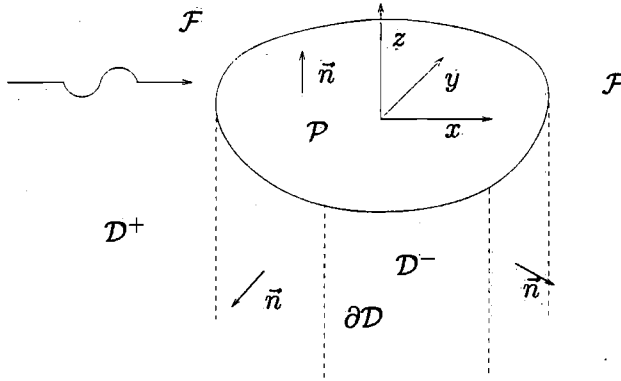


Figure 1.1: platform geometry

region underneath the platform is defined as \mathcal{D}^- and the region towards infinity \mathcal{D}^+ while the interface is denoted as $\partial\mathcal{D}$.

The fluid is assumed incompressible and inviscid. We introduce the velocity potential so that $\mathbf{V} = \nabla\Phi(\mathbf{x}, t)$. Under those assumptions we have the following equations for the potential

$$\nabla^2\Phi = 0 \quad \text{for } z < 0 \quad (1.1)$$

$$\frac{\partial\Phi}{\partial z} = 0 \quad \text{for } z = -\infty \quad (1.2)$$

$$-\rho gW - \rho \frac{\partial\Phi}{\partial t} = \begin{cases} P & \text{for } z = 0, (x, y) \in \mathcal{P} \\ 0 & \text{for } z = 0, (x, y) \in \mathcal{F} \end{cases} \quad (1.3)$$

where W is the free surface elevation, P the pressure applying on the plate and ρ the water density.

The displacement of the free surface is related to the velocity potential by the kinematic condition

$$\Phi_z = \frac{\partial W}{\partial t} \quad (1.4)$$

In addition, suitable radiation condition must hold at infinity.

The platform is assumed to be an elastic plate of thickness h where bending moments and transverse shears are active. We invoke the basic hypothesis of the Bernoulli-Euler theory to describe its dynamic behavior. This carries the assumptions that slopes and transverse deflections W are small and that the rotatory-inertia effects are neglected. Complete requirements for this theory can be found in Graff [19].

The dynamic equation for the plate reads then

$$D \nabla^4 \bar{W} + \rho_s h \frac{\partial^2 \bar{W}}{\partial t^2} = P \quad (1.5)$$

where $D = EI/(1 - \nu^2)$ is the flexural rigidity (E is the Young's modulus, I the moment of inertia of the plate). The Laplacian of the Laplacian is designated as the biharmonic operator ∇^4 and ρ_s is the mass density per unit area.

We assume that the plate is a thin layer at the free surface $z = 0$ and we denote $m = \rho_s h$ its mass per unit area of the plate.

The free edge boundary conditions can be found to be

$$\frac{\partial^2 \bar{W}}{\partial n^2} + \nu \frac{\partial^2 \bar{W}}{\partial s^2} = 0 \quad \text{and} \quad \frac{\partial^3 \bar{W}}{\partial n^3} + (2 - \nu) \frac{\partial^3 \bar{W}}{\partial n \partial s^2} = 0 \quad \text{on } \partial \mathcal{P} \quad (1.6)$$

where $\partial \mathcal{P}$ is the platform boundary, ν the Poisson's ratio, n is in the normal direction, in the horizontal plane, and s denotes the arc of length along the edge.

Combining (1.3) and (1.5) we obtain

$$\left\{ \frac{D}{\rho g} \left(\frac{\partial^2}{\partial x^2} + \frac{\partial^2}{\partial y^2} \right)^2 + \frac{m}{\rho g} \frac{\partial^2}{\partial t^2} + 1 \right\} \frac{\partial \Phi}{\partial z} + \frac{1}{g} \frac{\partial^2 \Phi}{\partial t^2} = 0 \quad \text{on } \mathcal{P} \quad (1.7)$$

The waves are monochromatic with frequency ω and wave number $k_0 = \omega^2/g$. The pressure P , the potential Φ and the vertical elevation W have an harmonic time dependence and we write $W(x, y, t) = \Re(w(x, y) e^{-i\omega t})$, $\Phi(x, y, z, t) = \Re(\phi(x, y, z) e^{-i\omega t})$ and $P(x, y, t) = \Re(p(x, y) e^{-i\omega t})$

The undisturb incident potential equals

$$\phi^{inc}(\underline{x}) = \frac{g\zeta_0}{\omega} \exp\{ik_0(x \cos \beta + y \sin \beta) + k_0 z\}$$

The potential function in \mathcal{D}^+ is written as a superposition of the incident wave potential and a diffracted potential, as follows

$$\phi(\underline{x}) = \phi^{inc}(\underline{x}) + \phi^+(\underline{x}) \quad (1.9)$$

while the total potential is denoted as ϕ^- in \mathcal{D}^- .

ϕ^+ must satisfy the Sommerfeld radiation condition as $r \rightarrow \infty$, given by

$$\lim_{r \rightarrow \infty} \sqrt{r} \left(\frac{\partial \phi^+}{\partial r} - ik \phi^+ \right) = 0 \quad (1.10)$$

We introduce the Green's function $\mathcal{G}(\underline{x}, \underline{\xi})$, (where \underline{x} is the source point and $\underline{\xi}$ the field point) that fulfills $\Delta\mathcal{G} = 4\pi\delta(\underline{x} - \underline{\xi})$, the free surface condition and the radiation condition. Its expression can be found in *Wehausen and Laitone* [24].

$$\mathcal{G}(\underline{x}, \underline{\zeta}) = -\frac{1}{r} + \frac{1}{r_1} + \int_{\mathcal{L}} \frac{k}{k - k_0} e^{k(z+\zeta)} J_0(kR) dk \quad (1.11)$$

where the contour \mathcal{L} is in the complex k -plane from $k = 0$ to $k = \infty$ that passes, due to the radiation condition, the pole of the integrand $k = k_0$ underneath (fig:1.2), $R^2 = (x - \xi)^2 + (y - \eta)^2$, $r^2 = R^2 + (z - \xi)^2$ and $r_1^2 = R^2 + (z + \xi)^2$.

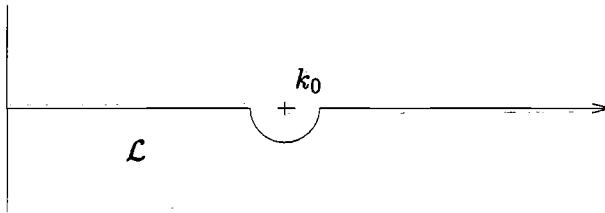


Figure 1.2: Contour of integration

Doing some contour of integration, it is possible to derive the asymptotic form for \mathcal{G} when $R \rightarrow \infty$

$$\mathcal{G} \sim i\pi k_0 e^{k_0(z+\zeta)} H_0^{(1)}(k_0 R) \quad (1.12)$$

1.2.1 Formulation of integral equation

Using Green's theorem for ϕ^- and ϕ^+ , for $\underline{x} \in \mathcal{D}^-$ we have

$$0 = - \iint_{\partial\mathcal{D} \cup \mathcal{F}} \left(\phi^+ \frac{\partial \mathcal{G}}{\partial n} - \mathcal{G} \frac{\partial \phi^+}{\partial n} \right) dS \quad 4\pi\phi^- = \iint_{\partial\mathcal{D} \cup \mathcal{P}} \left(\phi^- \frac{\partial \mathcal{G}}{\partial n} - \mathcal{G} \frac{\partial \phi^-}{\partial n} \right) dS \quad (1.13)$$

and for $\underline{x} \in \mathcal{D}^+$

$$4\pi\phi^+ = - \iint_{\partial\mathcal{D} \cup \mathcal{F}} \left(\phi^+ \frac{\partial \mathcal{G}}{\partial n} - \mathcal{G} \frac{\partial \phi^+}{\partial n} \right) dS \quad 0 = \iint_{\partial\mathcal{D} \cup \mathcal{P}} \left(\phi^- \frac{\partial \mathcal{G}}{\partial n} - \mathcal{G} \frac{\partial \phi^-}{\partial n} \right) dS \quad (1.14)$$

Due to the free surface condition for \mathcal{G} and ϕ^+ , the integral over \mathcal{F} vanishes and adding up the two expressions in (1.13) leads to

$$4\pi\phi^- = \iint_{\partial\mathcal{D}} \left([\phi] \frac{\partial\mathcal{G}}{\partial n} - \mathcal{G} \left[\frac{\partial\phi}{\partial n} \right] \right) dS + \iint_{\mathcal{P}} \left(\frac{\omega^2}{g} \phi^- - \phi_\zeta^- \right) \mathcal{G} dS \quad (1.15)$$

where the notation [...] has been used for the jump of the function concerned. At the dividing surface $\partial\mathcal{D}$ we require continuity of the total potential and its derivative and we have $[\phi] = \phi^- - \phi^+ = \phi^{inc}$. Injecting (1.7) in (1.15) leads for $\underline{x} \in \mathcal{D}^-$, $z < 0$ to

$$4\pi\phi^- = \iint_{\partial\mathcal{D}} \left(\phi^{inc} \frac{\partial\mathcal{G}}{\partial n} - \mathcal{G} \frac{\partial\phi^{inc}}{\partial n} \right) dS - \iint_{\mathcal{P}} \left(\frac{m\omega^2}{\rho g} \phi_\zeta^- - \frac{D}{\rho g} \left(\frac{\partial^2}{\partial\xi^2} + \frac{\partial^2}{\partial\eta^2} \right)^2 \phi_\zeta^- \right) \mathcal{G} dS \quad (1.16)$$

\mathcal{G} has a weak singularity so that we may take the limit when $z \rightarrow 0$ in the integral over \mathcal{P} . for $z < 0$, we write

$$\iint_{\partial\mathcal{D}} \left(\phi^{inc} \frac{\partial\mathcal{G}}{\partial n} - \mathcal{G} \frac{\partial\phi^{inc}}{\partial n} \right) dS + \iint_{\mathcal{P}} \left(\phi^{inc} \frac{\partial\mathcal{G}}{\partial n} - \mathcal{G} \frac{\partial\phi^{inc}}{\partial n} \right) dS = 4\pi\phi^{inc} \quad (1.17)$$

The integral over \mathcal{P} , where $\zeta = 0$, equals 0 for $z < 0$. We have to show that this still holds for $z = 0$.

Following Noblesse, we can write for $z < 0$

$$\frac{\partial\mathcal{G}}{\partial n} = \nu\mathcal{G} - \left(\frac{1}{r} + \frac{1}{r_1} \right)_\zeta + \nu \left(\frac{1}{r} - \frac{1}{r_1} \right) \quad (1.18)$$

Injecting this relation and equation (1.7) in (1.17) and taking the limit for $z \rightarrow 0$, the first integral over $\partial\mathcal{D}$ in (1.16) is found to be $4\pi\phi^{inc}$. We also notice that the integral over $\partial\mathcal{D}$ in (1.16) is independent of the parameters of the platform. If no platform is present m and D are set to zero and hence the integral equals $4\pi\phi^{inc}$.

We end up with an integral equation valid for $z = 0$ and unknown value ϕ_z^- .

$$4\pi \left(\mathcal{D} \left(\frac{\partial^2}{\partial x^2} + \frac{\partial^2}{\partial y^2} \right)^2 - (\mu - 1) \right) \phi_z^- =$$

$$k_0 \iint_{\mathcal{P}} \left(\mathcal{D} \left(\frac{\partial^2}{\partial \xi^2} + \frac{\partial^2}{\partial \eta^2} \right)^2 \phi_\zeta^- - \mu \phi_\zeta^- \right) \mathcal{G} dS + 4\pi \phi_z^{inc} \quad (1.19)$$

with parameters $\mathcal{D} \equiv \frac{D}{\rho g}$, $\mu \equiv \frac{m\omega^2}{\rho g}$

Once the integral equation is solved, adding the two expressions in (1.14) and following the same analysis as for ϕ_z^- , we can express ϕ^+ as follow

$$4\pi \phi^+ = \iint_{\mathcal{P}} \left(\mathcal{D} \left(\frac{\partial^2}{\partial \xi^2} + \frac{\partial^2}{\partial \eta^2} \right)^2 \phi_\zeta^- - \mu \phi_\zeta^- \right) \mathcal{G} dS \quad (1.20)$$

We notice that the equations do not provide an equality between the platform deflection and the water wave height at the edges. Using (1.20) and (1.19), it is possible to show that at the edge, the difference between the platform elevation w^- and the water wave elevation w^+ read

$$w^+ - w^- = -(\mathcal{D}\nabla^4 - \mu)w^- \quad (1.21)$$

We can compute the asymptotic field for ϕ^+ at infinity.

$$4\pi \phi^+ = \frac{F(\theta)}{\sqrt{r}} \quad F(\theta) = i\sqrt{k_0} \iint_{\mathcal{P}} \left(\mathcal{D}\nabla^4 \phi_\zeta^- - \mu \phi_\zeta^- \right) e^{-ik_0\rho \cos(\psi-\theta)} dS \quad (1.22)$$

In the following, we denote for simplicity ϕ^-, ϕ .

1.2.2 Drift force

The drift force \bar{F}_x is obtained by integrating the the dynamic pressure P over the platform hull and averaging it in time. This force can be split in two components. The first one is due to the pressure acting on the platform with slope $\bar{n} \cdot \bar{e}_x = \frac{\partial W}{\partial x}$. The second one originates in the difference between the platform elevation and the wave height at the edges of the structure (although the platform has no draft, it is supposed to have vertical walls at it's edges).

$$\bar{F}_x = \left\langle - \iint_{\mathcal{P}} P(t) \frac{\partial W(t)}{\partial x} dS + \int_{\partial\mathcal{P}} \frac{\rho g}{2} \overline{(W^+ - W^-)^2} dl \times n_x \right\rangle \quad (1.23)$$

where W^+ and W^- are the real wave elevation and the platform elevation on the platform edge ∂P and n_x the component of the normal vector in the x direction, (see Pinkster [5] for the derivation of the second integral in equation (1.23)).

The unsteady potential can be decomposed into a first- and second-order part as $\phi = \epsilon\phi^{(1)} + \epsilon^2\phi^{(2)} + \mathcal{O}(\epsilon^3)$. From Bernoulli's equation, we get for the pressure $P = -\epsilon\rho\phi_t^{(1)} + \frac{1}{2}\epsilon^2\nabla\phi^{(1)}\cdot\nabla\phi^{(1)} + \epsilon^2\phi_t^{(2)} + \mathcal{O}(\epsilon^3)$. Usually, the drift force calculus involves the computing of the second order potential $\phi^{(2)}$. But in the special case of an island with zero draft, only the first order terms in ϵ , involved in ϕ and P , influence the result.

Using the expression for the pressure given in equation (1.5) and after averaging in time, one can obtain for the expression of the drift force

$$\begin{aligned} \bar{F}_x = & -\frac{1}{2} \iint_P \left\{ \frac{\partial \Re(w)}{\partial x} (D\nabla^4 \Re(w) - m\omega^2 \Re(w)) - \right. \\ & \left. - \frac{\partial \Im(w)}{\partial x} (D\nabla^4 \Im(w) - m\omega^2 \Im(w)) \right\} dS + \frac{1}{4} \rho g \int_{\partial P} |D\nabla^4 w - \mu w|^2 dl e_x \end{aligned} \quad (1.24)$$

1.3 One-dimensional platform

One-dimensional model will be useful for the understanding of the difficulties which can arise in solving such a integro-differential equation and for providing computational validations involved for two-dimensional platforms. We consider a thin elastic beam of infinite extend in the y direction and width L . With a similar analysis in 1D, equations (1.19) and (1.6) transform into

$$2\pi \left(\mathcal{D} \frac{d^4 \phi_z}{dx^4}(x) - (\mu - 1) \phi_z(x) \right) = k_0 \int_0^L \left(\mathcal{D} \frac{d^4 \phi_\zeta}{d\xi^4}(\xi) - \mu \phi_\zeta(\xi) \right) \mathcal{G}(x, \xi) d\xi + 2\pi \phi_z^{inc} \quad \text{for } 0 \leq x \leq L \quad (1.25)$$

$$\frac{d^2 \phi_z}{dx^2} = \frac{d^3 \phi_z}{dx^3} = 0 \quad \text{for } x = 0 \quad \text{and} \quad x = L \quad (1.26)$$

The one-dimensional Green's function, at $z = 0$, $\zeta = 0$ reads

$$\mathcal{G}(x, \xi) = -2 \int_L \frac{1}{k - k_0} \cos k(x - \xi) dk$$

Using contour deformation, the Green's function is split in residue issue from the pole and an integration along the imaginary axis.

$$\mathcal{G}(x, \xi) = 2 \int_0^{+\infty} \frac{k}{k^2 + k_0^2} e^{-k|x-\xi|} dk - 2i\pi \exp ik_0|x - \xi|$$

To solve numerically equation (1.25), we use a finite difference method. The unknown value ϕ_z is assumed to be constant on each equidistant panel. The integration of the Green's function \mathcal{G} is first carried out analytically with respect to ξ and then numerically with respect to k . The fourth derivative is written as a five points central difference scheme and we introduce two extra grid points outside the platform. The two boundary equations (1.26) furnish the four missing extra equations.

In figure (1.3) we plot the deflection w , function of the platform abscissa x , for a wavelength of 150m. The parameters chosen are: $D = 10^{11} Nm^2$, $m = 250 Kg/m$, $L = 300m$. In figure (1.4), the rigidity and mass per unit area are unchanged but the platform is now 1500m long with an incoming wave with wavelength $\lambda = 100m$. The wavelength of the platform deflection, λ_p , is approximately 300m. It is given by the dispersion equation

$$(Dk^4 - \mu + 1)k - k_0 = 0 \quad (1.27)$$

In all cases, the displacement of the platform is found to be larger at the edges. In figure (1.6) we plot the reflection (R) and transmission (T) coefficients against the ratio λ/L (wavelength/platform length). The energy conservation relation is found to be fulfilled for all values of λ .

In figure (1.5) we plot the drift force \overline{F}_x for a 200m long platform, with rigidity $D = 2 \cdot 10^8 Nm^2$ and mass per unit length $m = 250 Kg/m$. Due to the small slope of the platform (the slope behaves like $1/\lambda_p^4$ when $L \gg \lambda_p$, \overline{F}_x is mainly due to the pressure integration on the vertical end walls of the platform. The force due to pressure acting on the platform slope is found to be very small, less than 70 N in the present computed case. We compare our result with *Maruo's* formula [8]: $\overline{F}_x = \frac{1}{2} \rho g R^2$. For very short wavelengths, our results differ. This is due to the fact that the computed elevation difference, involving a fourth order derivative at the edges of the platform, equation (1.21), is difficult to handle numerically.

1.4 Two-dimensional platform

This section presents the results obtained from computations for a two-dimensional rectangular barge.

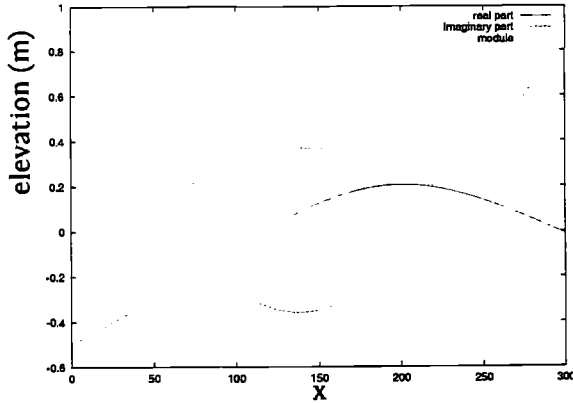


Figure 1.3: platform elevation, $L=300\text{m}$, $\lambda=150\text{m}$, $D = 10^{11}\text{Nm}^2$, $m = 250\text{Kg/m}$

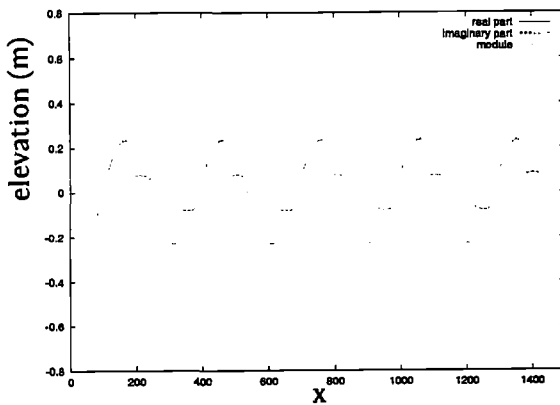


Figure 1.4: platform elevation, $L=1500\text{m}$, $\lambda=100\text{m}$, $D = 10^{11}\text{Nm}^2$, $m = 250\text{Kg/m}$

We employ as in the one-dimensional case a finite difference approach. In order to write the biharmonic operator and the boundary conditions, we introduce extra fictive points outside the platform, see figure (1.7). This leads to $n_x \times n_y$ collocation points inside the platform and $4(n_x + n_y) + 12$ fictive points outside the physical plane.

The integral equation and the boundary equations give $n_x \times n_y + 4(n_x + n_y)$ equations. We add 3 equations for the fictive points $\phi_z^{(2)}$ placed on each corner

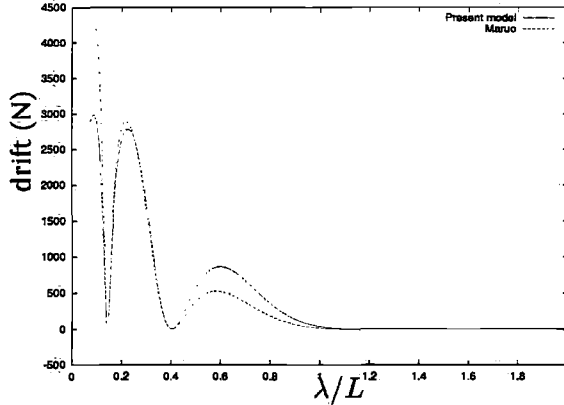


Figure 1.5: Drift force per unit width, $L=200\text{m}$, $D = 2 \cdot 10^8 \text{Nm}^2$, $m = 250 \text{Kg/m}$. Comparison between the present model and Maruo's formula

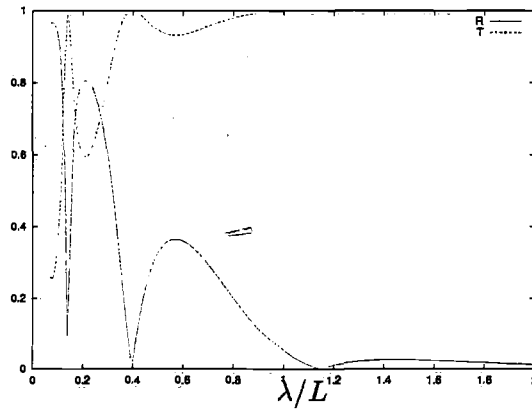


Figure 1.6: Reflection and transmission coefficients against λ/L , $L=300\text{m}$, $D = 10^{10} \text{Nm}^2$, $m = 250 \text{Kg/m}$

of the platform , see figure (1.7)

$$\frac{\partial \phi_z^{(2)}}{\partial x} = 0 \quad \frac{\partial \phi_z^{(2)}}{\partial y} = 0$$

$$\text{and } \phi_z^{(2)} = \frac{1}{2}(\phi_z^{(1)} + \phi_z^{(3)}) \tag{1.28}$$

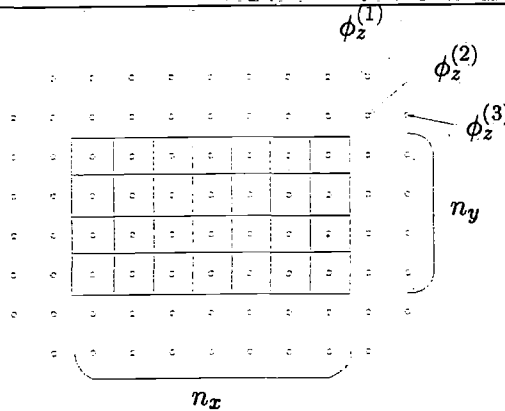


Figure 1.7: mesh of the plate

These arbitrary supplementary equations only influence the solution locally and their influence tends to zero when n_x and n_y are big enough.

Our numerical method presents some limitations when the parameter \mathcal{D} is very large, so that the platform is very stiff, almost rigid. A very small error in the numerical evaluation of $\iint_{P_i} \mathcal{G} dS$ on a panel will be strongly amplified by the

factor \mathcal{D} and produces erroneous results. In every practical cases of platforms we encounter, the rigidity stayed in the range of validity of our model. In the one-dimensional case, the integration in ξ is carried out analytically and the only error, due to the numerical integration in k is much smaller. Those limitations then never occur.

We present here some numerical results. In figures (1.8), (1.9) and (1.10) we plot the real part, imaginary part and module of the platform deflection with main dimensions and material property are given as $L = 800m$, $B = 300m$, $D = 10^{11} N.m^2$, $m = 1000 Kg/m^2$, $\nu = 0.3$. The incoming wavelength equals $200m$ and the incident angle $\beta = 0$. In figures (1.11), (1.12) and (1.13) we consider the deflection for the same platform with a plane wave incident under an angle $\beta = \pi/4$ with respect to the x -axis.

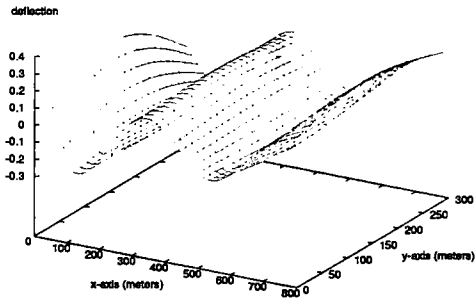


Figure 1.8: platform elevation, real part
 $L = 800m$ $B = 300m$ $D = 10^{11}N.m^2$,
 $\beta = 0$

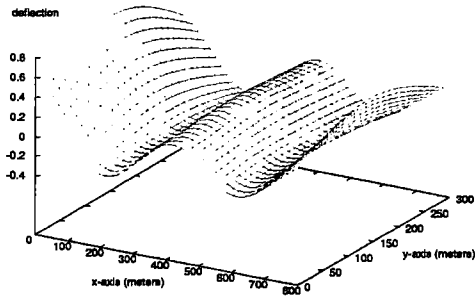


Figure 1.9: platform elevation, imaginary part
 $L = 800m$ $B = 300m$ $D = 10^{11}N.m^2$,
 $\beta = 0$

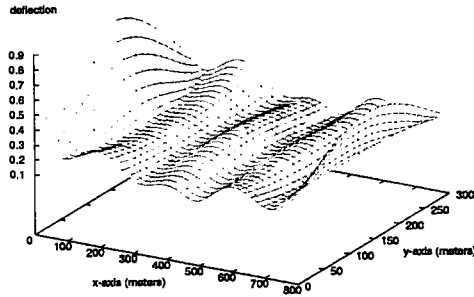


Figure 1.10: platform elevation, module
 $L = 800m$ $B = 300m$ $D = 10^{11}N.m^2$,
 $\beta = 0$

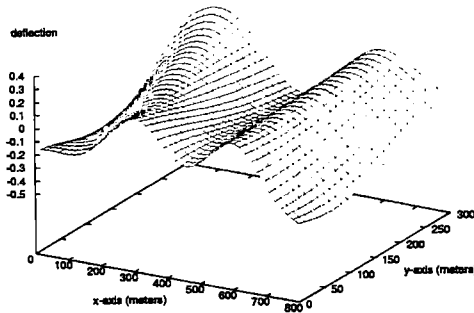


Figure 1.11: platform elevation, real part
 $L = 800m$ $B = 300m$ $D = 10^{11}N.m^2$, $\beta = \pi/4$

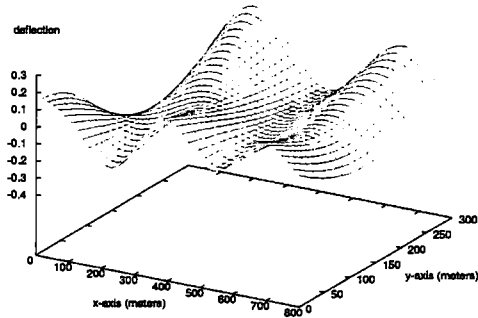


Figure 1.12: platform elevation, imaginary part $L = 800m$ $B = 300m$ $D = 10^{11}N.m^2$, $\beta = \pi/4$

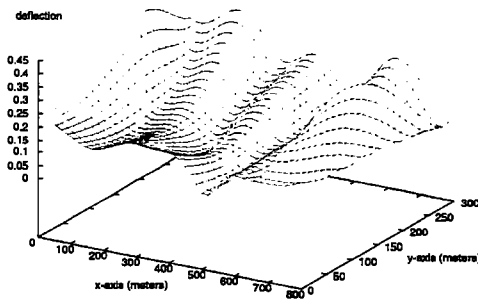


Figure 1.13: platform elevation, module $L = 800m$ $B = 300m$ $D = 10^{11}N.m^2$, $\beta = \pi/4$

1.5 Behavior of a ship with elastic distortions in periodic waves

It has been shown that it is possible to derive a formulation to describe the rigid body motion and the elastic behavior of a flexible platform by means of one differential-integral equation. This equation for the elevation can be solved numerically, without splitting the problem in the various rigid motion and eigenmode components, as is standard in the field of linear ship motions. In this section, we show that is easy to apply similar ideas to an elastic ship. For simplicity, we consider that the ship is mooring and then has no forward speed. The ship is not anymore considered as a rigid structure and we focus on the shears, bending moments and distortions due to the waves excitation. It is usually custom to distinguish between the motion responses and the distortion of a ship. Motion responses are obtained via the theory of sea-keeping that would be set for a rigid body, providing the pressure distribution on the hull. Stressing is then computed as a post calculus. But for very long and slender ship in severe sea conditions, deflection can be quite important and it is not possible to decouple the two phenomena.

Practical methods of estimating hydrodynamic actions on a hull depend on the assumption that the mechanical behavior of the hull is 'beamlike'. Strange as it may seem, large tankers are very well represented for the purpose of dynamic analysis as a *thin* beam (see *Bishop and Price* [16]). But for the hydrodynamic point of view, the ship is considered as a three dimensional body. We apply the boundary conditions for the velocity potential on the real hull and the summation of the pressure over the hull at a given abscissa is used for the one dimensional dynamic beam model.

We introduce some restrictions to our analyze. We only consider the time dependent distortions in the hull. It means that we don't take in account the strains due to gravity and buoyancy forces in still water. In this presentation we finally limit ourselves to the influence of head-seas on the heaving and pitching rigid-body motions. We also leave aside the slamming and restrict our analyze to harmonic waves.

We first derive a general formulation for a three dimensional ship, and then give some results for a ship in head waves for heave and pitch motion, and associated elastic distortion of the hull. In principle we can extend the formulation for the effect of waves on a ship traveling with steady forward speed.

1.5.1 Mathematical model

We derive a formulation for a ship without forward speed. We denote Ω the water region and $\partial\Omega$ the ship wetted hull. We have at the linearized free surface $z = 0$, the linearized kinematic condition $\Phi_z = \eta_t$, and the dynamic condition $\Phi_t = -g\eta$ where $\eta(x, t)$ denotes the wave elevation. On the hull, we have the following kinematic and dynamic conditions:

$$\frac{\partial \Phi}{\partial n} = v_n = \tilde{w}_t(x, t) \vec{e}_z \cdot \vec{n} + \tilde{\theta}_t(x, t) y \vec{e}_z \cdot \vec{n} - \tilde{\theta}_t(x, t) z \vec{e}_y \cdot \vec{n} \quad (1.29)$$

$$\frac{p}{\rho} = -\Phi_t - g \left(\tilde{w}(x, t) + \tilde{\theta}(x, t) y \right) \quad (1.30)$$

where v_n is the normal velocity of a point at the hull of the ship, $\tilde{w}(x, t)$ the deflection and $\tilde{\theta}(x, t)$ the angular rotation due to torsion respectively.

The ship is assumed to behave like a beam with no thickness. We use the linear beam theory to describe its deflection $\tilde{w}(x, t)$ and its angular rotation $\tilde{\theta}(x, t)$. The dynamic equations for the vertical force and moment read

$$\mu(x) \frac{\partial^2 \tilde{w}(x, t)}{\partial t^2} + \frac{\partial^2}{\partial x^2} \left(D(x) \frac{\partial^2 \tilde{w}(x, t)}{\partial x^2} \right) = \bar{Z}(x, t) \quad (1.31)$$

$$I_s \frac{\partial^2 \tilde{\theta}(x, t)}{\partial t^2} - \frac{\partial}{\partial x} \left(c \frac{\partial \tilde{\theta}(x, t)}{\partial x} \right) = \Gamma(x, t) \quad (1.32)$$

where D is the flexural rigidity, μ the mass per length, I_s the rotational inertia, Z and Γ the vertical force and the moment per length acting on the ship. The shear and bending moment vanish at the ends of the beam. Thus, it follows that the boundary conditions at the beam ends read

$$D \frac{\partial^2 \tilde{w}}{\partial x^2} = 0 \quad \frac{\partial}{\partial x} \left(D \frac{\partial^2 \tilde{w}}{\partial x^2} \right) = 0 \quad (1.33)$$

$$\frac{\partial \tilde{\theta}}{\partial x} = 0 \quad (1.34)$$

We consider a harmonic wave propagating in the direction β with respect with the main axis of the ship. The harmonic wave potential, deflection and angular rotation can be written as

$\Phi(\mathbf{x}, t) = \phi(\mathbf{x}) e^{-i\omega t}$ $\tilde{w}(x, t) = w(x) e^{-i\omega t}$ and $\tilde{\theta}(x, t) = \theta(x) e^{-i\omega t}$. The incident plane wave potential equals:

$$\phi^{inc} = \frac{g\zeta_0}{\omega_0} \exp\{ik_0(x \cos \beta + y \sin \beta) + k_0 z\} \quad (1.35)$$

The potential function is split in a incident wave potential and a diffracted wave potential.

$$\phi(\mathbf{x}) = \phi^{inc}(\mathbf{x}) + \phi^D(\mathbf{x}) \quad (1.36)$$

We notice that in most theories the diffracted potential is defined for the fixed ship, while here it also contains the effect of the rigid- and elastic-body motions.

We will make use of the Green's function \mathcal{G} , introduced in the previous chapters, that fulfills $\Delta \mathcal{G}(\mathbf{x}, \xi) = 4\pi\delta(\mathbf{x} - \xi)$, the free surface condition and the radiation condition.

For $\mathbf{x} \in \partial\Omega$

$$2\pi\phi^D = \int_{\partial\Omega} \left(\phi^D \frac{\partial \mathcal{G}}{\partial n} - \mathcal{G} \frac{\partial \phi^D}{\partial n} \right) dS \quad (1.37)$$

Equations (1.29), (1.30), (1.31), (1.32) and the general integral equation (1.37) lead to a system of the three integral equations

$$\begin{aligned} &= \mu\omega^2 w + \frac{\partial^2}{\partial x^2} \left(D \frac{\partial^2 w}{\partial x^2} \right) - i\rho\omega \left\{ \int_{\mathcal{C}(x)} \phi^D \vec{n} dl \right\} \cdot \vec{e}_z + \rho g b(x) w = \\ &i\rho\omega \left\{ \int_{\mathcal{C}(x)} \phi^{inc} \vec{n} dl \right\} \cdot \vec{e}_z \end{aligned} \quad (1.38)$$

$$\begin{aligned} &-I_s \omega^2 \theta - \frac{\partial}{\partial x} \left(c \frac{\partial \theta}{\partial x} \right) - i\rho\omega \left\{ \int_{\mathcal{C}(x)} \vec{OM} \wedge \phi^D \vec{n} dl \right\} \cdot \vec{e}_x + \mathcal{K}(x) \theta = \\ &i\rho\omega \left\{ \int_{\mathcal{C}(x)} \vec{OM} \wedge \phi^{inc} \vec{n} dl \right\} \cdot \vec{e}_x \end{aligned} \quad (1.39)$$

$$\begin{aligned} 2\pi\phi^D - \int_{\partial\Omega} \left\{ \phi^D \frac{\partial \mathcal{G}}{\partial n} + i\omega \mathcal{G} (w \vec{e}_z \cdot \vec{n} + \theta y \vec{e}_z \cdot \vec{n} - \theta z \vec{e}_y \cdot \vec{n}) \right\} dS = \\ \int_{\partial\Omega} \mathcal{G} \frac{\partial \phi^{inc}}{\partial n} dS \end{aligned} \quad (1.40)$$

where $b(x)$ is the width of the ship at abscissa x , $\mathcal{K}(x)$ the restoring moment for a slice at abscissa x and \mathcal{C} the line integral over the wetted hull at abscissa x .

1.5.2 Numerical method

The dynamic differential equations are discretized by means of a difference scheme, while the integral equation (1.5.1) is discretized by means of a piecewise constant panel distribution. The final set of equations is a matrix equation

for the coupled unknowns. For the purpose of calculation, the hull is divided into N slices. Each slice is supposed to have a constant displacement (w_i, θ_i) . The slices are denoted by $i = 1, 2, \dots, N$ starting from the bow.

As we are using a finite difference approach to solve the dynamic equations for the beam, we introduce 4 supplementary points for the mesh describing the beam in order to represent the fourth order derivative for the beam equation. We denote the diffracted potential on each of the M panels of the mesh describing the ship's hull by ϕ_i^D .

Equations (1.5.1), (1.5.1), (1.33), (1.34) and (1.40), lead to a linear system for the discretized problem. The solution vector is written in the form

$$\vec{X} = \{\phi_1^D, \phi_2^D, \dots, \phi_M^D, w_{-1}, w_0, w_1, w_2, \dots, w_N, w_{N+1}, w_{N+2}, \theta_0, \theta_1, \theta_2, \dots, \theta_N, \theta_{N+1}\} \quad (1.41)$$

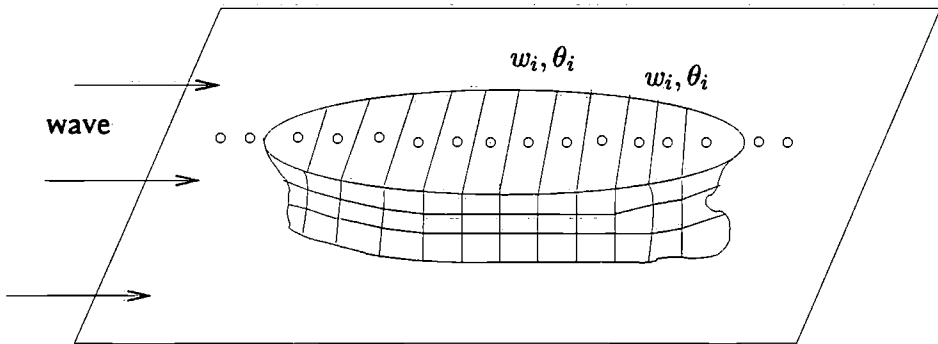


Figure 1.14: ship geometry and discretization

1.5.3 Numerical results for a parallelepiped barge

We present some numerical results for a thin barge of dimensions $l_x = 200m$, $l_y = 5m$, $l_z = 4m$. The ship is cut in 40 slices and has a constant flexural rigidity of $0.64 \cdot 10^{12} Nm^2$. The computations are carried out for a wave direction parallel to the ship direction, hence, $\theta(x) \equiv 0$ and the incoming wave has a wavelength of $\lambda = 80m$ and a unit amplitude. We are so here only interested in the motion associated with the heave and pitch motion and confined in a vertical plane. The graphs (1.15) and (1.16) represent the real part and the imaginary part of the total vertical deflection, representing the deflection at $t = 0$ and $t = T/4$, including the heave, pitch motion and the bending distortion due to the flexibility of the ship.

Figures (1.19) and (1.20) represent the flexural distortion (the rigid motion of the ship is subtracted) at $t = 0$ and $t = T/4$.

We can clearly see the first principal bending modes of an elastic vibrating uniform beam.

Figures (1.19) and (1.20) represent the amplitude of the bending moment for two different wavelengths, $\lambda = 80m$ and $\lambda = 100m$. In this last case, the bending moment vanishes at mid-point of the ship.

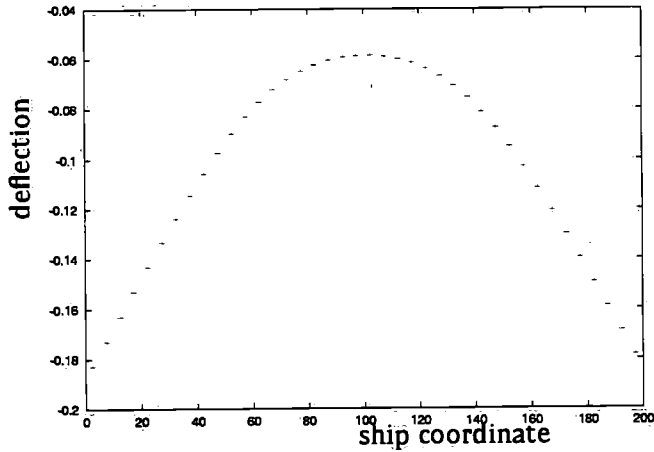


Figure 1.15: Real part of the total deflection, $\lambda = 80m$

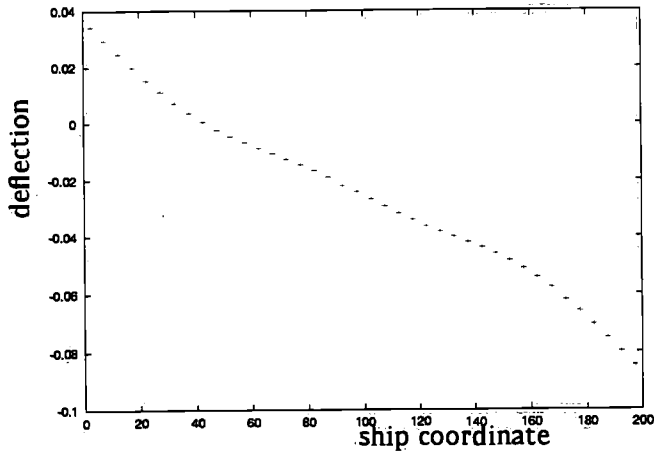


Figure 1.16: Imaginary part of the total deflection, $\lambda = 80m$

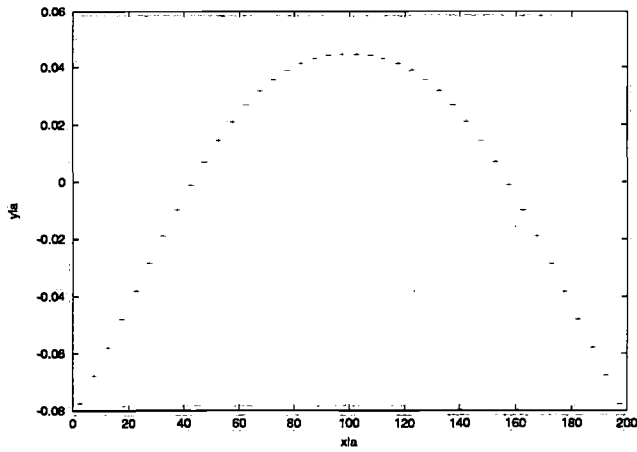


Figure 1.17: Real part of the flexural deflection, $\lambda = 80m$.

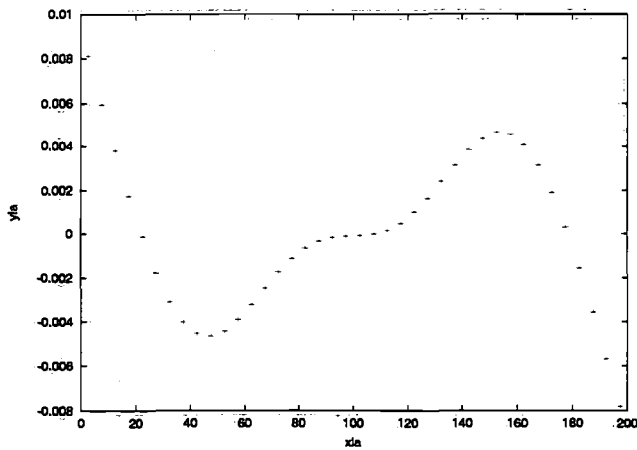


Figure 1.18: Imaginary part of the flexural deflection, $\lambda = 80m$.

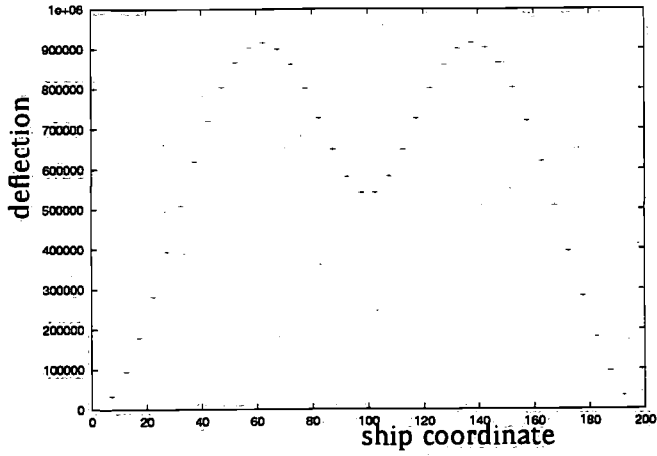


Figure 1.19: Amplitude of the bending moment,
 $\lambda = 80m$

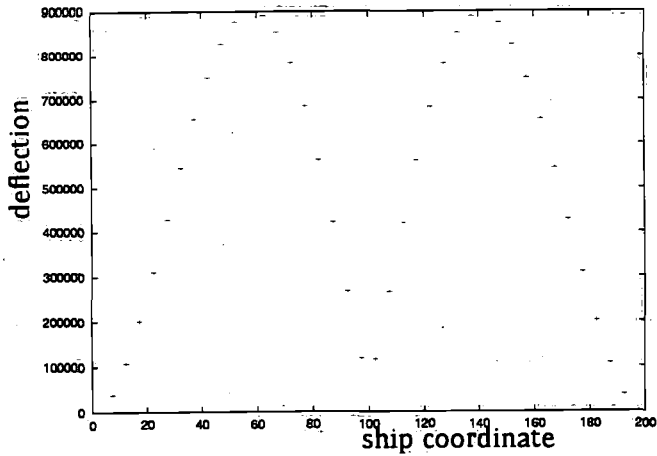


Figure 1.20: Amplitude of the bending moment,
 $\lambda = 100m$

Moving aircraft on a flexible platform

After having studied the deflection of a flexible platform by waves, we now compute the deflection created by a moving plane on a similar platform, with similar mechanical properties but of infinite extent.

2.1 Introduction

In this section we investigate the response of a transient dynamic load on a flexible platform in order to provide a model for landing and taking off airplanes. We focus our attention on the wave pattern produced by the moving load.

A time-domain analysis method is applied to the hydro-elasticity problem for this purpose. The dynamic load is modeled as a moving source point translating on a plate of infinite extent and we develop the mathematical solution of the deflection induced by this load.

Various authors tackled the related problem of a moving source with constant speed on a floating ice sheet using asymptotic Fourier analysis. (*Davys, Hoskind and Sneyd* [17], *Milinazzo, Shinbrot and Evans* [22], *Schulkes, Hoskind and Sneyd* [23]). Although this method is well suited to predict the wave elevation far from the source, the computations in the vicinity of the load lack of accuracy.

More recently, *Yeung & Kim* (1998) applied the method to airplanes moving on floating airports. They were mainly interested in the evaluation of the drag. Our solution for a general course of the moving load is derived in a different way, similar to the classical one presented by *Wehausen* [24] for a moving

source in water (no platform is present in this case). The general solution can easily be found with help of a Fourier and Laplace transform but it's numerical evaluation presents difficulties and is time consuming.

However, in the restricted case of a steady pattern, our analytical solution admits great simplifications and the fast decay of the wave amplitude with respect to the wave-number k enables us to use Neumann's addition theorem for decomposition of the involved Bessel function. A simple expression can then be obtained for the deflection w in term of a Fourier series expansion in the cylindrical coordinates attached to the moving source point. The coefficients of this series, expressed in a single integral over the k wave-number, are easily evaluated.

Our solution gives then an accurate description of the deflection over the entire field for all speeds. Three classes of platform responses depending on the source velocity, may be distinguished (supercritical, subcritical and critical) and an analytical solution is obtained for the critical speed and it's physical existence discussed.

2.2 Mathematical model

Since the dimensions of such floating airports are several kilometers both in length and width, we make the assumption that the platform is of infinite extend in the x and y direction. We consider a finite sea bottom at height H and we will investigate the influence of this parameter on the deflection.

The plane load is idealized as a moving point source translating along the x -axis at the position $x = a(t)$. The platform is in calm water and the only deflections are those due to the plane load. The only force exerted by the plane on the platform is the one due to its weight. It is assumed to be constant in time which means that the interactions between the plane and the flexible runway are discarded. The horizontal forces due to the possible acceleration or friction of the plane on the platform are also not taken in account.

The equations describing the physical problem are equation (1.1) to (1.4) exposed for the finite platform excited by wave except that equation (1.2) has to be replaced by a new equation expressing that no fluid particle can cross the sea bottom. We assume that the platform is initially at rest, providing two initial conditions for the potential.

The problem being linear, the calculations are hold for a plane weight of 1 N. Equations are solved via Fourier and Laplace transform for the moving pressure point following an arbitrary path $a(t)$. The numerical evaluation of the resulting integral solution is a fairly complicated process. However, in the case of moving pressure point with constant speed U , initiating it's course at $t = -\infty$, the deflection pattern in the coordinate system moving with the point is steady and it's evaluation can be drastically simplified. The originality of our approach is to compute, without approximation, the deflection on the whole physical plane as a single integral over the wave-number. This provides a fast

method for a numerical evaluation of the wave pattern. Asymptotic solutions when the speed U approaches the critical speeds can also be derived from those expressions.

2.2.1 mathematical formulation

We shall now give the mathematical statement of the problem. The governing equations are

$$\left\{ \frac{D}{\rho g} \nabla^4 + \frac{m}{\rho g} \frac{\partial^2}{\partial t^2} + 1 \right\} \frac{\partial \phi}{\partial z} + \frac{1}{g} \frac{\partial^2 \phi}{\partial t^2} =$$

$$= -\frac{1}{\rho g} \frac{\partial}{\partial t} [C(t) \delta(x - a(t)) \delta(y)] \quad \text{for } z = 0$$

$$\Delta \phi = 0 \quad \text{for } z < 0$$

$$\frac{\partial \phi}{\partial z} = 0 \quad \text{for } z = -H$$

with the homogeneous initial conditions $w(x, y, 0) = 0, \dot{w}(x, y, 0) = 0$ being assumed and $\phi_z = w_t$.

$C(t) = H(t)$ where $H(t)$ is the Heaviside function, for a landing plane and 1 if the plane is taking off.

We apply Fourier transform with respect to x and cosine transform with respect to y

$$\bar{\phi}(\alpha, \beta, z, t) = \int_{-\infty}^{\infty} \int_0^{\infty} e^{i\alpha x} \cos(\beta y) \phi(x, y, z, t) dx dy$$

and find

$$\left\{ \frac{D}{\rho g} (\alpha^2 + \beta^2)^2 + \frac{m}{\rho g} \frac{\partial^2}{\partial t^2} + 1 \right\} \frac{\partial \bar{\phi}}{\partial z}(\alpha, \beta, t) +$$

$$+ \frac{1}{g} \frac{\partial^2 \bar{\phi}}{\partial t^2}(\alpha, \beta, t) = -\frac{1}{\rho g} \frac{\partial}{\partial t} C(t) e^{i\alpha a(t)} \quad \text{for } z = 0$$

$$- (\alpha^2 + \beta^2) \bar{\phi} + \frac{\partial^2 \bar{\phi}}{\partial z^2} = 0 \quad \text{for } z < 0$$

$$\frac{\partial \bar{\phi}}{\partial z} = 0 \quad \text{for } z = -H$$

We apply the Laplace transform : $\bar{X}(\alpha, \beta, z, s) = \int_0^{\infty} e^{-st} \bar{\phi}(\alpha, \beta, z, t) dt$

$$\left\{ \frac{D}{\rho g} (\alpha^2 + \beta^2)^2 + \frac{ms^2}{\rho g} + 1 \right\} \frac{\partial \bar{X}}{\partial z} (\alpha, \beta, s) + \frac{s^2}{g} \bar{X} (\alpha, \beta, s) = -\frac{1}{\rho g} [s\mathcal{L}[e^{i\alpha a(t)}] - v] \quad \text{for } z = 0 \quad (2.2)$$

$$-(\alpha^2 + \beta^2) \bar{X} (\alpha, \beta, z, s) + \frac{\partial^2 \bar{X}}{\partial z^2} (\alpha, \beta, z, s) = 0 \quad \text{for } z < 0 \quad (2.3)$$

$$\frac{\partial \bar{X}}{\partial z} = 0 \quad \text{for } z = -H \quad (2.4)$$

For a landing plane $v = 0$, if the plane is taking off $v = 1$. This corresponds to the solution

$$w_{ini}(x, y, t) = \frac{1}{2\pi D} \int_0^\infty \frac{1}{k^3 (1 + \frac{\rho g}{Dk^4})} \cos(Kt) J_0(k\sqrt{x^2 + y^2}) dk \quad (2.5)$$

letting $\bar{W} = \mathcal{L}(\bar{w})$, $\alpha = k \cos \theta$ and $\beta = k \sin \theta$ and solving (2.3) and (2.4), leads to

$$s\bar{W} = k \tanh(kH) \bar{X}$$

$$\bar{W} = -\frac{f(s)}{s^2 + K^2} \frac{k}{[mk + \rho \coth kH]} \quad \text{with } K^2 = \frac{Dk^5 + \rho g k}{mk + \rho \coth kH} \quad (2.6)$$

Applying the inverse Laplace transform and noting that

$$\mathcal{L}^{-1} \left(\frac{1}{s^2 + K^2} \right) = \frac{1}{K} \sin(Kt)$$

we obtain

$$\bar{w}(\xi, t) = \frac{-k}{[mk + \rho \coth kH]} \times \int_0^t \frac{f(\tau)}{K} \sin K(t - \tau) d\tau$$

where $f(t) = e^{i\alpha a(t)}$. We apply inverse Fourier transform:

$$w(x, y, t) = -\frac{1}{4\pi} \int_0^\infty \int_{-\pi}^\pi \frac{k^2 e^{ikx \cos \theta} e^{iky \sin \theta}}{[mk + \rho \coth kH]} \times \int_0^t e^{ika(\tau) \cos \theta} \frac{\sin K(t - \tau)}{K(k)} d\tau d\theta dk \quad (2.8)$$

Using $J_0(x) = \frac{1}{2\pi} \int_{-\pi}^{\pi} e^{ix \cos \theta} d\theta$

we obtain

$$w = -\frac{1}{2\pi} \int_{k=0}^{\infty} H(k) \times \int_0^t \sin K(t - \tau) J_0[k\sqrt{(x - a(\tau))^2 + y^2}] d\tau dk \quad (2.10)$$

with $H(k) = \frac{k^2}{(mk + \rho \coth kH)^{1/2}} \times \frac{1}{(Dk^5 + \rho gk)^{1/2}}$

2.2.2 steady pattern in the moving frame with constant speed

Due to the fast oscillating character of the integrand, it is not an easy matter to carry out a numerical integration for w . We shall return to this problem later. We confine here our attention to the evaluation of this integral in a special case. We consider in this section the steady response of an infinite platform to the uniform motion of the load translating with constant speed U along the x axis. The platform deflection is expressed in the moving frame at coordinates (\bar{x}, \bar{y}) , translating at constant speed U with the load. Using Neumann's addition theorem for Bessel functions, the solution is expanded in Fourier series in the polar coordinates whose coefficients are easily computed as single integrals in the wave number k variable involving the radial coordinate τ . The analysis will be held for both finite and infinite depth. It is shown that the water depth can have a significant influence on the result.

The behavior of the wave pattern is classified in three mains categories, sub-critical, critical and supercritical depending on the moving point speed U .

To obtain the deflection due to a steadily moving pressure point source, we set $\bar{y} = y$, $x = Ut + \bar{x}$, $a(\tau) = U\tau$, and let t tend to infinity.

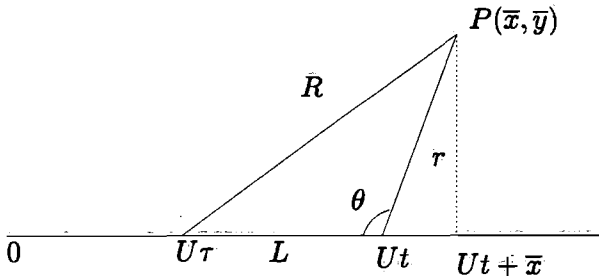


Figure 2.1: coordinate system

We introduce the angle θ so that

$$\begin{aligned}\bar{x} &= r \cos(\pi - \theta) & \bar{y} &= r \sin(\pi - \theta) \\ R^2 &= U^2(t - \tau)^2 + r^2 - 2U(t - \tau)r \cos \theta\end{aligned}$$

Using Neumann's addition theorem for Bessel's function, we have

$$J_0(kR) = \sum_{n=0}^{\infty} \epsilon_n J_n(kr) J_n(kU(t - \tau)) \cos(n\theta) \quad (2.11)$$

where ϵ_n denotes Neumann's factor and is defined as

$$\epsilon_n = \begin{cases} 1 & \text{if } n = 0 \\ 2 & \text{if } n > 0 \end{cases}$$

Injecting (2.11) into (2.10) and letting $t \rightarrow \infty$, it then possible to carry out analytically the integration in τ . We denote

$$\begin{aligned}G_n(k, U) &= \lim_{t \rightarrow \infty} \int_0^t \sin K(t - \tau) J_n(kU(t - \tau)) d\tau = \int_0^{\infty} \sin K\tau J_n(kU\tau) d\tau \\ &= \begin{cases} \frac{\sin[n \arcsin \frac{C}{U}]}{k(U^2 - C^2)^{1/2}} & \text{if } U > C(k) \\ \frac{\cos(n\pi/2)}{k(C^2 - U^2)^{1/2} [\frac{C}{U} + ((\frac{C}{U})^2 - 1)^{1/2}]^n} & \text{if } U < C(k) \end{cases} \quad (2.12)\end{aligned}$$

where $C(k) = \frac{K(k)}{k}$.

The deflection w is then found to be

$$w(r, \theta) = -\frac{1}{2\pi} \sum_{n=0}^{\infty} \cos(n\theta) g_n(r) \quad (2.13)$$

$$\text{with } g_n(r) = \int_0^{\infty} \epsilon_n H(k) G_n(k, U) J_n(kr) dk \quad (2.14)$$

In figure (2.3) and (2.5) we show $C(k)$ as function of k for various values of the parameters. We notice that due to the term $\cos(n\pi/2)$, for $U < C_{min}$, the wave pattern is symmetrical about the axis $\bar{x} = 0$. The energy transmitted by the wheel to the platform reads $\mathcal{P} = PU \frac{\partial w}{\partial x}(r = 0)$, where P is the plane weight. This shows that the speed of the moving load must be larger than the phase velocity $C(k)$ in order to have radiated waves at the corresponding wave-number k . Radiation is emitted in a band of frequencies for which

$$U > C(k).$$

Under the wheel, at $r = 0$, the deflection w_p equals

$$w_p = -\frac{1}{2\pi} \left\{ \int_0^{k_1} + \int_{k_2}^{\infty} \right\} \left[\frac{H(k)}{k(C^2 - U^2)^{1/2}} \right] dk \quad (2.15)$$

where k_1 and k_2 are solutions of the equation $C(k) = U$.

When the speed U tends to 0, the deflection under the wheel at $r = 0$ equals:

$$w_0 = \lim_{U \rightarrow 0} w_p = -\frac{1}{2\pi} \int_0^{\infty} \frac{H(k)}{K(k)} dk = -\frac{1}{2\pi} \int_0^{\infty} \frac{k}{Dk^4 + \rho g} dk = -\frac{1}{8} \frac{1}{\sqrt{\rho g D}} \quad (2.16)$$

This corresponds to the static deflection of the beam, independent of water height H , the fluid at rest exerting a upward supplementary restoring pressure of $\rho g w$.

In figure (2.2) we plot the deflection under the wheel w_p against the moving point speed U for a platform of flexural rigidity $D = 10^{11} \text{ Nm}^2$ for two different water depths $H = 40 \text{ m}$ and $H = \infty$. Results for the deflections have been divided by the static deflection value w_0 . The deflections present a peak for speed of 20 m/s for the finite depth and 35 m/s for the infinite depth. These speeds correspond to the minima of the function $C(k)$, representing the phase velocity of the wave, plotted against wave number k in figure (2.3).

For the infinite depth case, the minimum of the function $C(k)$ is found to be close to $C_{min} \sim 2(\frac{g^3 D}{27\rho})^{1/8}$ occurring at $k = k_c \sim (\frac{\rho g}{3D})^{1/4}$. At this speed, waves with wave number close to $k = k_c$, propagating with a speed close to C_{min} stay confined beneath the moving load vicinity. For k large, the phase velocity $C(k)$ tends to $C_{plate} = \sqrt{\frac{D}{m}} k$, the phase velocity given by the classical plate theory. Due to the fast growth of the function $C(k)$, the functions of k involved in integral (2.14) are rapidly decreasing ($H(k)$ decays in $1/k$) and only the wave numbers in the range $[0 \dots \sim 10k_c]$ contribute to the integrals g_n .

For the finite depth case, the function C tends to $C_g = \sqrt{gH}$, the wave velocities in shallow water in absence of platform, when $k \rightarrow 0$. In this wave number range, for large rigidity D (the literature gives values for D between 10^9 and 10^{12} for typical platforms) the factor $\rho \coth(kH)$ involved in K and H is predominant compared to mk . The influence of the mass per surface unit m is then negligible. We note that the graphs of the function C for $H = 40 \text{ m}$ and $H = \infty$ only differ for a narrow range of wavelength (approximately between $k = 0$ and $k \sim 2k_c$) This means that the presence of the sea bottom at a finite depth increases the influence of the very long waves ($\lambda > 500 \text{ m}$).

In figures (2.4) and (2.5) the deflection w_p and function $C(k)$ are plotted for a softer platform with a rigidity $D = 10^8 Nm^2$. The peaks for the deflection as well as their amplitude now hardly differ. The influence of sea bottom appears to be sensitive only for very rigid platform.

In figure (2.6) we plot the computed values of w_p , corresponding to equation (2.13), on the entire plane. The water depth is $H = 40m$, the mass per unit surface $m = 250Kg/m^2$ and the flexural rigidity $D = 10^{11} Nm^2$. The speed of the moving point is $U = 40m/s$. The results w are divided by the static deflection w_0 . In the next graphs, the solution being symmetrical about the x -axis, we will only plot the deflection for $y > 0$. We note the presence of waves in front of the moving load, even for large values of U . This is due to the fact that infinite wave velocity was predicted by the Euler theory for plate. Equation (2.13) also induces *instantaneous* far-field response for the same reason. The introduction of the shear and rotatory inertia would have as effect to bound the function $C(k)$ and remedy those problems.

Figures (2.8) and (2.7) show w_p for a water height of respectively $H = 40m$ and $H = \infty$ for the following parameters: $U = 25m/s$, $m = 250Kg/m^2$, $D = 10^{11} Nm^2$. The two waves patterns present major differences. In the infinite water depth case $U < C_{min}$ for all values of k ($C_{min} \sim 31.15m/s$). This correspond to the subcritical speed case. As we mentioned before, the deflection is symmetric about the x axis. The energy transmitted by the wheel to the platform is then equal to zero. There is no radiated wave and all the energy stays confined in the vicinity of the moving load. The waves decay very rapidly in amplitude with distance r to the load. This effect is analogous to field pattern emitted by a charged particle moving in a medium with a wave celerity greater than the particle speed. We find the maximal deflection under the wheel at $r = 0$, equaling 1.4 times the static deflection.

In the finite water case, $U > C_{min} \sim C_g$. This corresponds to the supercritical speed case. The symmetry about the $x = 0$ axis is broken and the maximum deflection is found to be close behind the wheel. We now note the presence of propagating waves.

We now investigate the wave pattern for a speed U slightly higher than the critical speed C_{min} , ($U = C_{min} + dU$). Let w^+ be the contribution on the deflection of the wavelength for which $C(k) > C_{min}$ and w^- the contribution on the deflection of the wavelength for which $C(k) < C_{min}$.

$$w = w^+ + w^- \quad (2.17)$$

We confine our attention on the value of w^+ when $C_{min} \rightarrow U$, $U - C_{min}$ staying positive

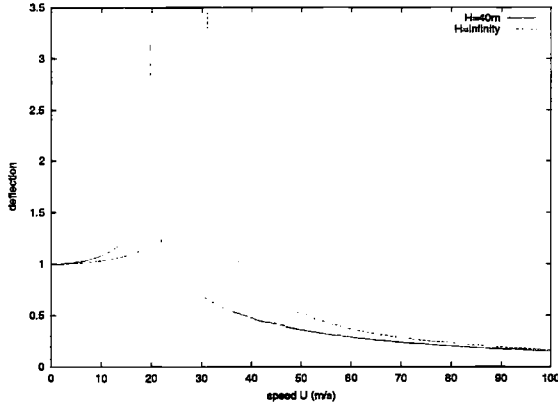


Figure 2.2: comparison of platform deflection under the wheel w_p , for $H = 40m$ and $H = \infty$, $D = 10^{11} Nm^2$, $m = 250Kg/m^2$

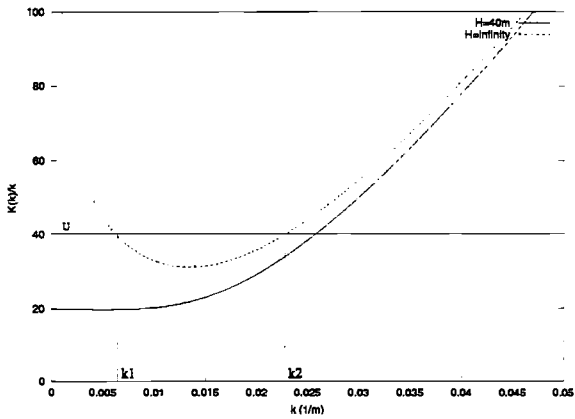


Figure 2.3: $K(k)/k$ for $H = 40m$ and $H = \infty$, $D = 10^{11} Nm^2$, $m = 250Kg/m^2$

We set

$$g_n^+ = \int_{k_1}^{k_2} \epsilon_n H(k) G_n(k, U) J_n(kr) dk = \int_{k_1}^{k_2} \epsilon_n \frac{H(k)}{k} \frac{\sin(n \arcsin \frac{C}{U})}{(U^2 - C^2)^{1/2}} J_n(kr) dk \tag{2.18}$$

Up to the first order in k

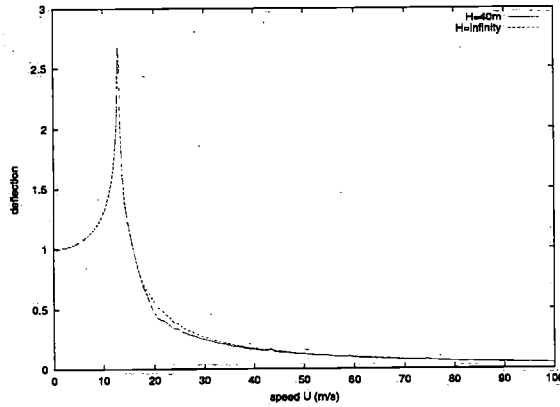


Figure 2.4: comparison of platform deflection under the wheel w_p , for $H = 40m$ and $\bar{H} = \infty$, $D = 10^8 Nm^2$, $m = 250Kg/m^2$

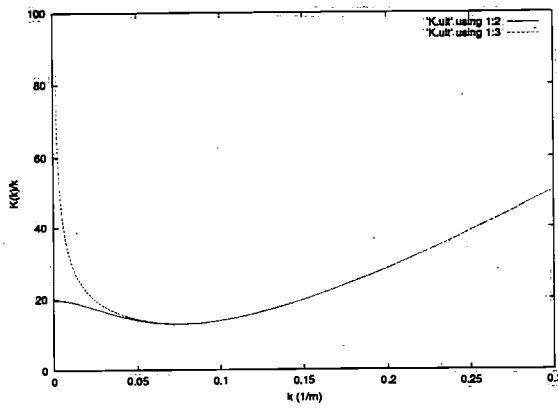


Figure 2.5: $K(k)/k$ for $H = 40m$ and $\bar{H} = \infty$, $D = 10^8 Nm^2$, $m = 250Kg/m^2$

$$\bar{C}(k) = C_{min} + \frac{(k - k_c)^2}{\delta k_c^2} dU \quad \text{with} \quad k_1 = k_c - \delta k, \quad k_2 = k_c + \delta k$$

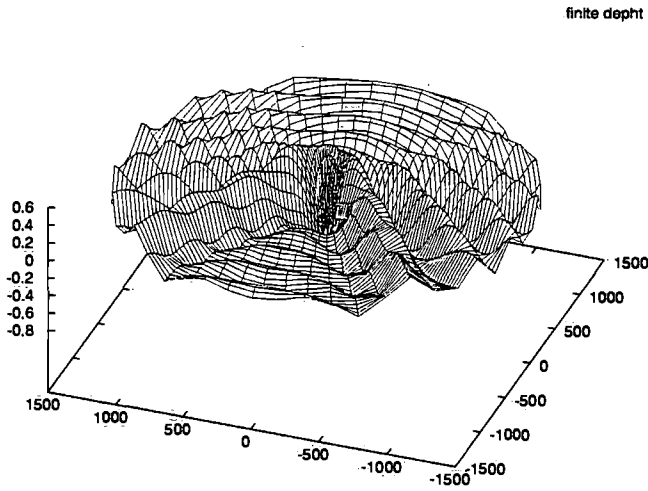


Figure 2.6: deflection w_p , $H = 40m$, $D = 10^{11}Nm^2$, $m = 250Kg/m^2$, $U = 40m/s$

$$U^2 - C^2 = 2UdU \left(1 - \frac{(k - k_c)^2}{\delta k_c^2} \right) \quad (2.19)$$

$$g_n^+ \approx \epsilon_n \frac{H(k_c)}{k_c} \sin(n\pi/2) J_n(k_c r) \int_{k_c - \delta k}^{k_c + \delta k} \frac{dk}{(U^2 - C^2)^{1/2}} \quad (2.20)$$

$$\text{and } \int_{k_c - \delta k}^{k_c + \delta k} \frac{dk}{(U^2 - C^2)^{1/2}} = \frac{\pi}{\sqrt{U C''}}, \quad C''(k_c) = 2 \frac{dU}{\delta k^2} \quad (2.21)$$

where $C''(k_c)$ is the second derivative of C with respect to k . Then w^+ equals

$$w^+ = -\frac{H(k_c)}{k_c \sqrt{U C''}} \sum_{n=1}^{\infty} (-1)^{n+1} J_{2n-1}(k_c r) \cos(2n-1)\theta \quad (2.22)$$

$$= \frac{2H(k_c)}{k_c \sqrt{U C''}} \sin(k_c x) \quad (2.23)$$

The last equality comes from the Jacobi-Anger formula [21].

In the case where $m = 0$, w^+ can be split in the sum of an even plus an odd function $w^+ = w_e^+ + w_o^+$.

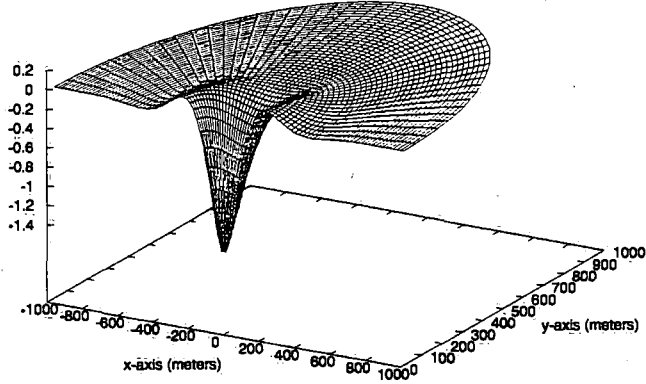


Figure 2.7: platform deflection w_p $H = \infty$, $D = 10^{11} \text{Nm}^2$, $m = 2500 \text{Kg/m}^2$, $U = 25 \text{m/s}$

$H(k) = \frac{k}{\rho} \frac{1}{C(k)}$ and introducing $\chi = \arcsin \frac{C(k)}{U}$, we have

$$w^+ = -\frac{1}{2\pi\rho U^2} \int_{k_1}^{k_2} \sum_{n=1}^{\infty} \frac{\sin n\beta \cos n\theta}{\cos \beta \sin \beta} J_n(kr) dk \quad (2.24)$$

Using the Jacobi-Anger formula, we can evaluate the sum under the integral

$$\begin{aligned} \sum_{n=1}^{\infty} \sin n\beta \cos n\theta J_n(kr) &= \frac{1}{4} \sin[kr \sin(\beta - \theta)] + \frac{1}{4} \sin[kr \sin(\beta + \theta)] + \\ &\frac{1}{2} \sum_{n=1}^{\infty} \sin 2n(\beta + \theta) J_{2n}(kr) + \frac{1}{2} \sum_{n=1}^{\infty} \sin 2n(\beta - \theta) J_{2n}(kr) \end{aligned}$$

and the odd term for w^+ is given by

$$w_o^+ = -\frac{1}{8\pi\rho U^2} \int_{k_1}^{k_2} \frac{\sin[kr \sin(\beta - \theta)] + \sin[kr \sin(\beta + \theta)]}{\cos \beta \sin \beta} dk \quad (2.25)$$

After some manipulations, w_o^+ can be expressed by the formula

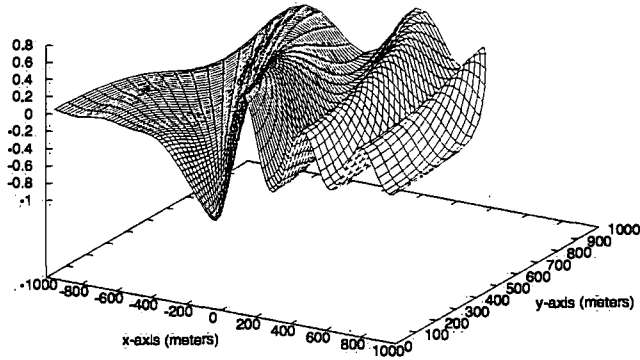


Figure 2.8: platform deflection w_p $H = 40m, D = 10^{11}Nm^2, m = 2500Kg/m^2, U = 25m/s$

$$w_o^+ = -\frac{1}{4\pi\rho U^2} \int_{k_1}^{k_2} \frac{\sin[kx \sin \chi] \times \cos[ky \cos \chi]}{\cos \chi \sin \chi} dk \quad (2.26)$$

If U approaches C_{min} , w^+ is then a two-dimensional monochromatic wave propagating with the moving pressure point at speed $U = C_{min} = C_g$ (fig 2.10). Indeed, for $k_1 < k < k_2$, $\frac{dC}{dk} \approx 0$ and the associated wave number celerities are approximately constant. The plate can then be seen as a non dispersive medium and the case is analogous to the Cherenkov radiation problem in electrodynamics. The deflections are confined inside a cone of semi-vertical angle $\chi = \arcsin \frac{C}{U} = \pi/2$. The waves are then two-dimensional.

The finite water depth case is slightly different because of the existence of two critical speeds corresponding to C_{min} and C_g . The prove given ahead is only valid for $U \sim C_{min}$. The numerical results show that in the general case, when $U \sim C_g$ we wave pattern has not a two-dimensional aspect. However, when $C_g \sim C_{min}$ which seems to be the case for realistic parameters ($m = 250Kg/m^2, D = 10^{11}Nm^2, H = 40m$), the curve $C(k)$ presents a horizontal asymptote for a larger range of wave numbers when $k \rightarrow 0$. We then still have a two-dimensional wave pattern but the waves are not monochromatic anymore. (see fig (2.9) where the waves in front and behind the load point

have different wavelengths).

The physical existence of a two-dimensional wave pattern is questionable. We note that this pattern results of emitted waves with a small range of values and a celerity slightly smaller than the source speed. Hence, no wave can propagate forward of the source point. The solution is then a purely mathematical one. But one can expect in reality a deflection extending on long distances in the direction perpendicular to the direction of motion.

We have $w = w^+ + w^-$. But w^- is even in x . It's first derivative with respect to x is then null at $x = 0$ under the wheel. Conversely, w^+ is odd with it's derivative $\frac{\partial w^+}{\partial x} = \frac{2H(kc)}{\sqrt{UC''}}$. The minimum value of the deflection is then behind the wheel and not under as it can sometimes be found in the literature.

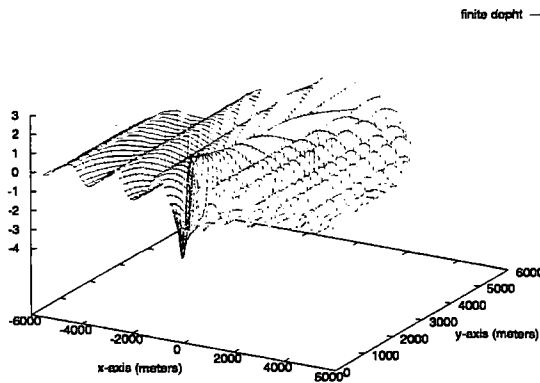


Figure 2.9: deflection w_p , $H = 40m$, $D = 10^{11}Nm^2$, $m = 2500Kg/m^2$, $U=19.75$ m/s

2.3 Pattern for an arbitrary path of the source

We now come back to the time dependent deflection of the platform for an arbitrary function $a(t)$ and note

$$R = \sqrt{(x - a(\tau))^2 + y^2}$$

Here, we focus our attention on the term

$$B = \int_0^{\infty} H(k) \sin(K(t - \tau)) J_0(kR) dk \quad (2.28)$$

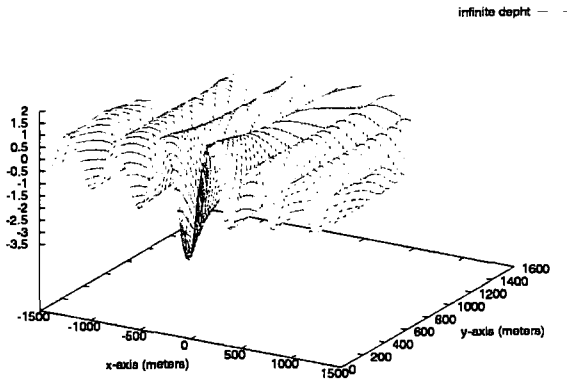


Figure 2.10: deflection w_p , $H = 40m$, $D = 10^{11} Nm^2$, $m = 2500Kg/m^2$, $U = 30.80 m/s$

This integral, evaluated as a contour integral, can be reduced to a form convenient for numerical analysis. Writing the sinus as a sum of complex exponentials, we making the change of variable $k = u \exp(i\pi/4)$ for the upper contour and $k = u \exp(-i\pi/4)$ for the lower contour.

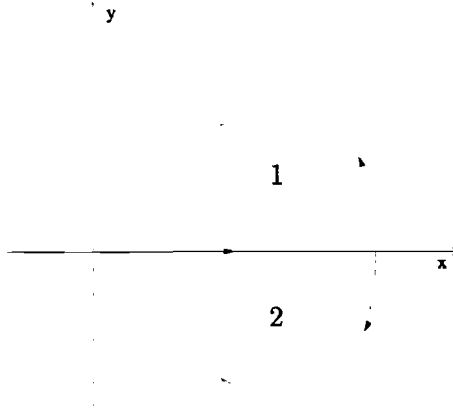


Figure 2.11: contour deformation

B is then found to be

$$B = \Im m \left\{ \int_0^{\infty} \frac{u^{3/2} e^{-i\pi/8}}{\sqrt{\rho}} \times \exp \left[\sqrt{u} e^{i\pi/8} \left(\frac{\rho g - Du^4}{\rho} \right)^{1/2} (t - \tau) \right] \times \right. \\ \left. J_0 [k e^{i\pi/4} \sqrt{(x - a(\tau))^2 + y^2}] du \right\} \quad (2.29)$$

This function of u under the integral has the advantage of decreasing exponentially when it starts oscillating rapidly and is easier to tackle out numerically. Once B is evaluated, we integrate it with respect to the variable τ , refining the time integration step when $\tau \rightarrow t$.

In figure (2.12) and (2.13) we plot the platform deflection for two different loading point courses. The flexural rigidity equals $D = 10^{11} Nm^2$ and the mass per unit area $250 Kg/m^2$. In figure (2.12), the plane is landing with constant speed $U = 25m/s$ and we plot the deflection at time $t = 5s$. This speed corresponded to the subcritical case for the steady deflection. The wave pattern is now wavelike but is found to be almost symmetric about the axis $x = 0$.

In figure (2.13) the plane is taking off, following the course $a(t) = 6t^2$. The graph corresponds to the time $t = 5s$. We can notice a strong slope of the deflection near the wheel corresponding to an important drag force acting on the plane.

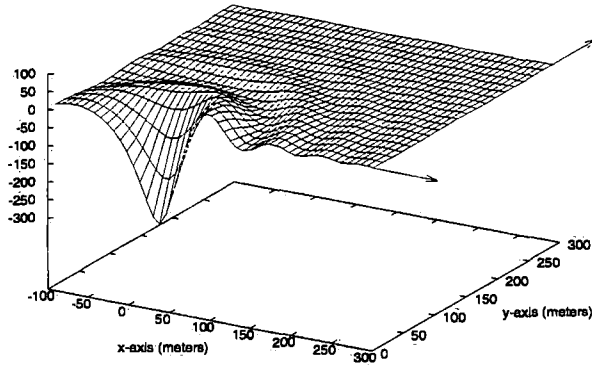


Figure 2.12: plate deflection for a plane landing with constant speed $U = 25\text{m/s}$, $t = 5\text{s}$, $D = 10^{11}\text{Nm}^2$, $m = 250\text{Kg/m}^2$

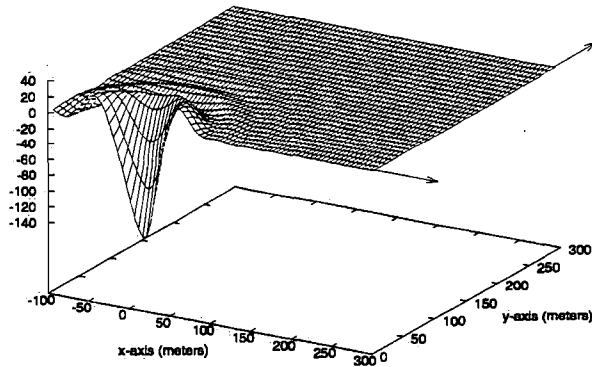


Figure 2.13: plate deflection for a plane taking off. $a(t) = 6t^2$, $t = 5\text{s}$, $D = 10^{11}\text{Nm}^2$, $m = 250\text{Kg/m}^2$

Chapter 3

Platform with air cushion

The previous chapters were concerned with large elastic floating platforms as a technical solution for floating airports. Indeed, the large scale of such construction induce large mechanical stresses and then, deflections in the structure. An engineering alternative should be the use of air cushion under the platforms in order to average the pressure applied on the body. This device can also be applied to platforms of smaller size for other purpose in oil-engineering. This chapter present a analysis of the phenomenon involved in such constructions in waves.

3.1 Introduction

Although the use of air cushions is not a new technique in offshore engineering, some new projects have recently renewed the interest in this field. Amongst them, we can mention the projects under consideration to built large floating barges for airports near the shore in Japan and USA or new types of FPSO. Actually, this kind of barges requires very long dimensions and the effect of the waves on a conventional rigid body would induce huge mechanical loads. One possible solution to remedy this problem is the use of air cushions. It provides several advantages:

If the size of these air chamber is reasonable, the pressure of the trapped air contained in the cavity can be considered as uniform in space. This contributes to average the pressure on the body and reduce the mechanical moments and stresses in the structure. Contrary to classical semisubmersible platforms which encounter structural difficulties as their size is increased, the performance of platforms with air cushion improve as their size increase. There is virtually no limit to their dimensions. A smaller value of the pitch and heave motions is as well expected, especially for frequencies of resonance. the compressibility of the gas playing the same roll as a spring, amortizing the platform.

One other main advantage of this device is the possibility to control the mean gas pressure, injecting some air in the cushion. Dynamically, this will change the frequencies of resonance for pitch and heave of such platform and provides the opportunity to adapt the platform to several given sea conditions that they may meet.

The study of the interaction of waves with this kind of platforms was first originated by *Pinkster* [6] who gave a mathematical description, developed a numerical code and carried out towing tank tests. *Cheung and al* [26] modeled the dynamic of a pneumatic platform composed of an array of open-bottom vertical cylinders. The air and the water mass inside each cylinder is modeled as a spring-mass system, the bottom of the platform is treated as continuous and they use a source method to solve numerically the problem. We notice that, contrary to other authors, they used an isotherm gas law for the gas compression description.

The platform consists of a rigid body and an air cavity beneath it, see figures (3.1) and (3.2). Most conventional floating platforms acquire their buoyancy forces by directly displacing the water with their hulls. A floating platform with air cushion utilizes indirect displacement, in which the platform rests on trapped air that displaces the water. The primary buoyancy force is provided by air pressure acting on the underside of the deck. We assume that there is no air leakage. The incoming water waves compress the air in the cushion and the resulting supplementary pressure forces the body to move. There is no energy exchange between the trapped air and the water. The gas compression is then supposed to follow an adiabatic law. It is possible to extend the method to several air cushions, connected or not.

In this chapter, we present a new integral equation to describe the motion of an air cushion supported platform, excited by waves. We assume that there is no current and tackle the problem with the linearized potential theory. A general mathematical model is developed as well as simplified cases suitable for the understanding of the phenomenon and comparison with other authors. We finally apply our model to a barge tested in a towing tank to compare with *Pinkster's* model tests.

For very large floating bodies (several hundreds of meters), the assumption of uniformity of pressure may not be valid anymore and there can be existence of acoustic waves traveling in the cushion and possible resonant modes. This requires a platform length L of same order of magnitude as $\pi c/\omega$ where c is the sound celerity. (Thin floating barges with length exceeding 500m fall in this category) *Lee and Newman* [10] took interest in this problem and developed a suitable mathematical model to that effect. Their results for a barge are very similar to ours for the RAO analyze although, the non-uniformity of the pressure can lead to different results concerning the pitch motion. The choice of an acoustic model for the gas law description has also important consequences. The force computations on the body are in fact erroneous for low incoming

wave frequencies and high compression of the gas. We analyze in a simplified one dimensional model, how the model differ to the one we developed and in which frequency and compressibility range they concur.

An air cushion device presents nevertheless several disadvantages. First at all, it deteriorates the static stability. Particular attention will be paid to the calculus of the restoring forces and moments which drastically differ from those computed in a rigid platform case.

The air cushion chamber also generates resonant waves which are reflected between the side walls. This affects the calculus of the hydrodynamic coefficients can lead to numerical difficulties in our model. The behavior of such a platform excited by waves is then considerably different from the one of a conventional rigid platform. There is then need of a predictive tool to compute the behavior of such a system. This is the goal of this chapter.

3.2 Physical problem

In this section, we present the mathematical equations which describe the physical problem. The fluid is assumed to be ideal (no viscosity), incompressible and the flow irrotational. Under these assumptions, we can describe the fluid velocity as the gradient of a potential satisfying the Laplace equation $\Delta\Phi = 0$. We consider the body as the rigid platform plus its air cushion. It oscillates sinusoidally about a state of rest, in response to long crested regular waves in a sea of infinite depth. The body is allowed to move in all directions and we assume the amplitudes of this motions to be small. We restrict then our analysis, in terms of the so called "linear harmonic theory" formulation. This theory, being well known, will be summarized briefly.

The problem being linear, we consider an incoming wave of unit height. At great distance from the body, the complex harmonic potential is defined by

$$\phi = \frac{g}{i\omega} e^{(i\nu x + \nu z - i\omega t)} \quad \text{with} \quad \nu = \omega^2/g \quad (3.1)$$

We define a system of axes with origin in the free surface. The incoming waves are propagating in the x direction, the vertical axis being the z axis, see figures (3.1) and (3.2).

The platform's boundary Σ is split into the boundary Σ_1 for the wetted part of the platform, and Σ_2 that marks the air-water interface underneath the platform and submitted to air cushion pressure. The normal \vec{n} on the hull surface is directed into the body. We denote S the surface of Σ_2 and V_0 the volume of the platform (air cushion included) under the free surface. G is the center of gravity of the platform and P his vertical projection on Σ_2 . We define η to be the surface elevation under the cavity or outside the platform, on S_F the sea free surface depending on the context. S_p is defined as the intersection of the platform with the plane $z = 0$ and its area is denoted s .

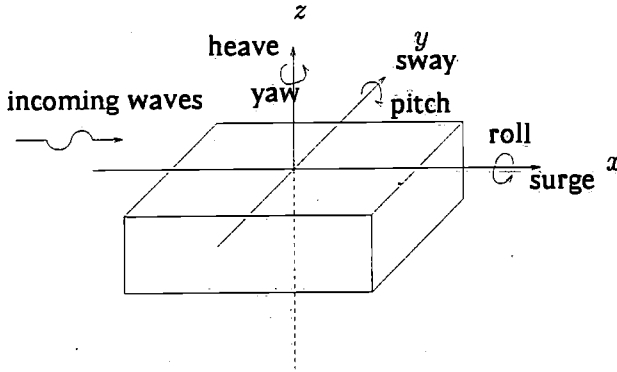


Figure 3.1: The six degrees of freedom

The interface of the cavity is at a distance of h_a meters from the free surface of the open sea. V_{cs} and P_{cs} are the volume and pressure in the cavity when the platform is at rest and the instantaneous pressure p_c is supposed to be uniform in space in the cavity.

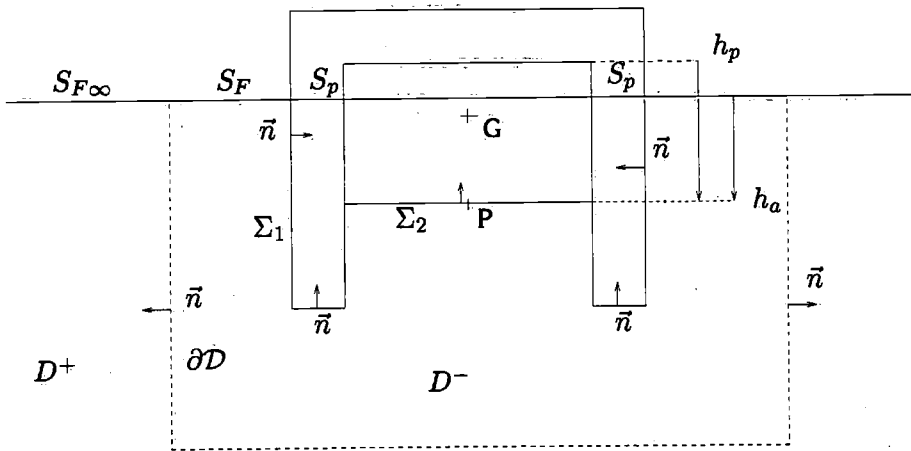


Figure 3.2: Definition of the geometry

3.3 Mathematical description

3.3.1 Boundary conditions

At the interface Σ_2 , the Bernoulli's equation and the kinematic condition (a particle can not leave the free surface) lead to the equations,

$$p_c = -\rho g h_a - \rho g \eta - \rho \frac{\partial \Phi}{\partial t}, \quad \frac{\partial \eta}{\partial t} = \frac{\partial \Phi}{\partial z} \quad (3.2)$$

The change of pressure Δp can be determined by the change of the volume of cavity ΔV . The air compression obeys the adiabatic law and we can write

$$\frac{\Delta p}{p_{cs}} = -\gamma \frac{\Delta V}{V_{cs}} \quad (3.3)$$

$$\begin{aligned} \Delta V = & \iint_{\Sigma_2} (\xi_3 + \xi_5(x - x_p) - \xi_4(y - y_p) - \eta) dS = \xi_3 S + \xi_5 a_x S \\ & - \xi_4 a_y S - \iint_{\Sigma_2} \eta dS \end{aligned} \quad (3.4)$$

$$\text{with } a_x = \frac{1}{S} \iint_{\Sigma_2} (x - x_p) dS, \quad a_y = \frac{1}{S} \iint_{\Sigma_2} (y - y_p) dS \quad (3.5)$$

where ξ_3, ξ_4, ξ_5 , are the heave, roll and pitch motions of the platform and $\gamma = 1.4$. If the platform admits symmetry about the x and y axis, we have $a_x = a_y = 0$. This is the case for a rectangular barge, as the one we compare our numerical results with, in an ulterior part. For simplicity, we restrict our analysis to this situation and report in appendix the changes in the equations when this conditions are not fulfilled anymore.

Then

$$\Delta V = \iint_{\Sigma_2} (\xi_3 - \eta) dS \quad (3.6)$$

Combining relations (3.2), (3.3) and (3.6) leads to the boundary condition on Σ_2 .

$$\frac{\partial^2 \Phi}{\partial t^2} + g \frac{\partial \Phi}{\partial z} - \frac{\gamma p_{cs}}{\rho V_{cs}} \frac{\partial \Delta V}{\partial t} = 0 \quad (3.7)$$

$$\text{or } \frac{1}{g} \frac{\partial^2 \Phi}{\partial t^2} + \frac{\partial \Phi}{\partial z} + \alpha \iint_{\Sigma_2} \frac{\partial \Phi}{\partial z} dS - \alpha S \frac{\partial \xi_3}{\partial t} = 0 \quad (3.8)$$

$$\text{with } \alpha = \frac{\gamma p_{cs}}{\rho g V_{cs}} \quad (3.9)$$

αS is a non-dimensional number. It represents the ratio of the force, due to air compression, exerted on the air cushion cavity as we push in the body in the vertical direction, to the force which would occur if the free surface was replaced by a solid surface. At rest, taking into account the atmospheric pressure has no influence on the equilibrium position - the atmospheric pressure applied on the platform above water is in equilibrium with the added pressure in water applied on the wetted hull-. However, adding this extra pressure will modify the value αS , leading to a stiffer system. In the case of a platform with a parallelepiped air chamber, as drawn in figure (3.2),

$$\alpha S = \frac{\gamma (P_{atm} + \rho g h_a)}{\rho g h_p} \quad (3.10)$$

where P_{atm} is the atmospheric pressure and h_p the height of the parallelepiped air chamber. It is then clear, as mentioned Cheung and al, that scaling the model will modify the air stiffness of the system.

We assume the potential $\Phi(\underline{x}, t)$ to be oscillatory and write $\Phi(\underline{x}, t) = \phi(\underline{x}) e^{-i\omega t}$. We have then the boundary conditions:

$$\left\{ -\nu\phi + \frac{\partial\phi}{\partial z} + \alpha \iint_{\Sigma_2} \frac{\partial\phi}{\partial z} dS + i\omega\alpha S\xi_3 = 0 \right\}_{\Sigma_2}, \quad \left\{ \frac{\partial\phi}{\partial n} = \vec{V} \cdot \vec{n} \right\}_{\Sigma_1} \quad (3.11)$$

where \vec{V} is the platform's velocity. $\xi_j, j = 1 \dots 6$ now denotes the complex values of the ξ_j .

At $z = 0$, on S_F , we have the usual free surface condition, $\frac{\partial\phi}{\partial z} - \nu\phi = 0$.

3.3.2 Boundary value problem

In this section, the expansion of the integral equation solution of the potential function ϕ is derived with help of the Green's function for a general body. However, for clarity, our analysis is restricted to the case where a_x and $a_y = 0$. The general expressions are postponed in the annex.

The fluid domain is split in two regions, separated arbitrary by an interface ∂D . The platforms stays in the region D^- and the region towards infinity is defined as D^+ . The potential function in D^+ is written as the superposition of the incident wave potential and a diffracted wave potential as follows

$$\phi(\underline{x}) = \phi^{inc}(\underline{x}) + \phi^+(\underline{x})$$

where ϕ^+ satisfies the radiation condition

$$\lim_{r \rightarrow \infty} r^{1/2} \left(\frac{\partial \phi^+}{\partial r} - i\nu \phi^+ \right) = 0 \quad (3.12)$$

In D^- , the total potential is denoted as $\phi^-(\underline{x})$. At the dividing surface ∂D we require continuity of the total potential and its normal derivative.

We recall that the Green's function $\mathcal{G}(\underline{x} - \underline{\xi})$, already introduced in chapter (1) fulfills $\Delta \mathcal{G} = 4\pi \delta(\underline{x} - \underline{\xi})$, the free surface and the radiation condition.

$$\mathcal{G}(\underline{x}, \zeta) = -\frac{1}{r} + \frac{1}{r_1} + \int_{\mathcal{L}} \frac{k}{k - \nu} e^{k(z+\zeta)} J_0(kR) dk \quad (3.13)$$

Applying Green's theorem for ϕ^+ and ϕ^- leads to the following formula:

for $x \in D^-$:

$$\begin{aligned} 0 &= - \iint_{S_{F\infty} \cup \partial D} \left(\phi^+ \frac{\partial \mathcal{G}}{\partial n} - \mathcal{G} \frac{\partial \phi^+}{\partial n} \right) dS \\ 4\pi \phi^- &= \iint_{S_F \cup \Sigma \cup \partial D} \left(\phi^- \frac{\partial \mathcal{G}}{\partial n} - \mathcal{G} \frac{\partial \phi^-}{\partial n} \right) dS \end{aligned} \quad (3.14)$$

The integrals over $S_{F\infty}$ and S_F become zero, due to the free surface condition for \mathcal{G} , ϕ^+ and ϕ^- . Adding up the two expressions in (3.14), leads for $x \in D^-$ to:

$$\begin{aligned} 4\pi \phi^- &= \iint_{\Sigma} \left(\phi^- \frac{\partial \mathcal{G}}{\partial n} - \mathcal{G} \frac{\partial \phi^-}{\partial n} \right) dS + \iint_{\partial D} \left([\phi] \frac{\partial \mathcal{G}}{\partial n} - \mathcal{G} \left[\frac{\partial \phi^-}{\partial n} \right] \right) dS \\ \text{or } 4\pi \phi^- &= \iint_{\Sigma} \left(\phi^- \frac{\partial \mathcal{G}}{\partial n} - \mathcal{G} \frac{\partial \phi^-}{\partial n} \right) dS + 4\pi \phi^{inc} \end{aligned}$$

When \underline{x} tends to $\bar{\Sigma}$, we have then

$$2\pi \phi^- = 4\pi \phi^{inc} + \iint_{\Sigma_1 \cup \Sigma_2} \left(\phi^- \frac{\partial \mathcal{G}}{\partial n} - \mathcal{G} \frac{\partial \phi^-}{\partial n} \right) dS \quad (3.15)$$

We decompose the potential into a potential of diffraction and six potentials of radiation due to the motions of the body

$$\phi^- = \phi^D - i\omega \sum_{j=1}^6 \xi_j \phi_j^R \quad (3.16)$$

diffraction

From (3.16), we write the boundary conditions for ϕ^D :

$$\left\{ -\nu\phi^D + \frac{\partial\phi^D}{\partial z} + \alpha \iint_{\Sigma_2} \frac{\partial\phi^D}{\partial z} dS = 0 \right\}_{\Sigma_2} \quad (3.17)$$

$$\left\{ \frac{\partial\phi^D}{\partial n} = 0 \right\}_{\Sigma_1}$$

$$\text{let } \tau_D = \iint_{\Sigma_2} \frac{\partial\phi^D}{\partial z} dS$$

Integrating (3.17) on Σ_2 and re injecting the result in the equation, we obtain:

$$\tau_D = \frac{\nu}{1 + \alpha S} \iint_{\Sigma_2} \phi^D dS$$

$$\text{and } \frac{\partial\phi^D}{\partial n} = \nu\phi^D - \frac{\nu\alpha}{1 + \alpha S} \iint_{\Sigma_2} \phi^D dS$$

Following Noblesse [9], we can write:

$$\left(\frac{\partial\mathcal{G}}{\partial n} - \nu\mathcal{G} \right)_{\Sigma_2} = \mathcal{H}(r, r_1) = -\left(\frac{1}{r} + \frac{1}{r_1} \right)_{\zeta} + \nu \left(\frac{1}{r} - \frac{1}{r_1} \right)$$

The potential ϕ^D is then found to be solution of the integral equation:

$$2\pi\phi^D - \iint_{\Sigma_1} \phi^D \frac{\partial\mathcal{G}}{\partial n} dS - \iint_{\Sigma_2} \mathcal{H} \phi^D dS - \frac{\alpha\nu}{1 + \alpha S} \iint_{\Sigma_2} \mathcal{G} dS \times \iint_{\Sigma_2} \phi^D dS = 4\pi\phi^{inc} \quad (3.18)$$

radiation

We apply the same procedure for the radiated potential. The boundary equations read:

$$\left\{ -\nu\phi_j^R + \frac{\partial\phi_j^R}{\partial z} + \alpha \iint_{\Sigma_2} \frac{\partial\phi_j^R}{\partial z} dS - S\alpha = 0 \right\}_{\Sigma_2} \quad \text{for } j=3 \quad (3.19)$$

$$\left\{ -\nu\phi_j + \frac{\partial\phi_j^R}{\partial z} + \alpha \iint_{\Sigma_2} \frac{\partial\phi_j^R}{\partial z} dS = 0 \right\}_{\Sigma_2} \quad \text{for } j \neq 3 \quad (3.20)$$

$$\left\{ \frac{\partial\phi_j^R}{\partial n} = n_j \right\}_{\Sigma_1} \quad (3.21)$$

where (n_1, n_2, n_3) is the unit normal vector pointing into the body, and $(n_4, n_5, n_6) = \vec{x} \times \vec{n}$.

We introduce:

$$\tau_j = \iint_{\Sigma_2} \frac{\partial\phi_j^R}{\partial z} dS \quad \text{for } j=1 \dots 6 \quad (3.22)$$

We then find:

$$\tau_3 = \frac{1}{1 + \alpha S} \left\{ \nu \iint_{\Sigma_2} \phi_3^R dS + S^2 \alpha \right\}, \quad (3.23)$$

$$\frac{\partial\phi_3^R}{\partial n} = \nu\phi_3 - \frac{\nu\alpha}{1 + \alpha S} \iint_{\Sigma_2} \phi_3^R dS + \frac{\alpha S}{1 + \alpha S} \quad (3.24)$$

and for $j \neq 3$:

$$\tau_j = \frac{\nu}{1 + \alpha S} \iint_{\Sigma_2} \phi_j^R dS, \quad \frac{\partial\phi_j^R}{\partial n} = \nu\phi_j^R - \frac{\nu\alpha}{1 + \alpha S} \iint_{\Sigma_2} \phi_j^R dS$$

We obtain the integral equation for ϕ_j :

$$\begin{aligned}
2\pi\phi_j^R - \iint_{\Sigma_1} \phi_j^R \frac{\partial \mathcal{G}}{\partial n} dS - \iint_{\Sigma_2} \mathcal{H} \phi_j^R dS - \frac{\alpha\nu}{1 + \alpha S} \iint_{\Sigma_2} \mathcal{G} dS \times \iint_{\Sigma_2} \phi_j^R dS \\
= -\frac{\alpha S}{1 + \alpha S} \iint_{\Sigma_2} \mathcal{G} dS - \iint_{\Sigma_1} \mathcal{G} n_3 dS \quad \text{for } j=3 \\
= -\iint_{\Sigma_1} \mathcal{G} n_j dS \quad \text{for } j \neq 3
\end{aligned} \tag{3.25}$$

We mention here that our formulation introduce the potential ϕ as unknown function although it is generally customary, in sea keeping analysis, to introduce source distributions.

3.4 Wave forces on the body and hydrodynamic coefficients

Once the velocity potential has been computed, it is possible to determine the forces and moments acting on the body with pressure integration. The fundamental theorem of dynamics will then be applied in order to compute the platform motion.

The pressure integration can be split in two parts. On the wetted part Σ_1 and on the interface Σ_2 . We recall that the body is defined as the rigid platform itself plus the captive air in the cushion.

The pressure is given by the linearized theory,

$$p = -\rho g(z - z_0) - \rho \frac{\partial \Phi}{\partial t} \tag{3.26}$$

z being the vertical abscissa of the moving platform and z_0 its vertical abscissa at rest.

If the results for a rigid body are well known, a supplementary difficulty arises due to the air cushion deformation, the interface staying horizontal.

3.4.1 Restoring coefficients

Our goal in this paragraph is to compute the restoring moment for a body with an air cushion. By definition, this is the ratio of the moment and the angle of rotation of the body that produces it. In the hydrostatic case, forces and moments are computed in still water. It is convenient to compute these moments with respect to the point O , lying on the free surface at $z = 0$ and

barycenter of intersection of the body with the plane $z = 0$. We study here a restricted situation where the body is symmetric with respect to the x and y axis, crossing each other at the point O . This implies that the rotation of the body will have no effect, up to the first order, on the change of volume of the air cavity. In annex we give the generalized equations.

The assumption of small angle of rotation is then used and we will only take into account the first order terms in θ . We split the above described problem (f_1) in three simpler small problems. The moment exerted in (f_1) with respect to the point O equals the sum of the moments exerted on the three following fictive bodies in situations (f_2), (f_3) and (f_4). (see figure (3.3))

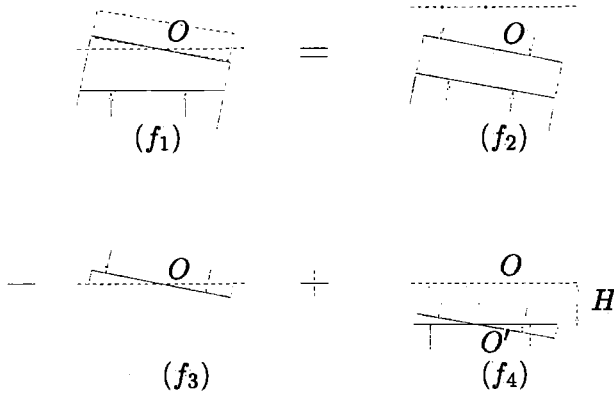


Figure 3.3: decomposition of the moment

- (f_2) moment exerted on a totally submerged rigid body.
 $\mathcal{M} = -\rho g V_0 O C \theta$ where V_0 is the volume of the platform with its air cushion and C the center of volume when the platform is at rest.
- (f_3) We subtract the moment exerted by a hydrostatic pressure on the surface represented by a solid line in (f_3).
 Up to the first order term in theta, we have: $\mathcal{M} = \rho g \iint_{S_c} x^2 dS \theta$
 S_c is the surface intersection between the platform at rest and the surface $z = 0$
- (f_4) We add the moment exerted by a hydrostatic pressure on the two surfaces represented by a solid line in (f_4).
 Let O' be the projection of O on Σ_2 . Up to the first order term in θ , the moment with respect to O' equals: $\mathcal{M} = \rho g \iint_{S_h} x^2 dS \theta$.
 where S_h is the projection of the interface Σ_2 on the plane $z = 0$. The total horizontal force on the inclined surface equals $\rho g H S_2$. Due to the rotation

of the body, the two surfaces are not centered anymore with respect to the point O . It will induce in O a supplementary moment of magnitude $\rho g H^2 S_2$.

We also take into account the moment exerted by the gravity forces

$$\mathcal{M} = \rho g V_p O G \theta$$

Adding these contributions, we find

$$\mathcal{M} = \left\{ \rho g \iint_{S_p} x^2 dS - \rho g V_0 (OC - OG) + \rho g H^2 S_2 \right\} \theta = \mathcal{R} \theta \quad (3.27)$$

S_p is the intersection of the platform with the plane defined by the equation $z = 0$. For a flat platform (barge type), the dominant term in this formula is $\rho g \iint_{S_p} x^2 dS$. Compared with the expression for a rigid platform, the integration only holds on S_p . This leads to a much smaller restoring coefficient and a deteriorate the stability of the body.

3.4.2 Added masses and damping

Due to continuity, the pressure is constant on the interface Σ_2 and can be computed via equation (3.3)

$$p = \rho g \frac{\alpha S}{1 + \alpha S} \left\{ \frac{i\nu}{\omega} \frac{1}{S} \iint_{\Sigma_2} \phi dS - \xi_3 \right\} \quad (3.28)$$

Denoting $X_j = \Re(\xi_j e^{i\omega t})$ and integrating the pressure over the wetted body and the air cushion walls, the vertical force on the platform can be written as follow

$$\begin{aligned} F_z(t) = & \rho g \frac{\alpha S}{1 + \alpha S} \left\{ -\omega \iint_{\Sigma_2} \Im(\phi^D) dS \cos \omega t + \omega \iint_{\Sigma_2} \Re(\phi^D) dS \sin \omega t \right. \\ & \left. - \sum_{j=1}^6 \iint_{\Sigma_2} \Re(\phi_j^R) dS \frac{d^2 X_j}{dt^2} - \sum_{j=1}^6 \omega \iint_{\Sigma_2} \Im(\phi_j^R) dS \frac{dX_j}{dt} - g S X_3 \right\} \\ & + \rho \left\{ -\omega \iint_{\Sigma_1} \Im(\phi_j^D) n_z dS \cos \omega t + \omega \iint_{\Sigma_1} \Re(\phi_j^D) n_z dS \sin \omega t \right. \\ & \left. - \sum_{j=1}^6 \iint_{\Sigma_1} \Re(\phi_j^R) n_z dS \frac{d^2 X_j}{dt^2} - \omega \sum_{j=1}^6 \iint_{\Sigma_1} \Im(\phi_j^R) n_z dS \frac{dX_j}{dt} - g S X_3 \right\} \quad (3.29) \end{aligned}$$

The pressure integration on Σ_2 has no contribution on F_x and F_y .

An analogous equation could be derived identically for the moment. This gives an easy expression for the value of the added masses and damping, the values of these terms being weighted with the non dimensional factor $\frac{\alpha S}{1+\alpha S}$ when the integrals apply on Σ_2 .

Collecting the terms in factor of $\frac{d^2 X_j}{dt^2}$ gives the added-masses (with a preliminary change of sign).

Collecting the terms in factor of $\frac{dX_j}{dt}$ gives the damping terms (with a preliminary change of sign).

Collecting the terms in factor of X_3 gives the restoring coefficient in heave (with a preliminary change of sign).

Collecting the terms in factor of $\cos(\omega t)$ and $\sin(\omega t)$ gives the forcing terms. (with a preliminary change of sign).

However, if the expressions can be expressed in a similar way than in a rigid body case, we keep in mind that the potentials involved in these expressions are solution of a different problem (equation (3.11)).

3.4.3 Equations of motion

We introduce the vectors $\vec{U}_D, \vec{W}_D, \vec{U}_j^R, \vec{W}_j^R$ for $j=1..6$ as follow

$$\vec{U}_D = \iint_{\Sigma_1} \phi^D \vec{n} dS + \frac{\alpha S}{1+\alpha S} \iint_{\Sigma_2} \phi^D \vec{n} dS \quad (3.30)$$

$$\begin{aligned} \vec{U}_j^R &= \iint_{\Sigma_1} \phi_j^R \vec{n} dS + \frac{\alpha S}{1+\alpha S} \iint_{\Sigma_2} \phi_j^R \vec{n} dS \quad \text{for } j=3 \\ &= \iint_{\Sigma_1} \phi_j^R \vec{n} dS \quad \text{for } j \neq 3 \end{aligned} \quad (3.31)$$

$$\vec{W}_D = \iint_{\Sigma_1} \vec{G}\vec{M} \wedge \phi^D \vec{n} dS + \frac{\alpha S}{1+\alpha S} \iint_{\Sigma_2} \vec{G}\vec{M} \wedge \phi^D \vec{n} dS \quad (3.32)$$

$$\vec{W}_j^R = \iint_{\Sigma_1} \vec{G}\vec{M} \wedge \phi_j^R \vec{n} dS + \frac{\alpha S}{1+\alpha S} \iint_{\Sigma_2} \vec{G}\vec{M} \wedge \phi_j^R \vec{n} dS \quad \text{for } j=1..6 \quad (3.33)$$

In the case where the air cushion is symmetrical with respect to the x and y axis, the integrals on Σ_2 involved in \vec{W}_D and \vec{W}_j^R vanish.

For simplicity, we restrict our results to a platform submitted to a front incoming wave. We are then interested in the surge, heave and pitch motion, ξ_1 , ξ_3 , ξ_5 . The equation of motion can then be written under the following vectorial system of equation

$$\begin{aligned} (m\omega^2 \vec{e}_1 + \rho\omega^2 \vec{U}_1^R) \xi_1 + (m\omega^2 \vec{e}_3 - \rho g [S_1 + \frac{\alpha S_2}{1 + \alpha S_2} S_2] \vec{e}_3 + \rho\omega^2 \vec{U}_3^R) \xi_3 \\ + \rho\omega^2 \vec{U}_5^R \xi_5 = -i\rho\omega \vec{U}_D \end{aligned} \quad (3.34)$$

$$\rho\omega^2 \vec{W}_1^R \xi_1 + [\mathcal{R} - \omega^2 I_{yy}] \dot{\xi}_2 \xi_5 + \rho\omega^2 \vec{W}_5^R \xi_5 = -i\rho\omega \vec{W}_D \quad (3.35)$$

Multiplying the first equation by \vec{e}_1 and \vec{e}_3 provides two scalar equations, and the second one by \vec{e}_2 gives the third scalar equation.

I_{yy} is the moment of inertia of the platform around the yy axis.

If the x and y axes are axes of symmetry for the air cushion, the dynamic pressure p does not contribute to the pitch and roll moment up to the first order of linearization with respect to η_4 and η_5 . The pressure integration for the moment on the internal walls of the air cushion cavity and its free surface is then zero.

3.5 Two dimensional test problem

In this section, we study the simple idealized 2D problem of the wave diffraction by an air-supported barge in order to test our algorithm. The air chamber, of length L and height h , is fixed and contains gas at the pressure equaling the atmospheric pressure P_{atm} . This means that there is no height level difference between the free surface mean level elevation, under and outside the platform. The platform is maintained in such way that its base does not extend below the free surface at rest. The waves are propagating along the x -axis and the first vertical wall encountered is located at $x = 0$, figure (3.4).

The general theory set up for a three-dimensional body still holds for a two-dimensional case. However, the integral equation has to be slightly modified in order to take in account that the water-gas interface Σ_2 , below the air chamber, lies at $z=0$. Indeed, in the Green's function formulation (3.13), both points \underline{x} and $\underline{\xi}$ are located at $z = 0$ and a correct treatment of the specific singularity is required.

Simple quasi-analytical solutions for the vertical force, exerted on the body by the incoming waves, are derived and compared with results of Newman [12]. The differences between our and his results are discussed.

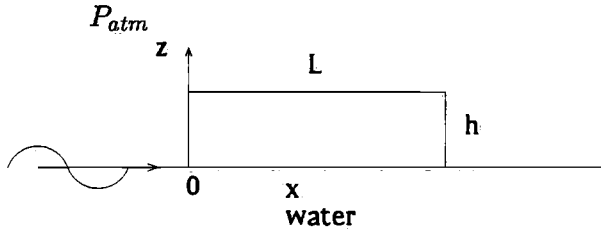


Figure 3.4: air chamber and incident wave

3.5.1 Present model

Denoting ϕ the diffracted potential ϕ^D , we recall the boundary condition for the free surface under the platform:

$$-\nu\phi + \frac{\partial\phi}{\partial z} + \alpha \int_0^L \frac{\partial\phi}{\partial z}(x) dx = 0, \quad \text{or} \quad \int_0^L \frac{\partial\phi}{\partial z} dx = \frac{\nu}{1 + \alpha L} \int_0^L \phi dx \quad (3.36)$$

Following the same analysis that for the flexible platform in chapter (1), the integral equation for the potential reads

$$2\pi\phi(x) - \frac{\alpha\nu}{1 + \alpha L} \int_0^L \mathcal{G}(x, \xi) d\xi \times \int_0^L \phi(\xi) d\xi = 2\pi\phi^{inc}(x) \quad (3.37)$$

(if the free-surface would be located below $z = 0$, the first term in the right hand side of equation (3.37) would be $\pi\phi(x)$ instead of $2\pi\phi(x)$.)

The Green's function $\mathcal{G}(x, \xi)$, for $z = 0$ obeying the radiation condition has the simplified form

$$\mathcal{G}(x, \xi) = -2 \int_C \frac{\cos k(x - \xi)}{k - \nu} dk \quad (3.38)$$

and the incoming potential ϕ^{inc} for an unit wave height

$$\phi^{inc}(x) = \frac{g}{i\omega} \exp(i\nu x)$$

We denote $\mathcal{I}(\nu L)$ such that

$$\int_0^L \int_0^L \mathcal{G}(x, \xi) d\xi dx = -4L^2 \mathcal{I}(\nu L), \quad \text{with} \quad \mathcal{I}(\nu L) = \int_C \frac{1 - \cos u}{u^2(u - \nu L)} du \quad (3.39)$$

The pressure reads $P(x) = i\rho\omega\phi(x) - \rho g\eta(x)$ with $-i\omega\eta = \frac{\partial\phi}{\partial z}$.

Denoting $\mathcal{A} = \int_0^L \phi(x) dx$ and integrating (3.37) from 0 to L , we find

$$\mathcal{A} \times \left[1 + \frac{2\alpha\nu L^2}{\pi(1 + \alpha L)} \mathcal{I}(\nu L) \right] = \int_0^L \phi^{inc}(x) dx$$

$$F_z = \int_0^L p(x) dx = i\rho\omega \int_0^L \phi(x) dx - \frac{i\rho g}{\omega} \int_0^L \frac{\partial\phi}{\partial z} dx = i\rho\omega \frac{\alpha L}{1 + \alpha L} \mathcal{A}$$

The normalized vertical force becomes

$$\frac{|F_z|}{\rho g L} = \frac{|\exp(-i\nu L) - 1|}{\nu L} \times \frac{\alpha L}{[1 + \alpha L + \alpha\nu L^2/\pi\mathcal{I}(\nu L)]} \quad (3.40)$$

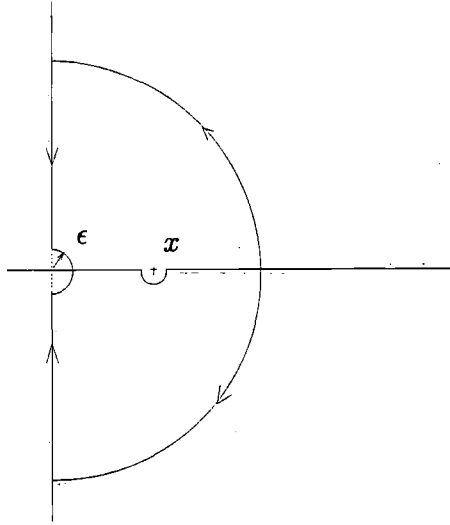


Figure 3.5: Path of integration in the complex plane

Splitting in (3.39) $1 - \cos u = \frac{1}{2}(1 - e^{iu}) + \frac{1}{2}(1 - e^{-iu})$ and denoting $u_0 = \nu L$, we deform the contours so that, in the neighborhood of $u=x$, they make a small semicircular detours into the lower half plane and and quarter circular detour around $u=(0,0)$ in the upper and lower half plane as shown in (3.5). Using residue theorem, we can then write

$$\lim_{\epsilon \rightarrow 0} \left\{ \int_{\epsilon}^{\infty} \frac{1 - e^{iu}}{u^2(u - u_0)} du + \int_{\infty}^{\epsilon} \frac{1 - e^{-u}}{-u^2(iu - u_0)} i du \right\} + \frac{\pi}{2u_0} = \frac{2i\pi(1 - e^{iu_0})}{u_0^2}$$

$$\lim_{\epsilon \rightarrow 0} \left\{ \int_{\epsilon}^{\infty} \frac{1 - e^{-iu}}{u^2(u - u_0)} du + \int_{-\infty}^{-\epsilon} \frac{1 - e^u}{-u^2(iu - u_0)} i du \right\} + \frac{\pi}{2u_0} = 0$$

And finally,

$$\mathcal{I}(u_0) = \frac{i\pi}{u_0^2}(1 - e^{iu_0}) - \frac{\pi}{2u_0} + \mathcal{T}(u_0), \quad \mathcal{T}(u_0) = \int_0^{\infty} \frac{(e^{-u} - 1)}{u(u^2 + u_0^2)} du$$

Using $\int_0^{\infty} \frac{e^{-u}}{u + iu_0} du = e^{iu_0} E_1(iu_0)$ $E_1(z) = -\gamma - \ln z - \sum_{n=1}^{\infty} \frac{(-z)^n}{nn!}$

We find

$$\begin{aligned}
\mathcal{T}(u_0) &= \lim_{\substack{A \rightarrow \infty \\ \epsilon \rightarrow 0}} \frac{1}{u_0^2} \left\{ E_1(\epsilon) - \frac{e^{iu_0}}{2} E_1(iu_0) - \frac{e^{-iu_0}}{2} E_1(-iu_0) \right\} - \\
&\quad - \frac{1}{u_0^2} \int_{\epsilon}^A \left(\frac{1}{u} - \frac{u}{u^2 + u_0^2} \right) du \\
&= \frac{1}{u_0^2} \left\{ \gamma(\cos(u_0) - 1) + \ln(u_0)(\cos(u_0) - 1) - \frac{\pi}{2} \sin(u_0) \right. \\
&\quad \left. + \cos(u_0) \sum_{n=1}^{\infty} \frac{(-1)^n u_0^{2n}}{(2n)(2n)!} + \sin(u_0) \sum_{n=0}^{\infty} \frac{(-1)^n u_0^{2n+1}}{(2n+1)(2n+1)!} \right\}
\end{aligned}$$

Recognizing in the sums the series expansions of the Sine and Cosine, $S_i(u_0)$ and $C_i(u_0)$, $\mathcal{I}(u_0)$ become

$$\begin{aligned}
\mathcal{I}(u_0) &= \frac{i\pi}{u_0^2} (1 - \cos(u_0)) + \frac{1}{u_0^2} \left\{ -\gamma - \ln(u_0) + \frac{\pi}{2} (\sin(u_0) - u_0) \right. \\
&\quad \left. + \cos(u_0) C_i(u_0) + \sin(u_0) S_i(u_0) \right\}
\end{aligned}$$

where $\gamma = 0.57721 \dots$ is Euler's constant.

It is easy to show that $u_0 \mathcal{I}(u_0) \rightarrow 0$ when $u_0 \rightarrow 0$. Then, the ratio $|F_z|/\rho g L$ tends to $\frac{\alpha L}{1+\alpha L}$ when the incoming wave frequency tends to zero. This limit value for F_z is the force exerted by the gas if we push in the platform of 1m in still water with an adiabatic compression. In figure (3.6) the vertical force has been plotted for $\alpha L = \infty$ against the parameter $\nu L/\pi$. Due to the interaction between the air cushion gas and the water, the maximum value for F_z is obtained for $\nu L \simeq 1.5\pi$ and not for $\nu L = \pi$. For $\nu L = 2n\pi$ with n integer, the mean value of the free surface elevation in the air cushion is null, the added pressure then cancels as well as F_z . In figure (3.7), we plot the non dimensional force function of αL and $\nu L/\pi$.

3.5.2 Newman's acoustic model

Similar calculations have been achieved by Newman, using a description of the acoustic disturbances and taking into account the coupling between acoustic waves (in the air chamber) and water waves. The platform has a length of $2a$ and a height b . We present briefly his method of resolution.

The velocities of the air and water are equal to the gradients of the complex potential $\Phi(x, z)$ and $\phi(x, z)$.

For the water domain the assumptions remain unchanged to our own model. The governing equation in the air chamber is the Helmholtz equation

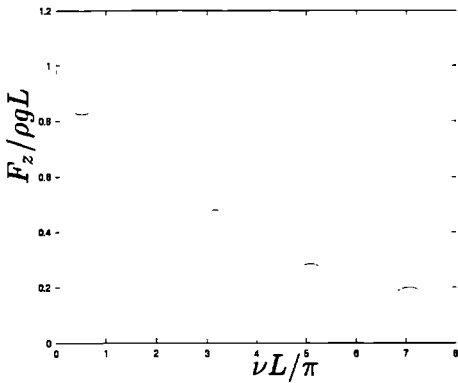


Figure 3.6: $F_z / \rho g L$ for $\alpha L = \infty$

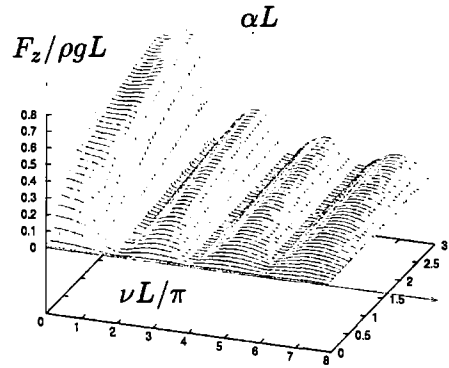


Figure 3.7: $F_z / \rho g L$ function of αL and νL

$$\nabla^2 \Phi + K^2 \Phi = 0 \tag{3.41}$$

where $K = w/c$ is the acoustic wave number and c the sound velocity. Neglecting the aerostatic pressure, the pressures in the air chamber and in water read

$$P(x, z) = -i\rho_a \omega \Phi(x, z), \quad p(x, z) = -i\rho_w \omega \phi(x, z) - \rho_w g z$$

Equalizing the pressures at the interface on the water-gas interface will furnish the dynamic condition. Combining this last relation with the usual kinematic one leads to the linearized free surface condition.

$$\rho_w \left(\omega^2 \phi - g \frac{\partial \phi}{\partial z} \right) = \rho_a \omega^2 \Phi \tag{3.42}$$

Zero normal velocity is prescribed on the ends and lid of the air chamber. The potential in the air chamber is expanded in the form

$$\begin{aligned} \Phi &= i\omega \sum_{m=0}^{\infty} \xi_m \Phi_m(x, y) & \Phi_m(x, y) &= f_m(x) \frac{\cosh v_m(b-y)}{v_m \sinh v_m b} \\ f_m(x) &= \cos u_m(x-a) & u_m &= \frac{m\pi}{2a} \end{aligned} \tag{3.43}$$

The coefficients v_m follow from the Helmholtz's equation $v_m^2 = u_m^2 - K^2$.

With the solution for an oscillatory pressure imposed on the free surface (Wehausen & Laitone, equation 21.17) we can write

$$\phi = \phi^{inc} - \frac{i\omega}{\pi\rho_w g} \int_{-a}^a P(\xi, 0) d\xi \int_0^\infty \cos k(x - \xi) e^{kz} \frac{dk}{k - \nu} \quad (3.44)$$

It is then possible to write

$$\phi = \phi^{inc} + i\omega \sum_{m=0}^{\infty} \xi_m \phi_m \quad \text{where} \quad (3.45)$$

$$\phi_m = -\frac{\nu\rho_a}{\pi\rho_w v_m \tanh v_m b} \int_{-a}^a f_m(\xi) d\xi \int_0^\infty \cos k(x - \xi) e^{kz} \frac{dk}{k - \nu} \quad (3.46)$$

After imposing the kinematic boundary condition $\phi_z = i\omega\eta$, multiplying by $f_n(x)/a$, and integrating over $(-a, a)$, a linear system of equations is derived for the unknown coefficients ξ_m in the form

$$\sum_{m=0}^{\infty} \xi_m C_{mn} = D_n \quad \text{where}$$

$$C_{mn} = \frac{1}{a} \int_{-a}^a f_n(x) \left[f_m(x) - \frac{k\rho_a}{\pi\rho_w v_m \tanh v_m b} \times \int_{-a}^a f_m(\xi) d\xi \int_0^\infty \cos k(x - \xi) \frac{kdk}{k - \nu} \right] dx$$

$$\text{and} \quad D_n = \frac{1}{a} \int_{-a}^a f_n(x) e^{-ikx} dx = -\frac{2i^n \nu a}{(u_n^2 - \nu^2) a^2} \sin(\nu a + \frac{n\pi}{2}) \quad (3.47)$$

It is possible to compute analytically this last integral and we find

$$C_{mn} = 2\delta_{mn} - \frac{k\rho_a}{\pi\rho_w v_m a \tanh v_m b} [1 + (-1)^{m+n}] \times \int_0^\infty \frac{[1 - (-1)^n \cos(2ka)] k^3}{(k - u_m)(k + u_m)(k - u_n)(k + u_n)(k - \nu)} dk \quad (3.48)$$

An elementary analysis shows that the only singularity of the integrand is for $\kappa = \nu$.

Neglecting the contribution to the pitch moment from the ends, the vertical force and the moment are given by

$$\begin{pmatrix} X_3 \\ X_5 \end{pmatrix} = \int_{-a}^a \begin{pmatrix} 1 \\ -x \end{pmatrix} P(x, 0) dx \tag{3.49}$$

Normalizing by the long-wavelength limits of the forces and moment for a flat rigid plate of the same width, we can write

$$\frac{X_3}{2\rho_w g a} = \frac{\rho_a \nu \xi_0}{\rho_w v_0 \sinh v_0 b}, \quad \frac{X_5}{\frac{2}{3}\rho_w g \nu a^3} = -\frac{12\rho_a}{\pi^2 \rho_w} \sum_{\substack{n=1 \\ (n \text{ odd})}}^{\infty} \frac{\xi_n}{n^2 v_n \sinh v_n b} \tag{3.50}$$

In figures (3.8) and (3.9) we show the vertical force and the moment acting on the air chamber for a value of $\alpha L \equiv 0.1$. The chamber is 300m long and 3m height. In figure (3.9) the peaks correspond to resonant modes for the acoustic waves.

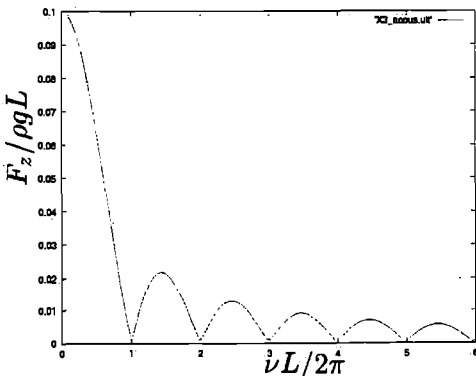


Figure 3.8: vertical force $\alpha L \equiv 0.1$

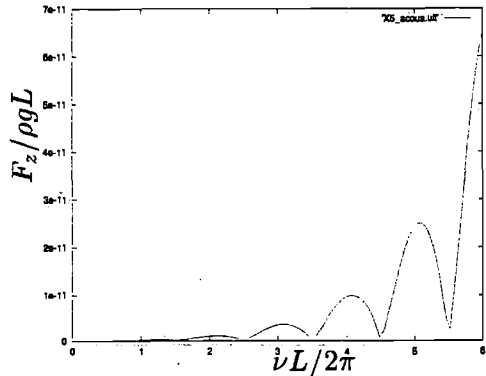


Figure 3.9: moment $\alpha L = 0.1$

3.5.3 Numerical results and comparison

In this section, we compare our results with those of Newman.

The ratio $|F_z|/\rho_w g L$, functions of the parameter νL , are shown for $\alpha L = 0.1, 0.5, 1, \text{ and } 2$, and compared with the acoustic model in figures (3.10), (3.11), (3.12) and (3.13). Agreement is good for small values of αL , but differences start to be significant beyond $\alpha L > 0.8$

In both models, the same physical assumptions have been used for the gas. In particular, the gas compression obeys the adiabatic law also in the acoustic theory where the celerity of sound is related to the pressure and density by the law

$\rho_a c^2 = \gamma p$ (see [1]). But in the acoustic theory, the disturbances are supposed weak enough so that nonlinear terms in the restoring forces associated with compressibility are neglected. Then the equation $\partial \rho / \partial t + \mathbf{u} \cdot \nabla \rho + \rho \nabla \cdot \mathbf{u} = 0$ is linearized in $\partial \rho / \partial t = -\rho \nabla \cdot \mathbf{u}$. As it can be shown, this assumption fails to predict the correct value of vertical force at very low frequencies.

It is possible to compute the long-wavelength limit of the vertical force in Lee and Newman's model. When $\nu \rightarrow 0$, then $\xi_0 \rightarrow 1$ and $\xi_m \rightarrow 0$ for $m > 0$. Then, using our notation, ($L=2a$), and the relation $\rho_a c^2 = \gamma p$, we find

$$\lim_{k \rightarrow 0} \frac{X_3}{2\rho_w g a} = \alpha L$$

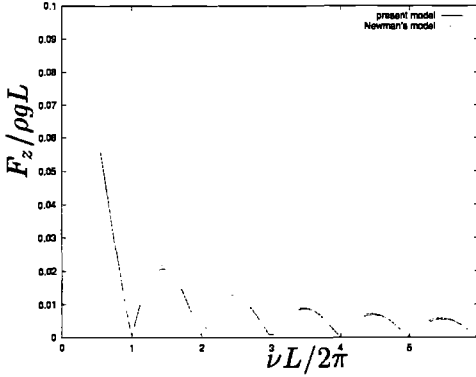
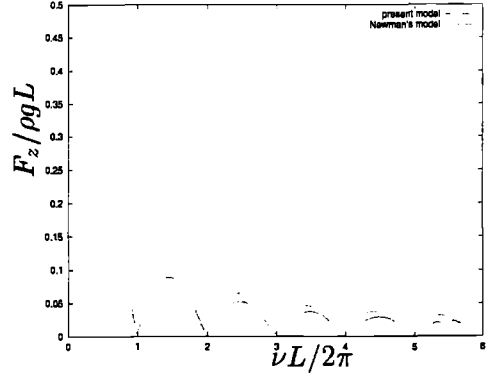
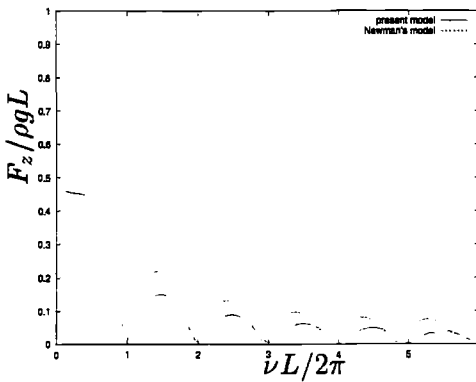
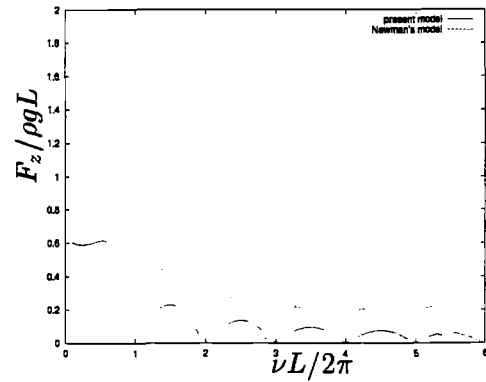
We recall that in our model, this value equals $\frac{\alpha L}{1+\alpha L}$ which is the right value for the hydrostatic case. The two models give then similar results when $\alpha L \ll 1$. This is confirmed by the numerical results. In the case of a platform with cavity height h_p , this implies $h_p \gg \frac{\gamma p c s}{\rho g}$. In practical cases, the pressure is always bigger than the atmospheric pressure $P_{atm} = 10^5 P_a$ and then we must have $h_p \gg 20m$, a value out of the range of practical applications. However, we notice that the discrepancy between our results is only sensitive for the very low frequencies. For $\alpha S = 0.5$ and $\nu L / 2\pi > 0.5$, the agreement is in fact still quite good.

In our model, the pressure being uniform in space, the theory predicts no moment acting on the platform. On the opposite, in Newman's model, the pressure is not uniform anymore and there are propagating gas waves in the air chamber, governed by the Helmholtz equation and leading to non null moment.

The calculation of this moment does not depend on the mean pressure value but on the spatial pressure variations. If the theory fails in predicting the first one for low frequencies, it should provide correct results for a much larger range of value for αL and ω for the second one.

We mention that if we can compute an equivalent compressibility ratio αL for the acoustic model, the vertical force F_z depends also of the length L , the two variables remaining independent (we can always choose the air chamber height h in this way). In the present case, we choose $L = 400m$.

We finally notice a phase difference in the force between Newman's results and ours, the vertical force canceling for smaller value of ω in the acoustic model. Indeed, a wave elevation will create a localized pressure excess above it, tending to level down the wave height. Similarly, a wave trough will generate a pressure depression leveling up the wave height. As a result, the canceling of F_z will always occur for wavelength slightly longer than the barge length.

Figure 3.10: $|F_z|/\rho g L$ $\alpha L = 0.1$ Figure 3.11: $|F_z|/\rho g L$ $\alpha L = 0.5$ Figure 3.12: $|F_z|/\rho g L$ $\alpha L = 1$ Figure 3.13: $|F_z|/\rho g L$ $\alpha L = 2$

3.6 Radiation problem for a cylindrical platform

In this section, we study the 3D radiation problem in heave (the platform is forced to oscillate harmonically in a vertical motion with an amplitude of one meter in the absence of incoming waves) in the case where the body has a very simplified geometry. The platform is cylindrical of radius R and has no vertical wall extending in the water.

The interface water-gas is denoted S . The problem has a radial symmetry and all functions depend only on the distance ρ from the vertical axis. As in the two dimensional test problem, the pressure of the gas contained in the air cushion equals the atmospheric pressure when the platform is at rest. We assume that there is no air leakage. The mathematical solution for the expression of the potential function is derived in a semi-analytical form and we compute the corresponding free surface elevation in the air cushion and outside the platform. The wave elevation is shown to present discontinuity at $\rho = R$ as expected. Expressions of the added mass in heave and damping coefficients are

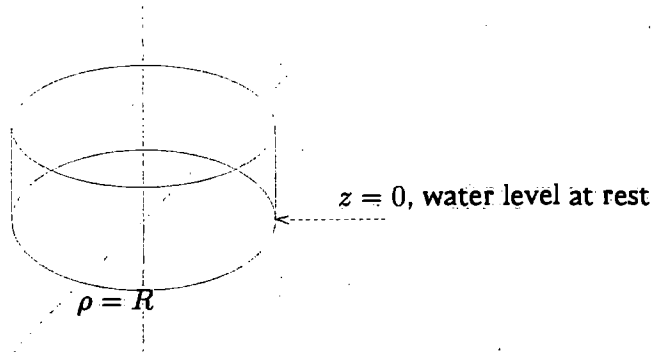


Figure 3.14: Definition of the geometry

also given.

This simplified model, although physically unrealistic, will be useful for the understanding of the mechanisms of the phenomenon and similar results will be found later in the case of more complex platform geometry.

We recall the mathematical problem. The potential function ϕ fulfills the Laplace equation plus the following boundary conditions at $z = 0$.

$$-\nu\phi + \frac{\partial\phi}{\partial z} + \alpha \iint_S \frac{\partial\phi}{\partial z} dS = \alpha\pi R^2 \quad 0 \leq \rho \leq R \quad (3.51)$$

$$-\nu\phi + \frac{\partial\phi}{\partial z} = 0 \quad \rho > R \quad (3.52)$$

The function ϕ is sought under the form

$$\phi = \int_0^{\infty} k^{-1} A(k) e^{kz} J_0(k\rho) dk \quad (3.53)$$

so that, it satisfies Laplace equation, with $A(k)$ an unknown function to be determined. This leads to the dual integral equation

$$\int_0^{\infty} (k - \nu) k^{-1} A(k) J_0(k\rho) dk + \alpha \int_0^{\infty} A(k) \times 2\pi \int_0^R \rho J_0(k\rho) d\rho dk = \alpha\pi R^2, \quad 0 \leq \rho \leq R \quad (3.54)$$

$$\int_0^{\infty} (k - \nu) k^{-1} A(k) J_0(k\rho) dk = 0, \quad \rho > R \quad (3.55)$$

Using the fact that $\int_0^R \rho J_0(k\rho) d\rho = \frac{R}{k} J_1(kR)$

and denoting $B(k) = A(k)(k - \nu)k^{-1}$, we have

$$\int_0^{\infty} B(k) J_0(k\rho) dk + 2\pi\alpha R \int_0^{\infty} \frac{B(k)}{k - \nu} J_1(kR) dk = \alpha\pi R^2 \quad 0 \leq \rho \leq R \quad (3.56)$$

$$\int_0^{\infty} B(k) J_0(k\rho) dk = 0 \quad \rho > R \quad (3.57)$$

We introduce the source density σ

$$\sigma(\rho) = \int_0^{\infty} B(k) J_0(k\rho) dk, \quad 0 \leq \rho \leq R \quad (3.58)$$

Using this expression and the fact that, due to equation (3.57), $\sigma(\rho) = 0$ if $\rho > R$, we find from the Hankel inversion theorem that

$$B(k) = k \int_0^R \rho \sigma(\rho) J_0(k\rho) d\rho = R\sigma(R) J_1(kR) - \int_0^R \rho \sigma'(\rho) J_1(k\rho) d\rho \quad (3.59)$$

Equation (3.57) is then automatically fulfilled. Injecting (3.59) in (3.56), we obtain

$$\begin{aligned}
 & R\sigma(R) \int_0^{\infty} J_1(kR)J_0(k\rho) dk - \int_0^{\infty} \int_0^R u\sigma'(u)J_1(ku)J_0(k\rho) du dk \\
 & + 2\pi\alpha R \int_0^R u\sigma(u) \int_0^{\infty} J_0(ku) \frac{k}{k-\nu} J_1(kR) dk du = \alpha\pi R^2 \quad 0 \leq \rho \leq R
 \end{aligned} \tag{3.60}$$

$$\text{Using the relation } \int_0^{\infty} J_0(ka)J_1(kb) dk = \begin{cases} 0 & b < a \\ 1/b & b > a \end{cases} \tag{3.61}$$

(3.60) transforms into

$$\sigma(R) - \int_{\rho}^R \sigma'(u) du = \sigma(\rho) = C \quad 0 \leq \rho \leq R \tag{3.62}$$

$$C = \pi R^2 \alpha - 2\pi\alpha R \int_0^R u\sigma(u) \int_0^{\infty} J_0(ku) \frac{k}{k-\nu} J_1(kR) dk du \tag{3.63}$$

C is a constant independent on ρ and the source strength σ is constant over the whole surface with a solution of the form

$$\sigma \equiv C_{ste} = \pi\alpha R^2 \left[1 + 2\pi\alpha R^2 \int_0^{\infty} \frac{1}{k-\nu} J_1^2(kR) dk \right]^{-1} \tag{3.64}$$

Using (3.59) we obtain

$$B(k) = \sigma R J_1(kR) \tag{3.65}$$

We can now compute the deflection η

$$\eta \equiv \frac{i\sigma R}{\omega} \int_0^{\infty} \frac{k}{k-\nu} J_1(kR) J_0(k\rho) dk \tag{3.66}$$

$$= \frac{i\sigma}{\omega} \begin{cases} 1 + \nu R \int_0^{\infty} \frac{1}{k-\nu} J_1(kR) J_0(k\rho) dk & 0 \leq \rho \leq R \\ \nu R \int_0^{\infty} \frac{1}{k-\nu} J_1(kR) J_0(k\rho) dk & \rho > R \end{cases} \tag{3.67}$$

In all integrals involving the factor $\frac{1}{k-\nu}$, the contour integration has to pass under the pole $k = \nu$ in order to assure the radiation condition at infinity.

Using (3.29), the added mass M_a and the damping coefficient D read

$$M_a = \rho g \frac{\alpha S}{1 + \alpha S} \iint_S \Re(\phi) dS, \quad D = \omega \rho g \frac{\alpha S}{1 + \alpha S} \iint_S \Im(\phi) dS \quad (3.68)$$

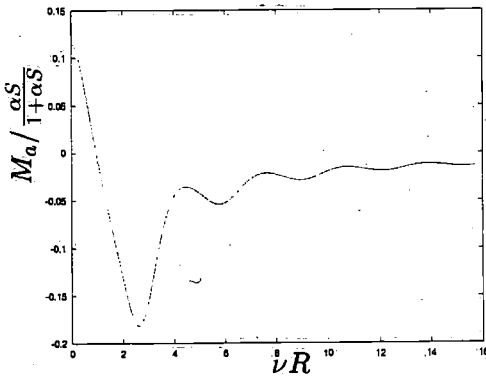
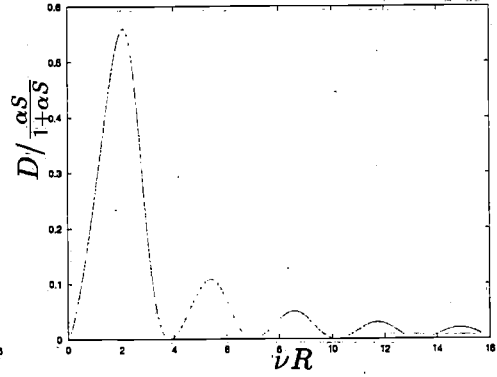
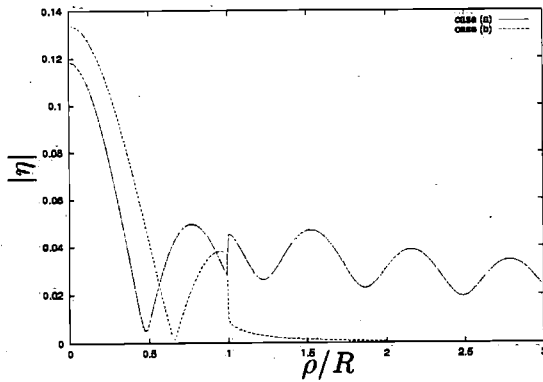
$$\text{with } \iint_S \phi dS = 2\pi R^2 \sigma \int_0^\infty \frac{1}{k(k-\nu)} J_1^2(kR) dk \quad (3.69)$$

In figures (3.15) and (3.16), we plot the added mass and damping coefficients divided by the factor $\rho g \frac{\alpha S}{1 + \alpha S}$ for $\alpha S = 0.15$. The added mass has negatives values for some range of frequencies. This phenomenon, unusual for classical platforms will be found again later when the method will be applied to a barge. The damping which represents the lose of energy due to outgoing waves, can vanish for some values of νR . Indeed, due to the idealized geometry and the absence of walls extending into water, the outgoing waves are only generated by the uniform pressure in the air chamber. For some frequencies, the mean value of the wave elevation in the air chamber is zero and there is then no pressure change. The power transmitted to the fluid is zero and there can be no outgoing wave. It can be shown that those frequencies correspond to the solution of the equation $J_1(\nu R) = 0$. In integrals (3.64) and (3.69) the pole at $k = \nu$ vanishes and the free surface elevation is in phase with the platform motion everywhere.

The wave elevation admits a discontinuity at $\rho = R$ and it's amplitude reaches its maximum value at $\rho = 0$. We can notice that the ratio between the waves elevation for $r = R^+$ and $r = R^-$ is independent of the value α which only determine the global wave elevation amplitude. However, due the presence of the exponential term in (3.53), the potential function ϕ is continuous everywhere for z negative.

In figure (3.17), we plot the absolute value of η for two different wave numbers $\nu R = 5$. and $\nu R = 3.831706$ which is the first root of $J_1(\nu R) = 0$. In the first case, the pattern is wave like implying the presence of outgoing wave. In the second case which corresponds to a null damping, the wave amplitude decays exponentially for $\rho > R$.

The integrals involved in the expressions of the wave elevation, added mass and damping can be rewritten in appendix (B) in a simpler form using contour deformation. The calculus of principal value integrals is then avoided.

Figure 3.15: Added mass, $\alpha S = 0.15$ Figure 3.16: damping, $\alpha S = 0.15$ Figure 3.17: wave elevation $\alpha S = 0.15$
case (a) $\nu R = 5.$, case (b) $\nu R = 3.831706$

3.7 Three-dimensional test problem, results for a barge

In the previous sections, we derived a general mathematical model to compute the forces acting on a body with an air cushion and the corresponding hydrodynamic coefficients (added mass and damping). This model has been tested against platforms with very simplified and unrealistic geometry for the understanding of the phenomenon. In this section, we now apply our model to a real parallelepiped barge. The numerical method used is described and we compute the hydrodynamic coefficients, forces due to harmonic incoming waves and response amplitude operators (RAO). The RAO represent the heave, surge and pitch motion of the platform when submitted to an incoming harmonic wave of one meter amplitude.

Pinkster [6] carried out a series of model experiments in the Delft Ships model basin and also modified his preexisting diffraction-radiation code to include the air cushion effects. After presenting briefly his mathematical model, the barge geometry and the basin test facility he used, we compare our numerical results with his both numerical and experimental ones he obtained. The agreement between our and his results is good.

Lee and Newman [10] developed an air cushion model for a general three dimensional body which is in a sense, the extension of the acoustical model of *Newman* presented in a previous section (3.5.2). They tested their numerical results against the experimental ones of *Pinkster*. We describe shortly their method of resolution and explain why the mathematical model differences highlighted in section (3.5.2), inherent in the choice of the gas law description in the air-chamber, do not lead to fundamental differences in our respective results.

A last comparison is finally done with the numerical results obtained by *Malenica* [3] with his code for a barge of similar shape but with different dimensions. Good similarity between our respective results is found.

The equations describing the barge motion are those presented in section 3.3. However, additional physical phenomena and numerical difficulties arise in the case of a real three dimensional barge.

First, the presence of a free surface under the platform, bounded by the verticals walls extending in water, will create a situation similar to the one of a water filled tank submitted to forced motion. In the basin test model and in our calculations, the incoming waves are front waves, propagating in a direction parallel to the axis in which is oriented the largest dimension axis of the barge.

At certain waves frequencies, so that $\nu L \simeq n\pi$ or $\nu l \simeq n\pi$, where L and l are the cavity length and cavity width respectively and n an integer, resonance modes will be generated, with sloshing waves of large amplitude propagating back and forth in between the side walls. If n is odd, the wave elevation integrated over Σ_2 will be small, a wave elevation compensating a wave trough and the pressure change will remain also small. But with n even, the waves

elevation and troughs do not cancel anymore. Important pressure change consequently occurs and strong variations for the hydrodynamic coefficients are expected.

A second difficulty originates from the peculiar geometry of the studied barge. The side walls are thin (see the mesh (3.20)) and have sharp angles. This generates singularities in the flow potential at the corners and numerical difficulties to obtain good numerical accuracy. Heave motion and the corresponding added mass and damping are not very affected by those problems because the vertical force on the body is due to the pressure in the gas chamber. However, as consequence of the uniform pressure in the chamber, the moment acting on the body are only due to the water pressure on the wetted part of the body. Especially, as result of the small ratio draft/length, on the horizontal inferior basis of the side walls, were the potential determination is numerically subject to errors.

3.7.1 Numerical aspects

We use a three dimensional panel technique method to solve the integral equation for ϕ^D and ϕ_j^R , $j = 1 \dots 6$. The barge boundaries, including the air cushion cavity, are discretized by means of flat perpendicular panels on which the potential is assumed to be constant. The boundary conditions are applied in one control point, centered on the middle on each element. For this purpose, we use an existing Fortran subroutine, written by Noblesse [9] to evaluate numerically the Green's function \mathcal{G} . A linear system of equations, with the discretized potential values on the hull and water-gas interface as unknown, is obtained and solved. Once the ϕ_i are computed, the hydrodynamics coefficients and excitations forces determination is straight forward. Due to the size of the barge, the range of frequencies which are of practical interest, is confined to $0 < \omega < 1.2$ for the full scale model.

3.7.2 Pinkster's model and results

Pinkster solved an identical problem and furnishes numerical calculations as well as model test results for a prototype barge. His approach is slightly different. He splits the gas-water interface of the air cavity in a given number of independent air cushions and associates to each one a potential induced by a vertical displacement. This leads to a multi-degrees of freedom problem, the equality of the pressures in each air cushion and the fulfillment of the boundary conditions for each sub interface, furnishing the supplementary equations. However, the global added masses and restoring coefficients can not be obtained directly. The comparison is then limited to the physical values (pitch, heave, surge) of the model.

The tests were carried out with a 1:100 scaled model of the platform described below. The full scale model is a 250m long and 78m wide rectangular platform with a parallelepiped cavity symmetrically centered with respect to its borders.

(see mesh (3.20)). The draft to the bottom of the wall is 15m and the water free surface in the air cushion is at distance of 5m from the mean sea level. The vertical walls thickness, surrounding the air cavity, is 6m for the 250m long side walls, and 6m for the 78m long end walls. The air cushion height between the free surface and the horizontal deck amounts 18m. The air chamber has an area of $242 \times 66 = 15.9710^3 m^2$. Some gas was introduced in the air cushion to obtain a mean water level in the cavity which was 5m below the still water level in the basin. Taking into account the atmospheric pressure influence, we find $p_{cs} = 1.49 atm$, $\alpha = 7.28 \cdot 10^{-5}$ and $\alpha S = 1.16$. Masses are placed on the barge lid in order to increase the metacentric height and the center of gravity is situated at $z = 0$.

The total number of rectangular panels for the computations amounts 872. The particulars of the platform are displayed in table (3.7.3) The tests are carried out with a head incoming wave. Due to the linearity of the problem, we assume it's amplitude of one meter.

3.7.3 Comparison with Pinkster and Newman's results

In this section, the numerical results of our model are presented and compared with Pinkster's towing tank test results as well as with Lee and Newman's numerical results.

The added masses and damping coefficients issued from our calculations are presented in the figures (3.21) through (3.26).

Discontinuities are clearly noticeable. These phenomenon occur for frequencies for which there is wave sloshing due to the resonant modes in the chamber bounded by the vertical sides. Physically, the flow should not be potential anymore, the waves of large amplitude breaking and the variations of these different coefficients should be smother. Unfortunately, we do not have experimental test results for these data. Numerical problems should also occur for these resonant frequencies. At this point, it is not clear in which extend these numerical problems play a role.

An interesting feature is the occurrence for certain frequencies of negative value for the added mass in heave. This phenomenon, already experienced in the one dimensional model, rarely occurs with classical rigid platform but can be explained by the air cushion presence. If in unbounded fluid the added mass represents a mass of the liquid entrained by the fluid, in presence of an air cushion and a free surface, this is just the in phase component of the fluid reactive force. The air compression generated by the water waves reacts like a spring which motion can be out of phase with the barge heave. This term could also be included in the restoring coefficient term and called "hydrodynamic spring coefficient". Oortmerssen [15] experienced similar behavior for the case of a tanker vertically oscillating near a quay. The presence of the vertical side walls can also accentuate the phenomenon by "guiding" the liquid in a vertical motion and preventing it to "escape" laterally.

Force in the incoming wave x direction and vertical force in figures (3.27) and (3.28) and added mass and damping in surge in figures (3.23) and (3.24). For frequencies so that $\nu \equiv 2(n+1)\pi/L$, we have as expected important peaks for the force F_x . this corresponds to sloshing modes for which the waves elevation at the two sides of the barge are in opposition of phase.

A interesting result is that the horizontal force F_x as well as the added mass in surge A_{11} (and more generally $\vec{U}_D \cdot \vec{e}_x$ and $\vec{U}_j^R \cdot \vec{e}_x$) are independent of the parameter α although the diffracted and radiated potentials are modified. In figures (3.18) and (3.19), forces F_x and F_z are plotted for different values of α . Indeed, a local wave elevation under the barge generates a extra pressure applying uniformly on the surface Σ_2 and the side walls. Due to linearity, modifying the value α is equivalent to applying an oscillating pressure in the air chamber. Due to the uniformity in space of the pressure, it's surface integration on the vertical side walls is then zero.

The potential induced by the imposed pressure having the same plans of symmetry as the barge, the resulting added mass and force for surge are then null.

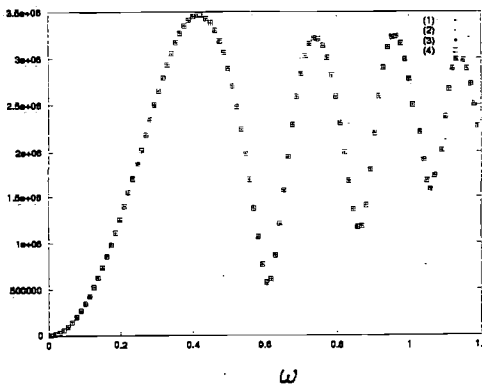


Figure 3.18: F_x

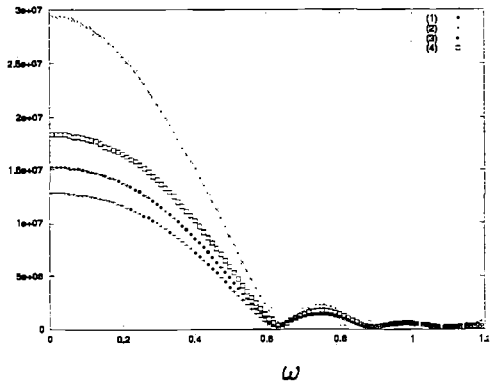


Figure 3.19: F_z

In figure (3.30) we compare our numerical model for heave with Pinkster's towing tank result. In figure (3.31) the comparison is made with Lee and Newman's acoustic model. In both cases, the agreement is good. For this last comparison, we notice that a small shift in frequency as in one dimension. On the other hand the comparison for the pitch motion lacks of precision. Actually, in our model, the pressure in the cavity does not contribute to the moment exerted on the body. Considering the small values of the draft compared to the length and width of the barge, this means that the moment on the body is mainly due to the pressure acting on the bases of the platform, the horizontal side walls, at $z = l_{z_2}$. Unfortunately, as it was already mentioned, the

computed values for ϕ lack of precision on those boundaries. The predicted pitch values plotted in figure (3.32) are far too small and unrealistic. The lack of numerical precision can also be noticed in figure (3.29) where the limit value of the surge, when $\omega \rightarrow 0$ is approximately 1.1 (it should be 1, the platform following the circular fluid particle motion). Increasing the number of panel elements remedy this problem although the convergence is slow.

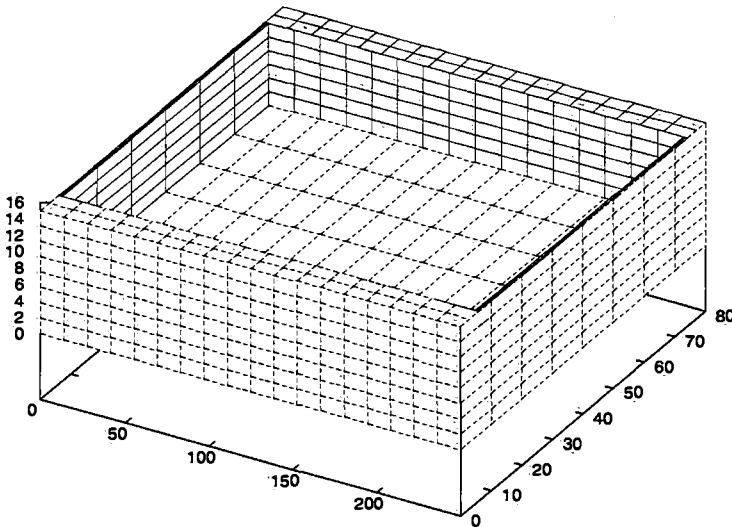


Figure 3.20: Panel description of the barge

We mention here the work of Lee and Newman who also developed a three dimensional code based on their acoustic model. As in 1D, the acoustic disturbances will give a non null value for the moment, exerted by the gas trapped in the air cushion, on the body. Their model can tackle any motion of the platform and gives added masses and different RAO coefficients. The method of resolution is very similar to the one presented for the one-dimensional case. The motion in the air chamber is represented by an eigenfunction expansion with a set of Fourier generalized modes. This reduces drastically the numbers of unknown values, especially in the case of a barge.

They tested their numerical results against Pinkster's towing tank test and numerical ones. The agreement is very good. Considering the mathematical differences in the two models, one based on an adiabatic gas law and the other on the acoustic theory, noticed in section 3.5.3, one could be surprised with a so good agreement between the results for the computed RAO. First, we no-

Quantity	Symbol	Units	Magnitude
Length	L	m	250
Breadth	l	m	78
Draft	l_{z2}	m	15
Depth	D	m	30
Displacement	V_0	m^3	$0.130 \cdot 10^6$
Center of gravity above keel	KG	m	30
Long. metacentric height	k_{yy}	m	75.1
Longitudinal side wall	d_y	m	6
Front side wall	d_x	m	2
γ	-	-	1.4
natural heave frequency	ω_ϕ	rad/s	4.97
natural pitch frequency	ω_H	rad/s	4.97
α	-	m^{-2}	$7.29 \cdot 10^{-5}$

Table 3.1: Particulars of the platform

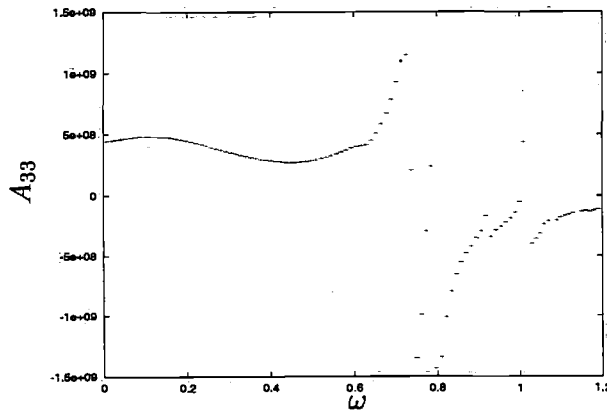


Figure 3.21: Added inertia in heave for Pinkster's model test barge

ticed that the calculus of the moment acting on the platform should be well predicted, and the agreement on the pitch motion could be expected. On the contrary we showed that the acoustic theory fails in predicting the forces at low frequencies. But for higher frequencies, a good agreement was also expected. In fact, when the incoming wave-lengths are very long, the heave motion of the body only depends on the restoring coefficient in heave and is always one, the barge "following" the waves, and this, whatever the value of the dynamic forces.

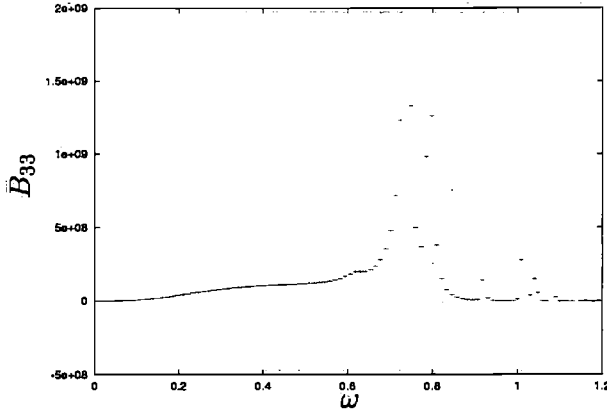


Figure 3.22: Damping in heave for Pinkster's model test barge

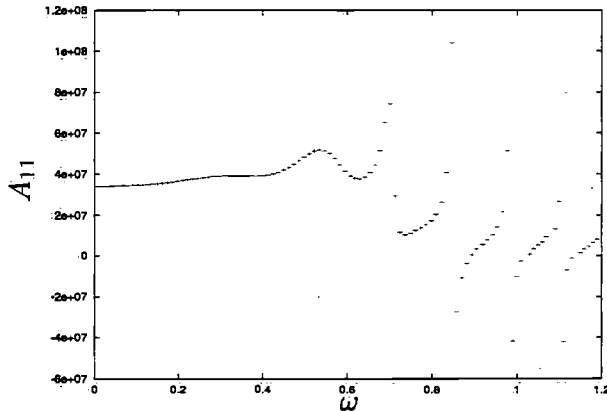


Figure 3.23: Added inertia in surge for Pinkster's model test barge

3.7.4 Comparison with Malenica's results

Malenica presented numerical results obtained his method which is similar to ours. It as been designed to be implemented in an existing diffraction-radiation code with a slightly different formulation. He tested his method on a barge similar to the one of Pinkster but with different dimensions. The barge is $150m$ long, $20m$ large and the draft amounts $10m$. The side walls are $4m$ wide and the water-gas interface in the air chamber is laying $5m$ below the sea level at rest. He presented results for the added mass and damping in heave which provide a good way to compare with our own computings.

Added masses and damping in heave for $\alpha = \infty$ and $\alpha = 0$ are plotted in

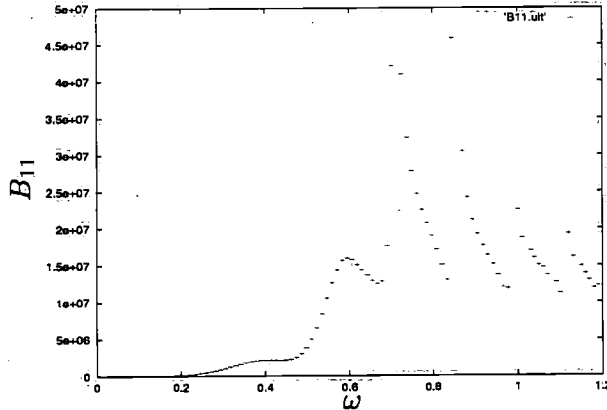


Figure 3.24: Damping in surge for Pinkster's model test barge

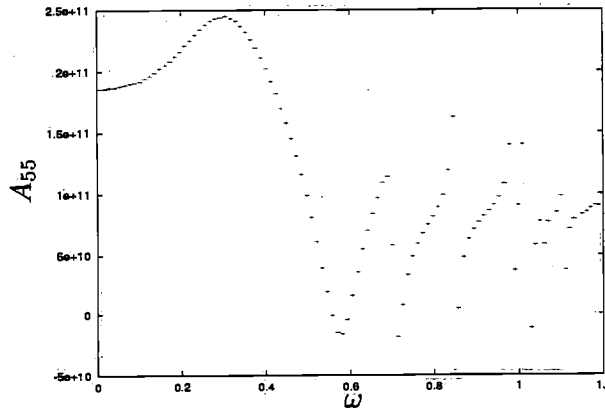


Figure 3.25: Added inertia in pitch for Pinkster's model test barge

figures (3.34), (3.35), (3.36) and (3.37).

The agreement between our results is good. A noticeable fact is that discontinuities are not present for the case $\alpha = \infty$. Numerical tests show that this is due to the low value of the ratio width/length although it is still not clear why. For $\alpha = 0$, our results slightly differ for the prediction of the resonant modes corresponding to high variation in the plots. This can be explained by the lack of accuracy of our code which is not optimized for industrial purposes. We finally mention the occurrence of negative values for the added mass as it was found for the previous analytical models and numerical results.

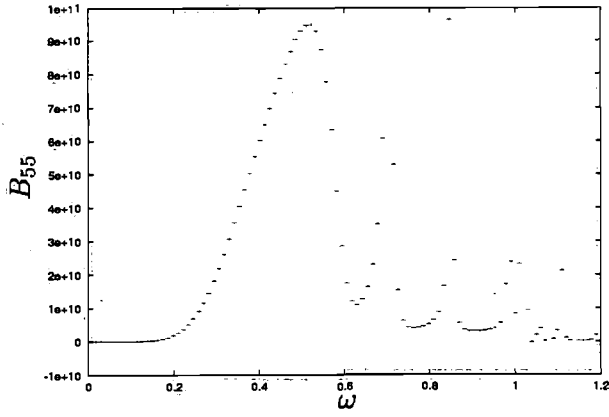


Figure 3.26: Damping in pitch for Pinkster's model test barge.

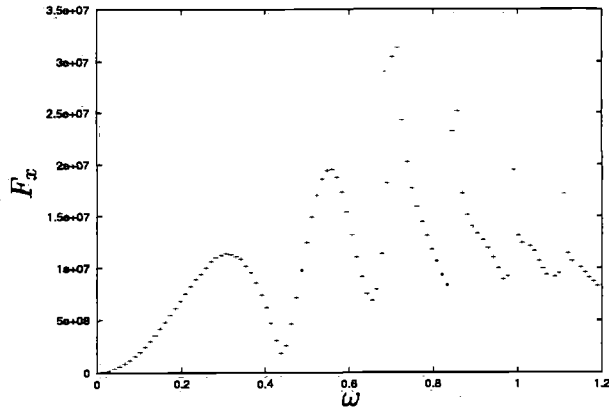


Figure 3.27: horizontal force F_x for Pinkster's model test barge

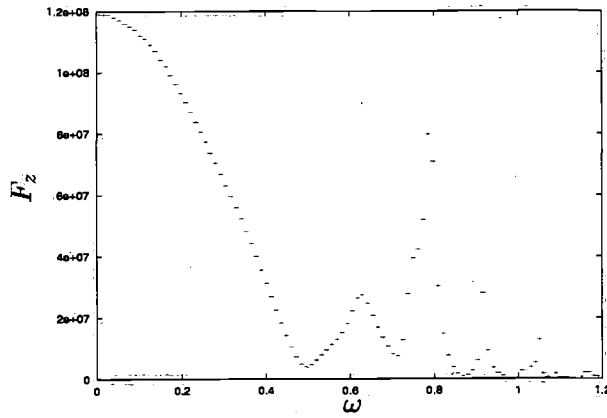


Figure 3.28: vertical force F_z for Pinkster's model test barge

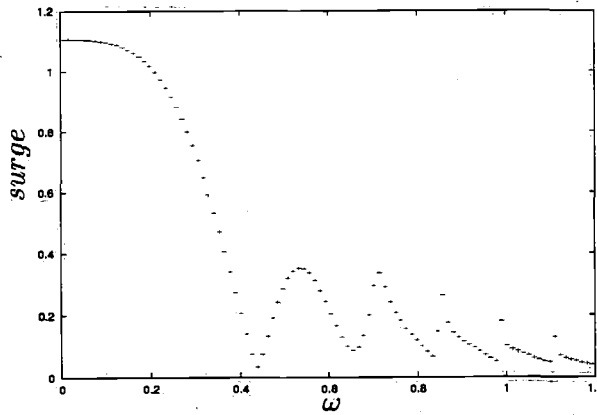


Figure 3.29: surge response for Pinkster's model test barge

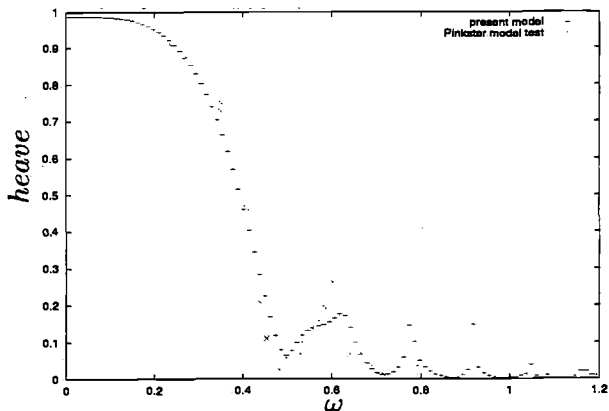


Figure 3.30: heave response, comparison with Pinkster's model test

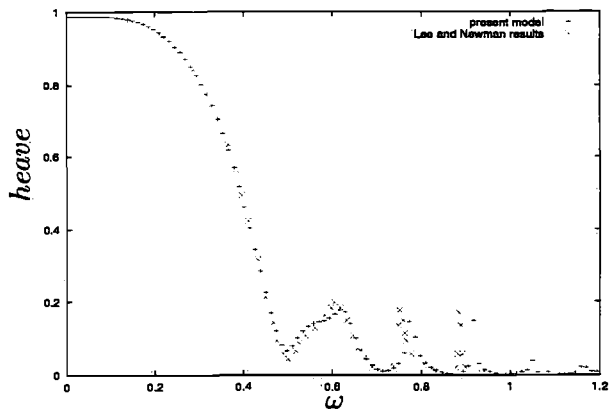


Figure 3.31: heave response, comparison with Lee and Newman's numerical model

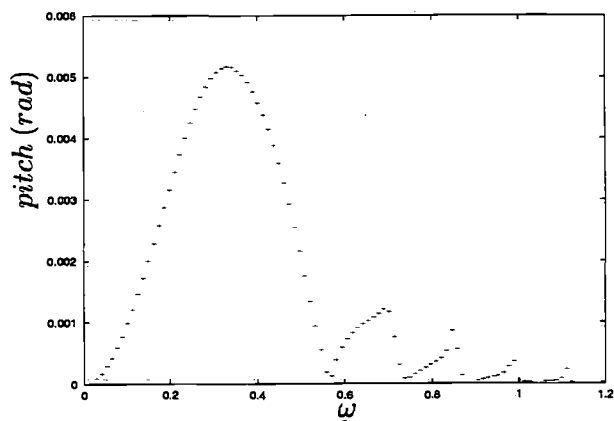


Figure 3.32: pitch response for Pinkster's model test barge

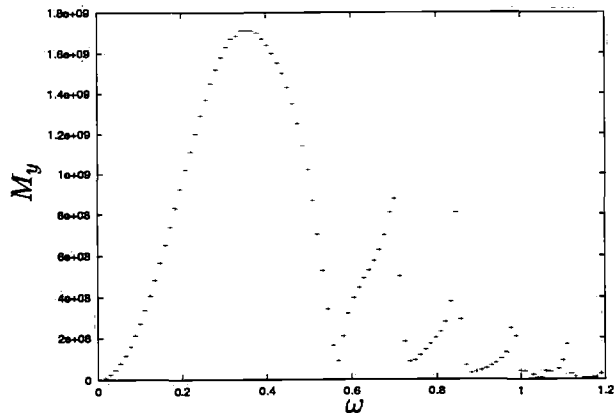


Figure 3.33: Moment /y for Pinkster's model test barge

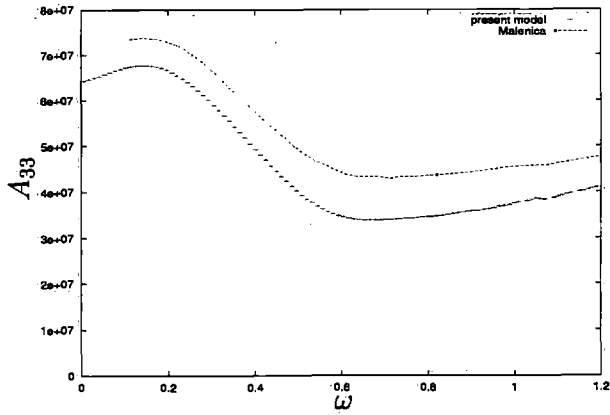


Figure 3.34: added mass in heave $\alpha = \infty$, Comparison with Malenica's result

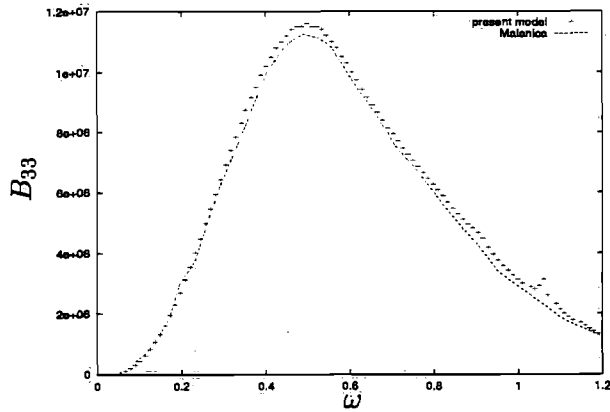


Figure 3.35: Damping in heave $\alpha = \infty$, Comparison with Malenica's result

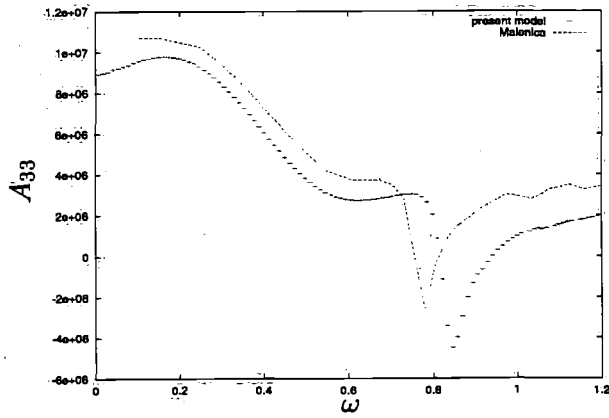


Figure 3.36: added mass in heave $\alpha = 0$,
Comparison with Malenica's result

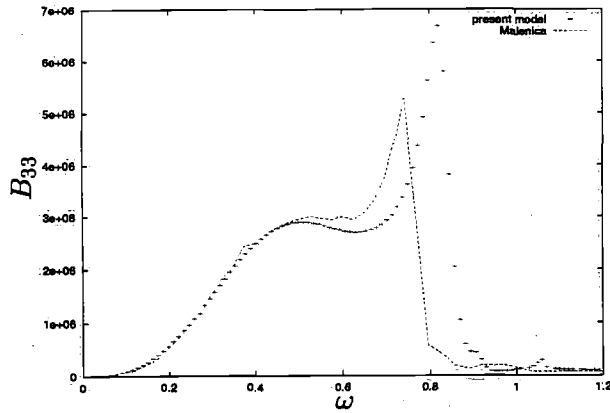


Figure 3.37: Damping in heave $\alpha = 0$,
Comparison with Malenica's result

Deformation of an elastic cylinder in waves

In this chapter, we investigate the deflection of a thin shell cylinder, mounted at the sea bottom by periodic waves. The motion of the shell is described by the well known thin shell theory. The harmonic water waves diffracted by the cylinder are described by means of the eigenmode expansion. We then solve the coupled equations for the cylinder using the same set of orthogonal functions. By developing the highest derivatives in series of these eigenmodes, we assure then convergence of our solutions.

4.1 Introduction

In this chapter we investigate the influence of periodic water waves on the deflection of a thin flexible shell, with large radius, mounted at the sea bottom at depth h and piercing through the free surface. The fluid is assumed to be inviscid and rotationless, hence the velocity potential obeys the Laplace equation. The motion of the shell is described by the classical theory of thin shells. The equations are then reduced to simplified "two dimensional" equations involving the normal, tangential and longitudinal motion u, v, w of the middle surface. This theory requires that the shell thickness d is small in comparison with shell radius R , and the water depth h . The other classical assumptions can be found in Markus [27]. We will focus on the periodic deflections only and we pay no attention to the static deflection due to hydrostatic pressure. By linearity, this effect can be added.

The harmonic water waves diffracted by a rigid cylinder will be described by means of the well known eigenmode expansion. These modes are solutions of

the Laplace equation and fit the boundary conditions at the free surface and the sea bottom. To solve the coupled equations for the refracted potential and the motion of the shell we use the same set of orthogonal functions. Due to the boundary conditions of the variables of motion of the shell this can not lead to a converging series. To assure convergence we expand these highest derivatives, as they occur in the equations of motions, in series of these eigenmodes. The lower order derivatives and the functions themselves follow from these expansions. This gives rise to a set of polynomials with unknown coefficients. Making use of the orthogonality relations of the eigenmodes and the expansion of the polynomials in these modes leads to a set of equations with a sparse block, structured by the orthogonality relation, combined with full rows due to the expansions of the polynomials. The boundary conditions of the variables describing the motion of the shell give an extra set of equations. The final 'square' matrix equation can be solved by a standard method.

In section 4.6, an application of this mathematical approach is treated for the case of a flexible beam loaded by a distribution described by the first eigenmode of the water-wave problem. Convergence of the deflection and its derivatives is shown. We then apply the mathematical model for the real shell and present results of our computations for several values of the flexural rigidity. The method is shown to be valid for a large range of shell rigidity.

4.2 Derivation of the main equations

We study the behavior of the thin cylindrical shell in periodic waves in a sea of constant depth h . The shell, emerging from the sea surface is fixed on the sea bottom (figure(4.1)). We denote u , v and w the normal, tangential and vertical shell deflections.

We assume the fluid to be potential and introduce the velocity potential $\mathbf{V} = \nabla\Phi(\underline{x}, t)$ where \mathbf{V} is the fluid velocity vector. We get for the potential $\Phi(\underline{x}, t)$ the Laplace equation $\Delta\Phi = 0$ in the fluid domain.

At the linearized free surface $z = 0$, the linearized free surface condition $g\Phi_z + \Phi_{tt} = 0$ holds. At the bottom, $z = -h$, we have $\frac{\partial\Phi}{\partial z} = 0$ and we add the linearized body boundary condition $\frac{\partial\Phi}{\partial n} = u$ on the shell, at $r = R$.

Following Love's theory, we derive the equations of motion of the shell.

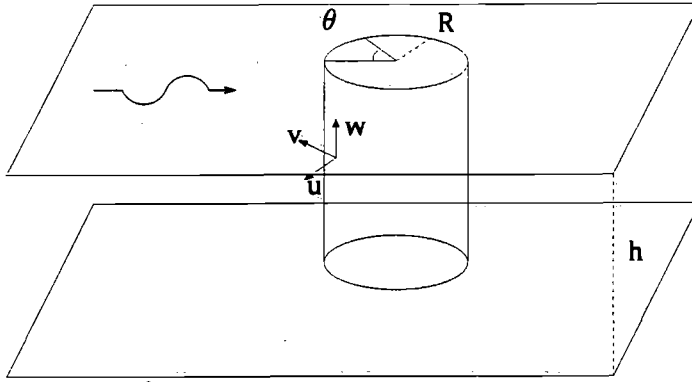


Figure 4.1: Cylinder geometry

$$-\nu R \frac{\partial u}{\partial z} + \frac{R}{2}(1+\nu) \frac{\partial^2 v}{\partial z \partial \theta} + R^2 \frac{\partial^2 w}{\partial z^2} + \frac{1}{2}(1-\nu) \frac{\partial^2 w}{\partial \theta^2} - \frac{\rho_0}{E}(1-\nu^2)R^2 \frac{\partial^2 w}{\partial t^2} = 0 \quad (4.1)$$

$$-\frac{\partial u}{\partial \theta} + \frac{\partial^2 v}{\partial \theta^2} + \frac{R^2}{2}(1-\nu) \frac{\partial^2 v}{\partial z^2} - \frac{\rho_0}{E}(1-\nu^2)R^2 \frac{\partial^2 v}{\partial t^2} + \frac{R}{2}(1+\nu) \frac{\partial^2 w}{\partial z \partial \theta} = 0 \quad (4.2)$$

$$-\chi \left(R^4 \frac{\partial^4 u}{\partial z^4} + 2R^2 \frac{\partial^4 u}{\partial z^2 \partial \theta^2} + \frac{\partial^4 u}{\partial \theta^4} \right) - u - \frac{\rho_0}{E}(1-\nu^2)R^2 \frac{\partial^2 u}{\partial t^2} + \frac{\partial v}{\partial \theta} + \nu R \frac{\partial w}{\partial z} = \frac{(1-\nu^2)R^2}{Ed} P(r, z, \theta, t) \quad (4.3)$$

with $\chi = \frac{1}{12} \left(\frac{d}{R} \right)^2$ and P the dynamic pressure due to water waves. From Bernoulli's theorem we can write

$$P(r, z, \theta, t) = -\rho \frac{\partial \Phi}{\partial t}(r, \theta, z, t) \quad (4.4)$$

By differentiating equation (4.2), one can obtain.

$$-\nu R \frac{\partial^2 u}{\partial z^2} + \frac{R}{2}(1+\nu) \frac{\partial^3 v}{\partial z^2 \partial \theta} + R^2 \frac{\partial^3 w}{\partial z^3} + \frac{1}{2}(1-\nu) \frac{\partial^3 w}{\partial z \partial \theta^2} - \frac{\rho_0}{E}(1-\nu^2)R^2 \frac{\partial^3 w}{\partial z \partial t^2} = 0 \quad (4.5)$$

The differentiation will allow us to expand later this equation in the same eigenfunctions than the two others shell equations. If we choose equation (4.2) to be zero at $z = -h$ it is automatically fulfilled everywhere.

We split the potential and the pressure into two parts.

The first ones (ϕ^d and p^d) are due to the diffraction when the shell is rigid. The second ones (ϕ and p) are due to the flexural deflections and the radiated water waves that the shell motion generates.

$$P(r, \theta, z, t) = (p^d(r, \theta, z) + p(r, \theta, z)) e^{-i\omega t} \quad (4.6)$$

$$\Phi(r, \theta, z, t) = (\phi^d + \phi) e^{-i\omega t} \quad (4.7)$$

The expression for $p^d(r = R)$ is well known and can be found in the literature.

$$p^d(r = R) = \frac{\rho g}{\cosh(kh)} \left(\frac{h + \sigma^{-1} \sinh^2(kh)}{2} \right)^{1/2} f_0(z) \times \sum_{n=0}^{\infty} \frac{2\epsilon_n(i)^{n+1}}{\pi k R \bar{H}'_n(kR)} \cos(n\theta) = \sum_{n=0}^{\infty} A_n \cos(n\theta) \times f_0(z) \quad (4.8)$$

$f_0(z)$ is given in the next section.

4.3 Expansion of the solutions in eigenfunctions

We first expand the potential ϕ in the usual eigenfunctions f_m .

$$\phi(r, \theta, z, t) = \sum_{n=0}^{\infty} \sum_{m=1}^{\infty} X_{mn} K_n^1(k_m r) \cos(n\theta) f_m(z) e^{-i\omega t} \quad (4.9)$$

$$+ \sum_{n=0}^{\infty} X_{0n} H_n^1(kr) \cos(n\theta) f_0(z) e^{-i\omega t}$$

Instead of following the standard approach for Sturm-Liouville boundary value problems where expansions in the eigenfunction space of the operator is sought, we assume that the fourth derivative of u , the second derivative of v and third derivative of w can be expanded in the same class of eigenfunctions. Then, if we integrate those functions and find for u , v and w

$$u(z, \theta, t) = \sum_{n=0}^{\infty} \left\{ \sum_{m=0}^{\infty} \frac{u_{mn}}{k_m^4} f_m(z) + \frac{1}{6} C_{1n}(z+h)^3 + \frac{1}{2} C_{2n}(z+h)^2 + C_{3n}(z+h) + C_{4n} \right\} \cos(n\theta) e^{-i\omega t} \quad (4.10)$$

$$v(z, \theta, t) = \sum_{n=1}^{\infty} \left\{ \frac{v_{0n}}{k^2} f_0(z) - \sum_{m=1}^{\infty} \frac{v_{mn}}{k_m^2} f_m(z) + C_{8n}(z+h) + C_{9n} \right\} \sin(n\theta) e^{-i\omega t} \quad (4.11)$$

$$w(z, \theta, t) = \sum_{n=0}^{\infty} \left\{ \frac{w_{0n}}{k^3} g_0(z) - \sum_{m=1}^{\infty} \frac{w_{mn}}{k_m^3} g_m(z) + \frac{1}{2} C_{5n}(z+h)^2 + C_{6n}(z+h) + C_{7n} \right\} \cos(n\theta) e^{-i\omega t} \quad (4.12)$$

with

$$f_0(z) = \frac{\sqrt{2} \cosh k(z+h)}{(h + \sigma^{-1} \sinh^2(kh))^{1/2}} \quad g_0(z) = \frac{\sqrt{2} \sinh k(z+h)}{(h + \sigma^{-1} \sinh^2(kh))^{1/2}} \quad (4.13)$$

with k given by the usual dispersion relation $\sigma = k \tanh(kh)$

$$f_n(z) = \frac{\sqrt{2} \cos k_n(z+h)}{(h - \sigma^{-1} \sin^2(k_n h))^{1/2}} \quad g_n(z) = \frac{\sqrt{2} \sin k_n(z+h)}{(h - \sigma^{-1} \sin^2(k_n h))^{1/2}} \quad (4.14)$$

k_n given by $\sigma = k_n \tan(k_n h)$

The f_n functions are orthonormal and form a complete set of eigenfunctions for the solution ϕ .

In order to guarantee the convergence of the termwise integrated series to the integral of the expanded function, we have to assume that the series of the successive derivatives converge uniformly. This requirement can be too strong and is not necessary as can be shown by a slightly different approach. However, numerical results confirm the convergence of the fourth derivative of u although slowly. The convergence of the series for u is then guaranteed and fast. The eigenfunctions f_n for ϕ are not eigenfunctions of the mechanical equations. It turns out that the polynomials are convenient to be added, the found solution lies in the proper function space. It fulfills the boundary conditions and in a weak sense the equations. It is reasonable to expect some local convergence problems for the series of the highest derivatives.

4.4 Boundary conditions

The boundary condition on the cylinder for the potential ϕ in frequency domain is as follow:

$$\frac{\partial \phi}{\partial n} = -i\omega u \quad (4.15)$$

The boundary condition at the bottom of the fluid domain also represents that the boundary is a rigid wall, therefore

$$\frac{\partial \phi}{\partial z} = 0 \quad \text{at } z = -h \quad (4.16)$$

The mechanical boundary conditions at the ends of the shell are then derived by considering that the shell is fixed at $z = -h$ but free at $z = 0$. Following Markus, the eight extra equations, for $r = R$, read

$$u = v = w = \frac{\partial u}{\partial z} = 0 \quad \text{for } z = -h \quad (4.17)$$

$$\frac{\partial w}{\partial z} + \frac{\nu}{R} \left(\frac{\partial v}{\partial \theta} - u \right) = 0 \quad (4.18)$$

$$\frac{\partial^2 u}{\partial z^2} + \frac{1}{R^2} \frac{\partial^2 u}{\partial \theta^2} = 0 \quad (4.19)$$

$$\frac{1}{R} \frac{\partial w}{\partial \theta} + \frac{\partial v}{\partial z} = 0 \quad (4.20)$$

$$\frac{\partial}{\partial z} \left[\frac{\partial w}{\partial z} + \nu \left(\frac{1}{R} \frac{\partial v}{\partial \theta} - \frac{u}{R} \right) \right] - \frac{(1-\nu)}{2R} \frac{\partial}{\partial \theta} \left[\frac{1}{R} \frac{\partial w}{\partial \theta} + \frac{\partial v}{\partial z} + 4 \frac{\partial^2 u}{\partial z \partial \theta} \right] = 0 \quad (4.21)$$

We have then to force equation (4.2) to be zero. Until now, only its derivative with respect to z equals zero. This gives an extra condition for the coefficients C_{8n} and C_{5n} :

$$\frac{nR}{2} (1 + \nu) C_{8n} + R^2 C_{5n} = 0 \quad (4.22)$$

4.5 Numerical method

For the numerical resolution of the problem, we truncate the sums to N for n , and to M for m . After multiplying each equation by $f_m(z)$, we integrate the equations (4.2), (4.3), (4.2) and (4.15) from $z = -h$ to $z = 0$ using the orthonormality of these functions. For each equation, we also expand the polynomials in the f_m series.

$$\delta_{0i} = \int_{-h}^0 f_i(z) dz \quad \delta_{1i} = \int_{-h}^0 (z+h) f_i(z) dz \quad (4.23)$$

$$\delta_{2i} = \int_{-h}^0 (z+h)^2 f_i(z) dz \quad \delta_{3i} = \int_{-h}^0 (z+h)^3 f_i(z) dz \quad (4.24)$$

This yields, for each $n \in [0 \cdots N]$, to a linear system of $4M + 13$ equations, with unknown values $U_{mn}, V_{mn}, W_{mn}, X_{mn}$ and the C_i coefficients. The force term of the system is logically found to be the pressure due to the diffracted problem for a rigid shell.

4.6 Numerical results and test of convergence

To make our method clearly understandable, let us first solve, for illustration a simplified case. Let describe the axisymmetric, radial vibration of a cylindrical shell under the symmetric load $q(z)$. The former system of equations can be reduced to the differential equation

$$D \frac{\partial^4 u}{\partial z^4} + \frac{Eh}{R^2} u = q(z) \quad \text{with} \quad q(z) = k f_0(z) \quad (4.25)$$

We assume that we have the following boundary conditions

$$u = 0 \quad u' = 0 \quad \text{at} \quad z = -h \quad (4.26)$$

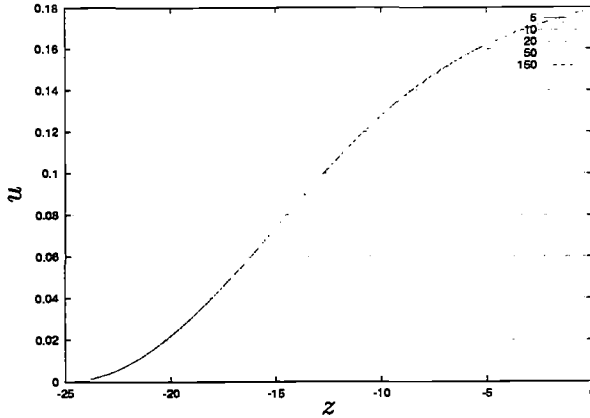
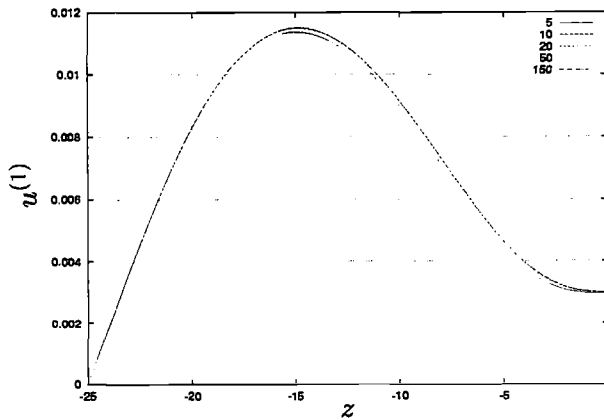
$$u'' = 0 \quad u''' = 0 \quad \text{at} \quad z = 0 \quad (4.27)$$

the function u writes

$$u(z) = \sum_{m=0}^M \frac{u_m}{k_m^4} f_m(z) + \frac{1}{6} C_1 (z+h)^3 + C_2 \frac{1}{2} (z+h)^2 + C_3 (z+h) + C_4 \quad (4.28)$$

Choosing $k = 1$, $D = 1Nm^2$, $h = 50$ and $\frac{Eh}{R^2} = 10^{-2} Nm$, we give the numerical solutions for u , $u^{(1)}$, $u^{(2)}$, $u^{(3)}$ and $u^{(4)}$ obtained for different values of $M(5, 10, 20, 50, 150)$.

The convergence of u appears very fast and we only need a couple of terms to have a very good approximation of our solution. The series of the fourth derivative seems to have a slow converge. Especially to obtain a right value at the point $z = 0$. This is due to the fact that the f_m functions do not obey the boundary equations of the mechanical problem.

Figure 4.2: convergence for u Figure 4.3: convergence for $u^{(1)}$

For the complete model it turns out that the convergence of the series for the deflection shows similar behaviour. Depending on the physical parameters we choose the upper bounds of the series. In general the choice $M = 50$ is reasonable. We present here some numerical results for a cylindrical shell with a diameter of 6 m, in a 25m depth sea. The thickness of the shell is 1cm and its density is 2500 Kg/m^3 . The rigidity equals $E = 10^9 \text{ Nm}^2$ and the incoming wave frequency $\omega = 0.3 \text{ rad/s}$. The chosen value for the rigidity is rather low, so the thin structure is very flexible

Examples of the computation of the amplitude of the deflection for u and w against z , for $\theta = 0$ are shown in figure (4.7). and (4.8). As we suggested we have chosen 50 terms for the series although, more terms are needed to obtain a good convergence of the highest derivatives.

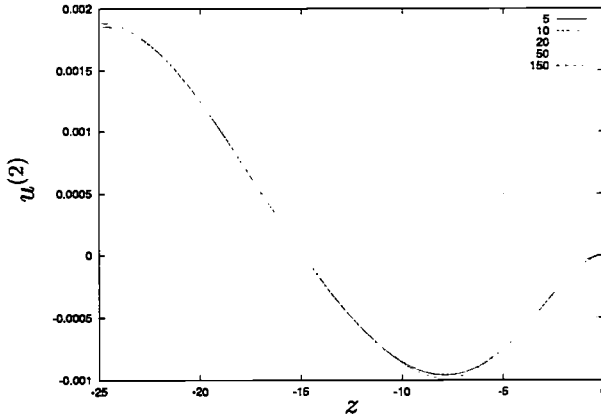


Figure 4.4: convergence for $u^{(2)}$

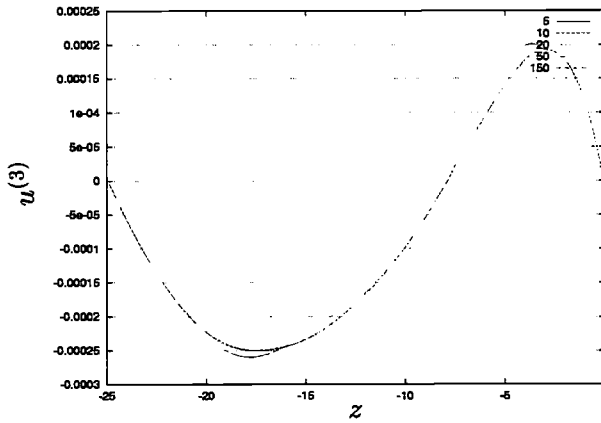


Figure 4.5: convergence for $u^{(3)}$

In figure (4.9) and (4.10), we show the cylinder displacement at two different depths ($z=-15\text{m}$ and $z=-5\text{m}$) and in five different time moments. The main contribution to the displacement is due to the bending of the cylinder.

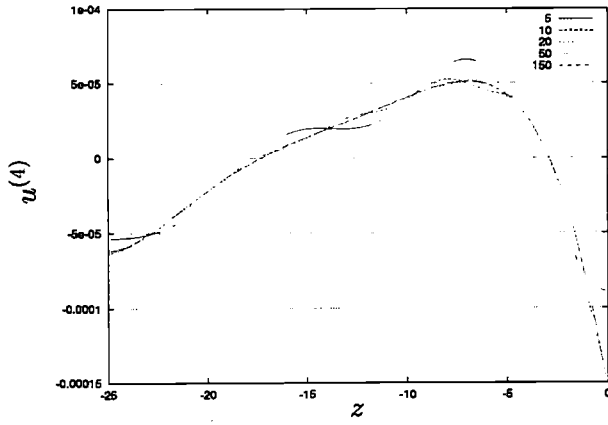


Figure 4.6: convergence for $u^{(4)}$

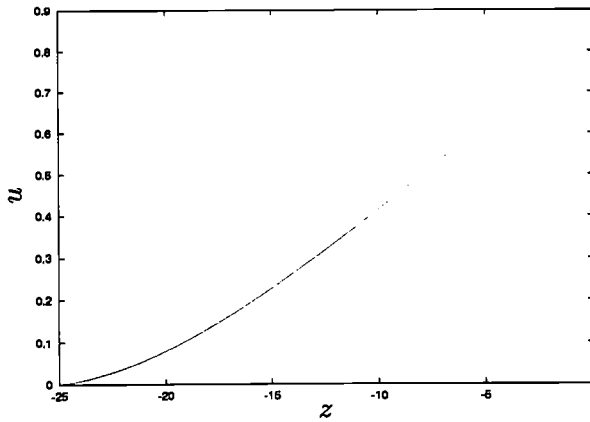


Figure 4.7: shell deflection u function of z

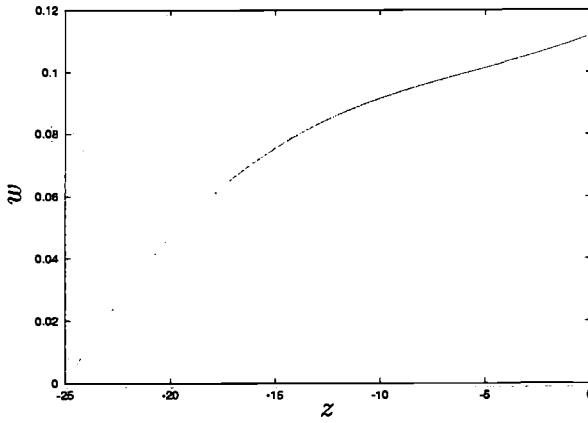


Figure 4.8: shell deflection w function of z

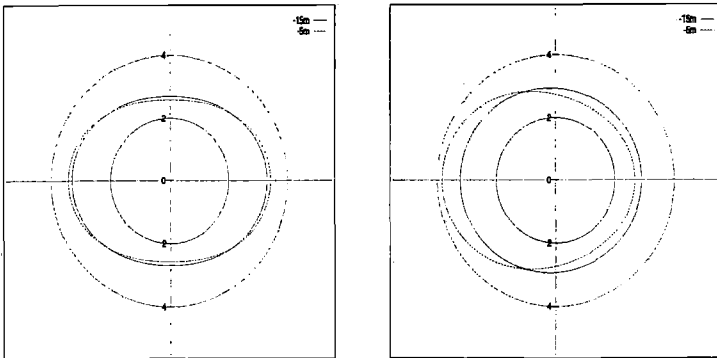


Figure 4.9: shell deflection

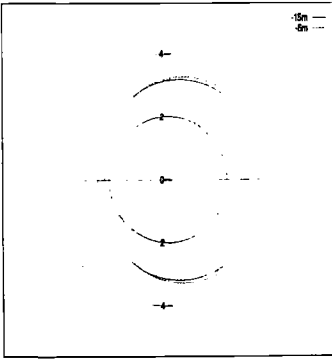
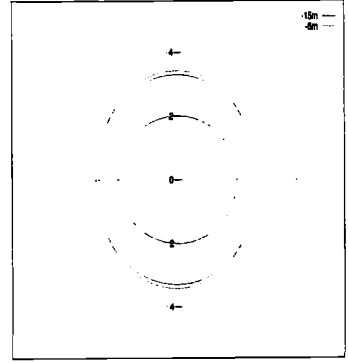
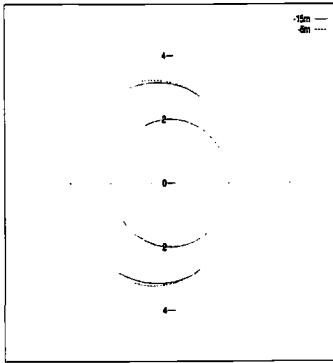


Figure 4.10: shell deflection

Appendix A

Integral equations

In this appendix, we give the integral equations that must fulfill the potentials of radiation ϕ_j^R when the body does not possess axis of symmetry, as it was the case in chapter(3).

A.1 General case for integral equations

This appendix contains the general case for equations when a_x and a_y are non null, this means, when the air cushion does not possess xx and yy as plans of symmetry. We indicate the changes with have to be made.

The boundary condition for the total potential (3.11) becomes

$$\left\{ -\nu\phi + \frac{\partial\phi}{\partial z} + \alpha \iint_{\Sigma_2} \frac{\partial\phi}{\partial z} dS + i\omega\alpha S\xi_3 + i\omega\alpha a_x S\xi_5 - i\omega\alpha a_y S\xi_4 = 0 \right\}_{\Sigma_2} \quad (\text{A.1})$$

the equations (3.19) and (3.20) for the potential of radiation ϕ_j^R become

$$\left\{ -\nu\phi_j^R + \frac{\partial\phi_j^R}{\partial z} + \alpha \iint_{\Sigma_2} \frac{\partial\phi_j^R}{\partial z} dS - \alpha S\chi = 0 \right\}_{\Sigma_2} \quad (\text{A.2})$$

$$\text{with } \chi = \begin{cases} 1 & : j = 3 \\ a_y & : j = 4 \\ -a_x & : j = 5 \\ 0 & : j = 1, 2, 6 \end{cases}$$

the integral equation (3.25) becomes

$$\begin{aligned}
 & 2\pi\phi_j^R - \iint_{\Sigma_1} \frac{\partial \mathcal{G}}{\partial n} \phi_j dS - \iint_{\Sigma_2} \left(\phi_j^R \frac{\partial \mathcal{G}}{\partial z} - \nu \mathcal{G} \phi_j^R \right) dS \\
 & - \frac{\alpha\nu}{1+\alpha S} \iint_{\Sigma_2} \mathcal{G} dS \times \iint_{\Sigma_2} \phi_j^R dS = -\frac{\alpha S \chi}{1+\alpha S} \iint_{\Sigma_2} \mathcal{G} dS - \iint_{\Sigma_1} \mathcal{G} n_j dS \quad (\text{A.3})
 \end{aligned}$$

Appendix **B**

Integral evaluation

In this appendix, we rewrite the integrals given in chapter (3), section 6) under a more convenient form to evaluate numerically by extending the path of integration to the complex plane.

B.1 Some integral calculus

In the problem of the radiation of a cylindrical platform in chapter (3), we encounter the three following integrals.

$$\mathcal{I}_1 = \int_0^{\infty} \frac{1}{(k - \nu)} J_1^2(kR) dk, \quad \mathcal{I}_2 = \int_0^{\infty} \frac{1}{k(k - \nu)} J_1^2(kR) dk \quad (\text{B.1})$$

$$\text{and } \mathcal{I}_3 = \int_0^{\infty} \frac{1}{k - \nu} J_1(kR) J_0(k\rho) dk \quad (\text{B.2})$$

The calculus of these integrals is performed by splitting the integrated functions in two separate parts and extending the path of integration in the superior quadrant for the first resulting integral and in the inferior quadrant for the second. Applying the residu theorem, we obtain a new expression for the integrals, making rid of the singularity at $k = \nu$.

It is recalled that the integration path in the upper plane embrasses the pole at $k = \nu$.

The contribution of the path integration along the superior vertical axis is denoted \mathcal{B}_1 , respectively \mathcal{B}_2 for the inferior vertical axis for each integral.

For \mathcal{I}_1 , we have

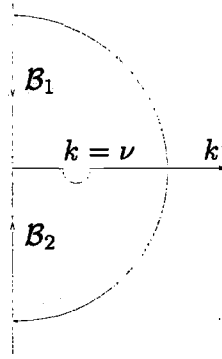


Figure B.1: path of integration

$$\mathcal{I}_1 = \frac{1}{2} \int_0^{\infty} \frac{1}{(k-\nu)} J_1(kR) \left[H_1^{(1)}(kR) + H_1^{(2)}(kR) \right] dk, \quad (\text{B.3})$$

$$\mathcal{B}_1 = - \int_0^{\infty} \frac{I_1(kR) K_1(kR)}{\pi(ik-\nu)} dk, \quad \mathcal{B}_2 = \int_0^{\infty} \frac{I_1(kR) K_1(kR)}{\pi(ik+\nu)} dk \quad (\text{B.4})$$

$$\text{so that } \mathcal{B}_1 + \mathcal{B}_2 = \frac{2}{\pi} \int_0^{\infty} \frac{\nu}{k^2 + \nu^2} I_1(kR) K_1(kR) dk \quad (\text{B.5})$$

and then

$$\mathcal{I}_1 = - \frac{2}{\pi} \int_0^{\infty} \frac{\nu}{k^2 + \nu^2} I_1(kR) K_1(kR) dk + i\pi J_1(\nu R) H_1^{(1)}(\nu R) \quad (\text{B.6})$$

The integral \mathcal{I}_2 can be obtained noticing that $\frac{1}{k(k-\nu)} = \frac{1}{\nu(k-\nu)} = \frac{1}{\nu k}$

$$\mathcal{I}_2 = \int_0^{\infty} \frac{1}{k(k-\nu)} J_1^2(kR) dk = \frac{\mathcal{I}_1}{\nu} - \frac{1}{\nu} \int_0^{\infty} \frac{J_1^2(kR)}{k} dk \quad (\text{B.7})$$

The last integral has a well known value [[14]]

$$\int_0^{\infty} \frac{J_1^2(kR)}{k} dk = \frac{1}{2} \quad (\text{B.8})$$

And then, taking in account the residu we obtain

$$\mathcal{I}_2 = -\frac{2}{\nu\pi} \int_0^{\infty} \frac{\nu}{k^2 + \nu^2} I_1(kR) K_1(kR) dk - \frac{1}{2\nu} + i\frac{\pi}{\nu} J_1(\nu R) H_1^{(1)}(\nu R) \quad (\text{B.9})$$

To compute \mathcal{I}_3 , we write

$$J_1(kR) J_0(k\rho) = \frac{1}{2} J_1(kR) (H_0^{(1)}(k\rho) + H_0^{(2)}(k\rho)) \quad \text{for } \rho > R \quad (\text{B.10})$$

$$J_1(kR) J_0(k\rho) = \frac{1}{2} (H_1^{(1)}(kR) + H_1^{(2)}(kR)) J_1(k\rho) \quad \text{for } \rho < R \quad (\text{B.11})$$

so that, the integrals along the quarter circle in the complex plane vanish and we find after calculation

$$\mathcal{I}_3 = \begin{cases} \frac{2}{\pi} \int_0^{\infty} \frac{k}{k^2 + \nu^2} I_1(kR) K_0(k\rho) dk + i\pi I_1(\nu R) H_0^{(1)}(\nu\rho) & \text{for } \rho > R \\ \frac{2}{\pi} \int_0^{\infty} \frac{k}{k^2 + \nu^2} K_1(kR) I_0(k\rho) dk + i\pi H_1^{(1)}(\nu R) J_0(\nu\rho) & \text{for } \rho < R \end{cases} \quad (\text{B.12})$$

Conclusions and recommendations

This thesis contains four different studies that are, apart from the first two chapters, independent from each other.

In the first chapter, we investigate the response of a platform of large dimensions and shallow draft excited by waves. Due to these peculiar geometrical properties, it is possible to describe the dynamical behavior of the structure with a beam model. Combining the kinematic condition with the plate model leads to an integro-differential equation, valid at $z = 0$. The initial three-dimensional problem is then reduced to a two-dimensional one, the platform presence modifying the free surface condition. We use the simplest beam model (Bernoulli-Euler) which is well suited for low frequencies but the method can be extended to more elaborated models including damping for example. A direct application is floating airports which are moored near the shore in shallow water. To take into account the finite water depth (it is supposed to be infinite in the presentation of our results) can be done without any problem by simply replacing the Green's function by a new one, fulfilling the slip condition on the ocean bottom. It seems that in real cases, the use of pillars for preventing the platform to drift is considered. The inclusion of this constraint in our model can be achieved by adding new boundary conditions ($w = 0$ at each pillar location). This does not represent a great interest mathematically and it has not then been done in this thesis. We mention that, due to the simplicity of our model, our numerical program is very fast - less than a few minutes on a PC for 2000 panels - and can be used for industrial purposes.

We show that our method can also be applied to ships, taking into account their three-dimensional geometry, as long as they can dynamically be described with a rod model. We nevertheless limit our investigations to deflections caused by harmonic waves when there is no forward speed. Various other hydrodynamic phenomena, such as slamming, are responsible of ship deflections but a complete survey of these aspects would furnish an entire new thesis subject by

itself, far from our original objective.

To complete our study on floating airports, we analyze the wave pattern that a moving plane (landing or taking off) generates in the beam structure when translating on the platform. With the model previously developed in the first chapter and the use of integral transforms (Laplace and Fourier), the expression of the deflection is carried out in the most general case. In the case of a translation with constant speed, the expression admits great simplifications and it is possible to extract characteristic values, such as critical speeds, which allows us to understand the physical phenomena involved. Our derivation of the solution is very simple and can be computed with high accuracy within a minute on the far field as well as in the vicinity of the wheel.

Returning to the initial problem of a plane motion with acceleration or deceleration, we show how deforming in the complex plane one of the integrals involved in w can reduce the computing time necessary to determine the deflection.

The third chapter deals with another subject which also could furnish technological solutions for an engineering problem: the behavior of floating platforms with an air cushion device. We first recall the advantages that such platforms would give. The pressure in the air chamber being uniform, the pressure is averaged on the body hull and the stresses in the material are then reduced. It is also possible to change the static and dynamic properties of the body, injecting some air in the chamber and modifying therefore the mean pressure value. To describe the air pocket dynamics, we assume that the compression is adiabatic, the pressure change in the air cushion being linearly dependent of its instantaneous volume change. After deriving the main equations governing the platform behavior and reducing the problem to the resolution of an integro-differential equation on the hull of the platform (and the interface water-gas in the air chamber), we derive simplified models in two and three dimensions to understand the nature of the involved phenomena. Then, we apply our model on a real barge and made some comparisons obtained with *Pinkster's* test model and numerical results. The agreement is good even if the pitch moment is underestimated. Our code has not been optimized for industrial purpose and more accurate results could be obtained by more elaborated numerical panel method. It is nevertheless questionable if this represents a great interest.

Finally, in the fourth chapter, we study the deformations of a cylindrical shell, with its inferior base on the sea bottom, by harmonic waves. We use an eigenfunction expansion for the water domain and show that it is possible to use the same set of functions to describe the shell deflections. Particular attention has been paid to the convergence of such mathematical series and the method proved to furnish correct results.

Bibliography

- [1] James Lighthill. *Waves in Fluids*. Cambridge University Press, 1978.
- [2] A.J. Hermans. *A boundary element method for the interaction of free-surface waves with a very large floating flexible platform*. J. of fluids and structures, vol 14, pp. 943-956, 2000.
- [3] Š Malenica, A. Espanet & M. Zalar. *Tenue à la mer des objets flottants supportés par des coussins d'air*. Huitièmes journées de l'hydrodynamique, 2001.
- [4] Š Malenica & M. Zalar. *An alternative method for linear hydrodynamics of air cushion supported floating bodies*. 15th International Workshop on Water Waves and Floating Bodies, Caesarea, Israel, 2000.
- [5] J.A. Pinkster. *Low frequency second order wave exciting forces on floating structures*. PhD Thesis, Delft 1980.
- [6] J.A. Pinkster, E.J.A. Meervers Scholte. *The behaviour of a large air-supported MOB at sea*. Marine Structures 14 163-179, 2001.
- [7] J.A. Pinkster, A. Fauzi, Y. Inoue and S. Tabet. *The behaviour of a large air cushion structures in waves*. Proceedings of the second international conference on hydroelasticity in marine technology Fukuoka/Japan, 1998.
- [8] Hajine Maruo. *The drift force of a body floating in waves*. Journal of ship research, 1960.
- [9] F. Noblesse. *The Green function in the theory of radiation and diffraction of regular water waves by a body*. J. Engineering Mathematics 16, 137-169, 1982.
- [10] C.-H Lee, J.N. Newman. *Wave effects on large floating structures with air cushions*. Marine Structures 13 315-330, 2000.

- [11] C.-H. Lee & J.N. Newman. *An assessment of hydroelasticity for very large hinged vessels*. Journal of Fluids and Structures, vol 14, pp. 957-970, 2000.
- [12] J.N. Newman. *Diffraction of water waves by an air chamber*. 15th International Workshop on Water Waves and Floating Bodies, Caesarea, Israel, 2000.
- [13] IAN N. Sneddon. *Mixed boundary value problems in potential theory* North-Holland Publishing Company, Amsterdam, 1966.
- [14] G.N. Watson. *Theory of Bessel Functions*. Cambridge University press, 1922.
- [15] G. van Oortmerssen. *The motions of a moored ship in waves*. PhD thesis, Delft Univ. of Techn., The Netherlands, 1976.
- [16] R.E.D Bishop & W.G Price. *Hydroelasticity of ships*. Cambridge University Press, 1979.
- [17] Davys J.W., Hosking R.J. and Sneyd A.D. *Waves due to a steadily moving source on a floating ice plate*. J. Fluid Mech. , vol 158, pp 269-287, 1985.
- [18] M. Abramowitz and I.A. Stegun. *Handbook of Mathematical Functions*. Dover Publications inc., New York, USA, 1964.
- [19] Karl F. Graff. *Wave Motion in Elastic Solids in Fluids*. Dover publications, 1973.
- [20] C.-H. Lee & J.N. Newman. *An assessment of hydroelasticity for very large hinged vessels*. Journal of Fluids and Structures, vol 14, pp. 957-970, 2000.
- [21] W. Magnus & F. Oberhettinger. *Formulas and Theorems for the Special Functions of Mathematical Physics*. Chelsea Publishing Company, 1943.
- [22] F. Milinazzo, M. Shinbrot & N.W. Evans. *A mathematical analysis of the steady response of floating ice to the uniform motion of a rectangular load*. J. Fluid Mech., vol 287, pp. 173-197, 1995.
- [23] R.M. Schulkes, Hosking R.J. & Sneyd A.D. *Waves due to a steadily moving source on a floating ice plate. Part 2*. J. Fluid Mech., vol 180, pp. 297-318, 1987.
- [24] J.V. Wehausen and E.V. Laitone. *Surface Waves*. Springer-Verlag, Berlin, Germany, 1960.
- [25] R. W. Yeung & J.W. Kim. *effects of a translating load on a floating plate - structural drag and plate deformation*. Journal of Fluids and Structures, vol 14, pp. 993-1011, 2000.

- [26] K.F. Cheung, A.C. Phadke, D.A. Smith, S.K. Lee & L.H. Seidl. *Hydrodynamic response of a pneumatic floating platform*. Ocean Engineering 27 1407-1440., 2000.
- [27] Štefan M̄arkus. *The Mechanics of Vibrations of Cylindrical Shells Studies in Applied Mechanics*, 1988.
- [28] J.J. Stoker. *Water Waves, The Mathematical Theory with Applications*. Interscience Publishers, INC., New York, 1957.
- [29] Jang Whan Kim & Cengiz Ertekin. *An Eigenfunction-expansion method for predicting hydroelastic behavior of a shallow-draft VLFS*. Proceedings of the second international conference on hydroelasticity in marine technology Fukuoka/Japan, 1998.

Samenvatting

Wisselwerking tussen watergolven en elastische platforms en platforms met luchtkussen

Het probleem van de hydrodynamische krachten die op een drijvend platform werken is allang bekend. Theorieën zijn gewoonlijk geschikt voor massieve, zware en stijve offshore constructies die de olie-industrie met succes gebruikt. Kort geleden zijn nieuwe platform prototypen voor verschillende toepassingen verschenen. In het bijzonder is er veel belangstelling voor drijvende luchthavens in Japan en in de V.S. Deze constructies hebben bijzondere vormen - ze zijn veel langer, breder en hebben een kleine diepgang - en kunnen onderworpen zijn aan de krachten van opstijgende en landende vliegtuigen. Nieuwe ontwerpen roepen om nieuwe wiskundige modellen en nieuwe wiskundige modellen roepen om nieuwe AIO's met nieuwe proefschriften.

In dit proefschrift is speciale aandacht besteed aan twee mogelijke oplossingen die voor dit probleem waren voorgesteld: kunstmatige eilanden en platforms met een zogenaamd "luchtkussen".

In het eerste hoofdstuk bestuderen wij de invloed van golven op de bewegingen van drijvende en buigzame eilanden. Aangenomen wordt dat het eiland geen diepgang heeft en dat het mogelijk is zijn dynamische gedrag met een plaatmodel te beschrijven. De plaatvergelijking is met de waterdeflectie vergelijking gekoppeld om een nieuwe vrije oppervlakte conditie voor de plaat af te leiden. Met behulp van een rand-integraalmethode is een integro-differentialvergelijking verkregen om de plaatdeflectie te beschrijven en we lossen het probleem numeriek met een panelen methode op. In tegenstelling tot klassieke methoden wordt er geen hydrodynamische coëfficiënt (toegevoerde massa en demping) berekend. De potentiaalfunctie wordt niet in componenten opgesplitst maar het volledige probleem wordt in een keer opgelost.

De verticale plaatverhoging is op elk paneel constant genomen en die waarden

vormen de oplossing van het probleem. De verre veld golfhoogte is afgeleid en de uitgestraalde energie wordt bepaald. We testen de methode op een tweedimensionaal platform want het probleem is klein en snel uit te rekenen, en tonen de limieten van het algoritme voor erg stijve eilanden. Uiteindelijk is de methode op rechthoekige platformen toegepast.

De methode is uitgebreid voor een buigzaam driedimensionaal schip. Daarvoor nemen we aan dat het schip zich dynamisch als een balk gedraagt. Haar romp wordt gediscrètiseerd in een verzameling doorsneden met constante massa en stijfheid. Een rand-integraalmethode is gebruikt om de hydrodynamische vergelijkingen te beschrijven en de vergelijkingen zijn door middel van de relatie tussen de balkdeflectie en de water beweging op de romp gekoppeld.

In het tweede hoofdstuk, bepalen we de deflectie die door een landend of opstijgend vliegtuig op een platform wordt veroorzaakt. Aangenomen wordt dat het eiland oneindig uitgestrekt is en dat de enige kracht op het platform uitgeoefend, het constante gewicht van het toestel is. Voor de beschrijving van het dynamische gedrag van het platform wordt het plaatmodel van het vorige hoofdstuk gebruikt. Met behulp van Laplace en Fourier transformatie, bepalen we de oplossing van de verhoging over de hele platform voor een translatie, met variabele snelheid, van het vliegtuig. In het geval van een constante snelheid wordt de oplossing vereenvoudigd. De plaatgolven, door het toestel uitgestraald, zijn in drie klassen- subkritisch, kritisch en superkritisch-afhankelijk van de snelheid, te verdelen. Aangetoond wordt dat voor alle snelheden, de verhoging naast het vliegtuigwiel, een begrensde waarde heeft. Wij schenken bijzondere aandacht aan het golfpatroon voor het geval waarin de vliegtuigsnelheid gelijk is aan de kritische snelheid.

In het derde hoofdstuk worden de krachten op een platform met luchtkussen berekend, welke door inkomende regelmatige watergolven worden uitgeoefend. Een adiabatisch model is voor het gas in de luchtkamer onder het platform gekozen. Dit leidt tot een constante druk in de kamer. De vrije oppervlakteconditie voor het interface tussen het gas en het water in de luchtkamer is afgeleid en door middel van een rand-integraalmethode, volgt een integraalvergelijking voor de snelheidspotential. De uitdrukkingen voor toegevoegde massa en demping worden berekend.

Er wordt bijzondere aandacht aan de stabiliteit van het platform besteed want de aanwezigheid van het luchtkussen verandert de opdrijvende kracht en statische momenten van stabiliteit drastisch. Het evenwicht van dit soort platforms is inderdaad slecht.

Om de fysische verschijnselen die door de aanwezigheid van het luchtkussen veroorzaakt worden te analyseren, gebruiken we eerst platforms met eenvoudige vormen. Analytische resultaten zijn gepresenteerd in het geval van de verstrooiing van inkomende golven op een een-dimensionaal platform en uitstraling bij een cilindrisch platform. Onze resultaten zijn met een akoestisch model van andere auteurs vergeleken.

Uiteindelijk wordt de algemene methode op een echt platform toegepast. De resultaten zijn vergeleken met resultaten van Pinkster, uit modelproeven verkregen. De stampbeweging van het platform is in overeenstemming met de metingen maar er zijn verschillen voor het dompen.

In het vierde hoofdstuk wordt de vervorming van een slanke verticale cilinder door inkomende golven bepaald. De cilinder staat op de zeebodem en de bovenkant ervan is gelijk met de zeespiegel. De verstrooie golven zijn door middel van een reeks van harmonische eigenfuncties beschreven en we ontwikkelen de cilindervervorming in hetzelfde reeks van eigenfunctie. De dynamische vergelijkingen voor de cilinder en het hydrodynamische probleem zijn uiteindelijk gekoppeld waarbij bijzondere aandacht aan de convergentie van de oplossing wordt besteed.

Remerciements

Le travail présenté dans cette thèse et effectué à l'Université de Delft durant ces quatre dernières années n'aurait jamais été possible sans la contribution de nombreuses personnes.

Tout d'abord, je voudrais remercier le professeur Hermans pour l'encadrement qu'il m'a fourni. Je lui suis particulièrement reconnaissant pour son intérêt constant pour mes travaux et son infinie disponibilité pour répondre à toutes sortes de questions. Tout en disposant d'un soutien permanent, j'ai toujours pu avoir une large autonomie dans mes recherches.

J'ai apprécié son intérêt et sa curiosité scientifique pour des sujets qui allaient au delà de cette thèse et de l'hydrodynamique en général et je le remercie chaleureusement d'avoir toujours eu pour but d'enrichir les connaissances de son étudiant et pour ses nombreux conseils de lecture.

Je voudrais aussi remercier Marleen Keijzer avec qui j'ai eu la chance de partager le bureau mes deux dernières années de thèse. Son optimisme et son amitié m'ont été d'un grand soutien dans les moments de découragement. Je la remercie aussi grandement pour sa patience à m'écouter écorcher le Néerlandais. Je lui dois d'avoir pu pratiquer quotidiennement cette langue (bien que mon niveau soit malheureusement resté passable).

Kees Lemmens et Eef Hartman sont de même de tout coeur remerciés pour l'assistance technique qu'ils m'ont apporté en informatique et leur patience à réparer les dégâts que je m'évertuais à faire sur mon ordinateur.

Un certain nombre de personnes extérieures au département ont aussi collaboré à ce travail. Je suis reconnaissant au professeur Pinkster de m'avoir fourni les fichiers numériques concernant les résultats de tests en bassin pour la barge avoir coussin d'air et pour les discussions que j'ai pu avoir avec lui. Sime Malenica a bien voulu attentivement relire ma thèse et m'a apporté de nombreux commentaires et conseils durant toute ma thèse.

Enfin, je remercie tous les membres du département pour l'atmosphère agréable dans laquelle j'ai pu travailler.

Curriculum vitae

Geboren: 30 januari 1973 te Clermont-Ferrand (Frankrijk).

Vorbereidend onderwijs, Lycée: 1988-1991
"Lycée Aux Lazaristes" te Lyon.

"Mathématiques supérieures, mathématiques spéciales" te Lyon.
(vorbereiding voor ingenieursopleiding): 1991-1994

Ingenieursopleiding: 1994-1997,
"Ecole supérieure d'ingénieur de Marseille"

Diploma wiskundig ingenieur: september 1997

Militaire dienst : 1997-1998

Promotie-onderzoek uitgevoerd bij de vakgroep Toegepaste
Analyse (Mathematische Fysica) van de Faculteit der
Technische Wiskunde en Informatica: 1998-2002